NTNU

Norwegian University of
Science and Technology

Techno-economic and thermodynamic optimization of Rankine cycles

Inés Encabo Cáceres

Natural Gas Technology
Submission date: June 2018
Supervisor: Lars Olof Nord, EPT
Co-supervisor: Roberto Agromayor, EPT

Norwegian University of Science and Technology
Department of Energy and Process Engineering

NTNU

Norwegian University
of Science and Technology

Department of Energy
and Process Engineering

EPT-M-2017-26

MASTER THESIS

for

Student Inés Encabo Cáceres

Spring 2018

English title:
Techno-economic and thermodynamic optimization of Rankine cycles

Background and objective

Organic Rankine cycles (ORC) is one of the most interesting power cycles for various applications, including waste heat recovery and geothermal. Other options include steam Rankine cycles and Brayton cycles. Much of the focus in the literature is on *thermodynamic* optimization of such systems. However, when a decision is to be made for a potential new development, cost will be the main decision factor. Therefore, *techno-economic* optimization is a vital part when analysing such cycles.

The thesis will be based on the specialization project where an in-depth literature review was done, a techno-economic optimization MATLAB code was developed, and preliminary results were presented. The code needs refinement to decrease the computational time and proper documentation for future use. Validation of the model, the heat transfer coefficients and the cost results are needed. The specialization project was based on a given geothermal case study. For the thesis, the work should be generalized to apply to a range of heat source and cold sink temperatures.

The following tasks are to be considered:

1. Refine and document MATLAB code
2. Validate model
3. Compare thermodynamic and techno-economic optimization results
4. Evaluate different process configurations and components
5. Generalize results

When the thesis is evaluated, emphasis is put on processing of the results, and that they are presented in tabular and/or graphic form in a clear manner, and that they are analyzed carefully.

The thesis should be formulated as a research report with summary, conclusion, literature references, table of contents etc. During the preparation of the text, the candidate should make an effort to produce a well-structured and easily readable report. In order to ease the evaluation of the thesis, it is important that the cross-references are correct. In the making of the report, strong emphasis should be placed on both a thorough discussion of the results and an orderly presentation.

The candidate is requested to initiate and keep close contact with his/her academic supervisor(s) throughout the working period. The candidate must follow the rules and regulations of NTNU as well as passive directions given by the Department of Energy and Process Engineering.

Risk assessment of the candidate's work shall be carried out according to the department's procedures. The risk assessment must be documented and included as part of the final report. Events related to the candidate's work adversely affecting the health, safety or security, must be documented and included as part of the final report. If the documentation on risk assessment represents a large number of pages, the full version is to be submitted electronically to the supervisor and an excerpt is included in the report.

Pursuant to “Regulations concerning the supplementary provisions to the technology study program/Master of Science” at NTNU §20, the Department reserves the permission to utilize all the results and data for teaching and research purposes as well as in future publications.

The final report is to be submitted digitally in DAIM. An executive summary of the thesis including title, student’s name, supervisor's name, year, department name, and NTNU's logo and name, shall be submitted to the department as a separate pdf file. Based on an agreement with the supervisor, the final report and other material and documents may be given to the supervisor in digital format.

☐ Work to be done in lab (Water power lab, Fluids engineering lab, Thermal engineering lab)
☐ Field work

Department of Energy and Process Engineering, 15 January 2018

Lars O. Nord
Academic Supervisor

Co-supervisors:
Roberto Agromayor, PhD candidate, NTNU

Preface

The decision of focusing this project work on the optimization of Rankine cycles came from the interest I developed in the field after having worked an entire semester on the thermodynamic optimization of the same technology. The satisfying feeling of having reached interesting results that allowed me to publish a scientific paper and to participate in the first conference of my life encouraged me to dig much more into the topic.

Since Organic Rankine Cycles constitute a developing field that offers great possibilities of improvement through research, I wanted to promote the unfolding of such an innovative and environmentally friendly way of producing power. Also, I saw in this project an opportunity to lead my career, thanks to the great future forecast that Rankine Cycles present.

I really hope that the effort I put on this work can inspire future students to get interested in a topic I never thought I could enjoy so much.

I hope you enjoy the reading.

Inés Encabo Cáceres

Norwegian University of Science and Technology
Department of Energy and Process Engineering
Trondheim. June, 2018

Abstract

Rankine Cycles are an effective and efficient way of producing power from low-medium temperature heat sources when combined with low-medium critical temperature working fluids. The technology provides high flexibility in design, not only because of the great number of working fluids that can be selected for the system, but also because of the wide range of possible configurations and layouts the cycle allows to work with. When designing a Rankine cycle, the thermodynamic assessment alone is not an exhaustive indicator of the optimal configuration, mainly because every working fluid has very different properties, which have a great impact not only on the performance of the cycle, but also on its size and, therefore, on its cost.

This work is focused on the thermodynamic and techno-economic optimization of simple subcritical Rankine cycles for a low-medium temperature geothermal heat source application. Two case studies were analyzed. The first one consists on optimizing the Specific Investment Cost of the plant for 4 different heat exchangers configurations and a given scenario (a heat source of 10 kg/s water flow rate at 120 ºC and a cold sink inlet temperature of 10 ºC), and determining which configuration gives the best results and for which set of working fluids. The second case study lies in evaluating and comparing the optimum thermodynamic and techno-economic performance of the plant for different varying heat source and heat sink conditions, for the best set of working fluids that was found in the previous case study (plus benzene and pentane) and the most suitable heat exchangers configuration. For both case studies, the geometry design of the cycle heat exchangers was determined by an optimization code developed in MATLAB, computing all the thermodynamic states of the cycle, pressure drops and heat transfer coefficients in the heat exchangers, and cost components.

Results show that resorting to plate heat exchangers minimizes the Specific Investment Cost of Rankine cycles, especially when using working fluids with a T_{max}/T_{crit} close to 1. The working fluid selection, and the heat source and cold sink inlet conditions, have a great impact on the performance and cost of the system, which are always reaching the best results when ammonia is used as the system working fluid. Moreover, the techno-economic and thermodynamic optimizations give completely dissimilar results, not only when analyzing the size of the system components, but also when looking at the heat exchangers geometry design, the operating pressures, or the degree of super-heating at the inlet of the expander, among others. In general, better cycle performances can only be reached in exchange for higher investment costs.

Acknowledgements

In truth, I could not have achieved any success without the support and help from people who have been around me during the realization of this project.

First of all, I would like to thank my supervisor, Professor Lars O. Nord, for having been an important source of knowledge through his guidance during the three years I have spent at the Norwegian University of Science and Technology. You were the only one who gave me the opportunity to prove my aptitudes when I came to Trondheim and, since then, your trust in me made me grow as a researcher, directing my steps to successes I never thought I could achieve, such as participating in a conference. I will always be grateful to you.

I would also like to mention PhD candidate Roberto Agromayor, my co-supervisor, to the one I must express my gratitude for having awaken my interest in a programming tool I had always been afraid of: MATLAB. You know you will always be my example to follow, because, as I say: “no matter where I go, I will never meet anyone as intelligent and magnificent as Roberto”. Thank you very much for your patience, for your fast responses to my annoying questions at the wrong time (even when you were busy), and for your efforts on keeping me calmed when things were not going as I expected. You always pushed me to discover my abilities, and that is the reason why I can now say that, more than just my co-supervisor, you are a real friend I am taking from Norway.

Furthermore, I want to thank all the friends I have made in Trondheim, for having been there when I really needed to get my head away from work and for having made each one of my hardest days a bit better. This gratitude is specially directed to John, Edvard, Rubén, Jairo, Tina, and obviously to my Spanish crew from Moholt. I will never forget you and I really hope our paths can cross soon again. Having a home in so many different parts of the world is something I cannot express with words.

To my parents and sister, for having supported me with their understanding, even from the distance, and for having given me the chance of living the student experience abroad, making a big effort to make sure I could fulfill my dreams. Thanks for not letting me underestimate myself, and for making each one of my less important successes your biggest pride. You made me fly without wings.

Finally, to my grandparents. I really hope you are proud of me wherever you are.

Contents

List of figures

List of tables

Nomenclature

C_{BM}	Bare module equivalent cost	[$]
c_p	Specific heat	[J/(kg·K)]
C_P	Basic cost	[$]
d_e	Equivalent diameter	[m]
d_h	Hydraulic diameter	[m]
$\dot{E}$	Exergy flow rate	[W]
F_{bm}	Aggregate multiplying factor	[-]
F_m/F_p	Multiplying factors	[-]
h_{lg}	Enthalpy of vaporization	[-]
$\dot{I}$	Rate of exergy destruction	[W/K]
$\dot{m}$	Mass flow rate	[kg/s]
p_r	Reduced pressure	[Pa/Pa]
$\dot{q}$	Heat flux	[W/m^2]
$\dot{Q}$	Heat flow rate	[W]
$\dot{V}$	Volume flow rate	[m^3/s]
$\dot{W}$	Power	[W]
A	Area	[m]
Bo	Boiling number	[-]
C	Cost	[$]
CF	Capacity Factor	[m^2] or [W]
d	Diameter	[m]
e	Specific exergy	[J/kg]
E	Energy	[J]
G	Mass velocity / mass flux	[kg/(m^2·s)]
h	Specific enthalpy	[kJ/kg]
k	Thermal conductivity	[W/m·K]
N_S	Stage specific speed	[-]
Nu	Nusselt number	[-]
p	Pressure	[Pa]

PPTD	Pinch Point Temperature Difference	[ºC]
Pr	Prandtl number	[-]
Re	Reynolds number	[-]
s	Specific entropy	[J/kgK]
SIC	Specific Investment Cost	[$/kW]
SP	Size Parameter	[-]
T	Temperature	[ºC]/[K]
u	Velocity	[m/s]
U	Overall heat transfer coefficient	[W/(m^2·K)]
V_R	Volume Ratio	[-]
x	Vapour quality	[-]

Shell-and-tube heat exchanger geometry parameters

A_s	Shell characteristic area	[m^2]
d_e	Equivalent diameter	[m]
d_i	Inside diameter	[m]
d_o	Outlet diameter	[m]
d_s	Shell diameter	[m]
G_s	Shell mass velocity	[kg/(m^2·s)]
L_b	Baffle cut (baffle length)	[m]
L_t	Tube length	[m]
N_b	Number of baffles	[-]
N_p	Number of passes	[-]
N_s	Number of shells	[-]
N_t	Number of tubes	[-]
P_T	Tube-pitch	[m]
B	Baffle spacing	[m]
CL	Tube Layout Constant	[-]
CTP	Tube Count Constant	[-]
t	Thickness	[m]
φ	Tube layout	[º]

Plate heat exchanger geometry parameters

C_h, n, K_p, m	Kumar constants	[-]
L_h / L_w	Plate width	[m]
L_p / L_v	Plate height	[m]
N_{ch}	Number of channels per pass	[-]
N_p	Number of passes	[-]
N_t	Number of plates	[-]
b	Corrugation height	[m]
t	Thickness	[m]
β	Chevron angle	[º]

Greek letters

η_I	First law efficiency	[-]
η_{II}	Second law efficiency	[-]
$\dot{\sigma}$	Rate of entropy generation	[W/K]
f	Friction factor	[-]
α	Convective heat transfer coefficient	[W/(m^2·K)]
β	Chevron angle	[º]
δ	Thickness	[m]
η	Efficiency	[-]
λ	Conductive heat transfer coefficient	[W/(m·K)]
μ	Dynamic viscosity	[kg/(m·s)]
ρ	Density	[kg/m^3]

Subscripts

amb	Ambient
c / cold	Cold
cond	Condenser
crit	Critical

ch	Channel
eq	Equivalent / equality
fl	Fluid
gen	Generator
h / hot	Hot
i	Inside / initial conditions
in	Inlet
ineq	Inequality
l	Liquid
max	Maximum
min	Minimum
o	Outside / dead state (surrounding conditions)
out	Outlet
pp	Pinch point
sat	Saturated
sp	Single-phase
tot	Total
tp	Two-phase
turb	Turbine
v	Vapour
w	Wall
wf	Working fluid

Acronyms

BWR	Back Work Ratio
CEPCI	Chemical Engineering Plant Cost Index
CRC	Capital Recovery Cost
GWP	Global Warming Potential
H.E	Heat Exchanger
HCC	Hydrocarbon
HFC	Hydrofluorocarbon

HTC	Heat Transfer Coefficient
lb	Lower bound
LCOE	Levelized Cost of Electricity
LMTD	Logarithmic Mean Temperature Difference
O&M	Operation and Maintenance
ODP	Ozone Depletion Potential
ORC	Organic Rankine Cycle
PrHE	Primary heat exchanger
SCP	Specific Cost of the Plant
SIC	Specific Investment Cost
TIT	Turbine Inlet Temperature
ub	Upper bound

Acronyms for the heat exchanger configurations

Acronym	*Type of primary heat exchanger*	*Type of condenser*
PP	Plate	Plate
PS	Plate	Shell-and-tube
SP	Shell-and-tube	Plate
SS	Shell-and-tube	Shell-and-tube

1 Introduction

1.1 Project background

With the increasing concern on environmental problems, more and more renewable energy resources are being installed and big efforts are being put on their development. Nowadays, in large stationary power generation scale, natural gas and coal fueled gas cycles and vapour cycles play a dominant role [1]. However, the renewable energy boom has led to the need of developing new technologies for power production, as vapour and gas cycles are not a technical nor an economical viable solution when the temperature available from the heat source is low, which may be the case for certain renewable energy sources such as biomass energy, solar energy or geothermal energy.

Among the listed renewable energy sources, geothermal energy shows a promising future, since it has advantages that none of the rest can provide. These advantages are related to its availability and stability, and to the fact that it does not depend on ambient conditions, offering the possibility of renewable energy base-load operation [1]. Being able to make the most of these advantages is one of the principal goals of new research studies, mainly focused on the investigation and development of Organic Rankine Cycles (ORCs), the primary technology that is used to produce power from low-temperature heat sources.

1.2 Motivation

During the last years, ORC technology has become a strong player in the market, showing a promising future in the renewable energy power production. Improving the performance and decreasing the cost of these systems has become one of the most demanding activities for engineers and researchers.

With this aim, from January to June (2017), I worked on a project related to the thermodynamic optimization of Rankine cycles, reaching results that included fluid selection, cycle layout choices or the influence of the pump and turbine efficiencies on

the overall performance, among others. As a fruit of the labor, professor Lars O. Nord, PhD candidate Roberto Agromayor, and I, published a conference paper (see [2]).

After this project, I came to the conclusion that the thermodynamic assessment alone is not an exhaustive indicator of the optimal configuration of a Rankine cycle, mainly because every working fluid presents different properties, which have a great influence not only on the performance of the cycle, but also on its size and, therefore, on its cost [3]. In order to provide the right assessment of a Rankine cycle project, the optimization process must include both a thermodynamic and techno-economic analysis.

1.3 Objectives of the work

The objectives of this project are:

1. Perform a literature review on the design of Rankine cycles components, heat transfer correlations, cost correlations, working fluids and cycle layouts for a varying geothermal heat source.
2. Develop a MATLAB program able to execute the steady-state cycle optimization of the Specific Investment Cost and the second-law efficiency by computing all cost, heat transfer and pressure drop correlations, as well as all thermodynamic states of the cycle.
3. Validate the model.
4. Select a case study and execute the Specific Investment Cost cycle optimization for different heat exchanger configurations and working fluids.
5. Select the most suitable heat exchanger configuration and a set of working fluids, and compare the thermodynamic and techno-economic optimization results for different heat source and heat sink scenarios.
6. Generalize the results.

An assessment of the accomplishment of these objectives is presented in Section 11.3.

1.4 Risk Assessment

This work is purely theoretical and no risk assessment was required.

1.5 Organization

The project has been divided in 11 chapters:

The first two chapters constitute an introduction to Organic Rankine Cycles, which includes a brief description to their development through history and their current situation in the market, a technical overview of the different configurations and layouts that can be implemented, and a general description of the main components that are part of the cycle. After having introduced the theoretical basis, Chapter 4 presents the heat exchanger geometry parameters and design considerations that are required for reckoning these components. Chapter 5 includes the thermodynamic fundamentals that allow to compute all the thermodynamic states of the cycle and to define the thermodynamic objective function. The definition of all heat transfer coefficients and pressure drop correlations can be found in Chapter 6, while cost correlations are included in Chapter 7, digging into depth in the basis behind all calculations, and leading to the definition of the techno-economic objective function. Chapter 8 introduces the optimization process, including the methodology for the selection of degrees of freedom and constraints, the objective functions and the different algorithms that may be used in the simulations. Chapter 9 presents the starting case study, accompanied by the assumptions and boundary conditions, and the implemented degrees of freedom, constraints, optimization algorithm, etcetera. Chapter 10 addresses the challenges related to the model validation, and includes the obtained results and their discussion, leading to the final conclusions and suggested further work presented in Chapter 11. Finally, some of the most important and complex concepts have been included in a glossary, and a final section of appendixes provides some extra information that might help to understand the theory behind this work and to support the presented results.

1.6 Limitations

The main limitation of this work was the impossibility of carrying out the model validation. In order to compute the cycle and to reach the desired results, many different cost, heat transfer coefficient and pressure drop correlations needed to be implemented in the model. This implied having to resort to a great amount of different literature sources and to combine correlations from different authors (as none of them covers all the aspects we did at the same time). For this reason, when trying to execute the validation process, no model including the same correlations as the ones we had chosen could be found. Furthermore, authors do not provide all information nor data related to assumptions, design of heat exchangers nor boundary conditions for their developed models, making it not possible to compute the same cycle conditions and hence, to compare the obtained results. The validation challenges will be further treated in Section 10.1.

Although studying transcritical Rankine cycles would have been of interest, the field is still under research, and no accurate heat transfer coefficient correlations nor pressure drop formulas that could be applied to compute this kind of cycles could be found in open literature. The omission of transcritical cycles is then the second limitation of this work, and it will be further addressed in Section 3.3.2.

2 The Organic Rankine Cycle: a historical and market approach

The increasing number of studies focused on the development of the ORC technology has led to the achievement of a better performance of power generation from low-temperature heat sources. For this reason, ORCs are winning more and more significance in the electricity market, as more companies are interested on investing in new promising alternative ways of producing electricity against the most conventional, but still environmentally harmful, carbon fueled power cycles.

Even though ORCs current technology progress tendency seems to be defined, there is still a lack of information about their future development in the market. How has this technology developed through the last years? Which global factors have motivated its arrival to the electricity market? What are the expectations for the next years? Will the installed ORC capacity increase? In order to answer these questions, an introduction to the development of ORCs over time and an overview of their current situation in the electricity market are presented in this chapter.

2.1 A brief introduction to ORCs history

Since 1970, the ORC technology has considerably developed, mainly because of the economic incentives and the explosion of energy prices [4]. However, considering the wide range of applications it encompasses, and the great number of manufacturing companies and countries that are backing their integration into the electricity market, determining the tendency of its acceptance and development in the market through the last years is not simple.

The theoretical basis that defines the performance of ORCs was established in 1826 by T. Howard, who used ether as the working fluid for its power cycle model. Some launches engines were constructed based on his idea, but due to the numerous number of accidents they were involved in, ORCs development reached a halt [5]. It was not until 1936 when

D'Amelio developed the first ORC, using monochloroethane as the cycle working fluid. From then on, many investigators applied the same ideas for a couple of low-temperature geothermal heat source power plants. However, not too many companies were willing to invest their capital in such a new technology, due to the uncertainty of its market development and payback period [1].

The founding of ORMAT (in 1964) [4] and Turboden (in 1970) [4] hastened the development of ORCs. These companies highly promoted the study of the technology with large investments, and, since then, many institutions have focused their attention on it. During the last years, new companies have been set up, developing their own technology and proposing innovative configurations. This reflects the dynamics of the industry. Nowadays, ORMAT, Turboden and Exergy are leading the market (the former owns 62.9% of the total installed capacity, while Turboden and Exergy together own a 11.1%) [4]. They expect a great future forecast thanks to their strong connection with academic research [4].

The ORC potential for the conversion of thermal energy coming from renewable sources is large. What is more, the ORC technology is possibly the most flexible one in terms of capacity and temperature levels. For this reason, academic research is interested and focused on its further development [6]. Institutions such as Naples University, The National Physical Laboratory of Israel, Politecnico de Milano and Lappeenranta University of Technology, have put big efforts on improving the performance of ORCs, and have contributed to their development through studies related to fluid selection, more efficient turbines and the use of this technology in the automotive industry and aerospace, among others [1].

2.2 ORC market current situation

One of the main problems related to the promotion of ORCs in the electricity market is that the current number of installed power plants and cycles based on this technology is uncertain [4]. This provokes that local governments cannot foster their development as a

solution to the environmental problems related to the carbon fueled power cycles, as no suitable data can support the great investments they require [4].

In order to cooperate to solve this problem, T. Tartière and M. Astolfi [4] collected information related to the installed ORC capacity from 1975 up to the present, creating the first reliable data-base that can be used to predict the development of the market based on its historical trend. Figure 1 shows a plot of the results they obtained through their research[1].

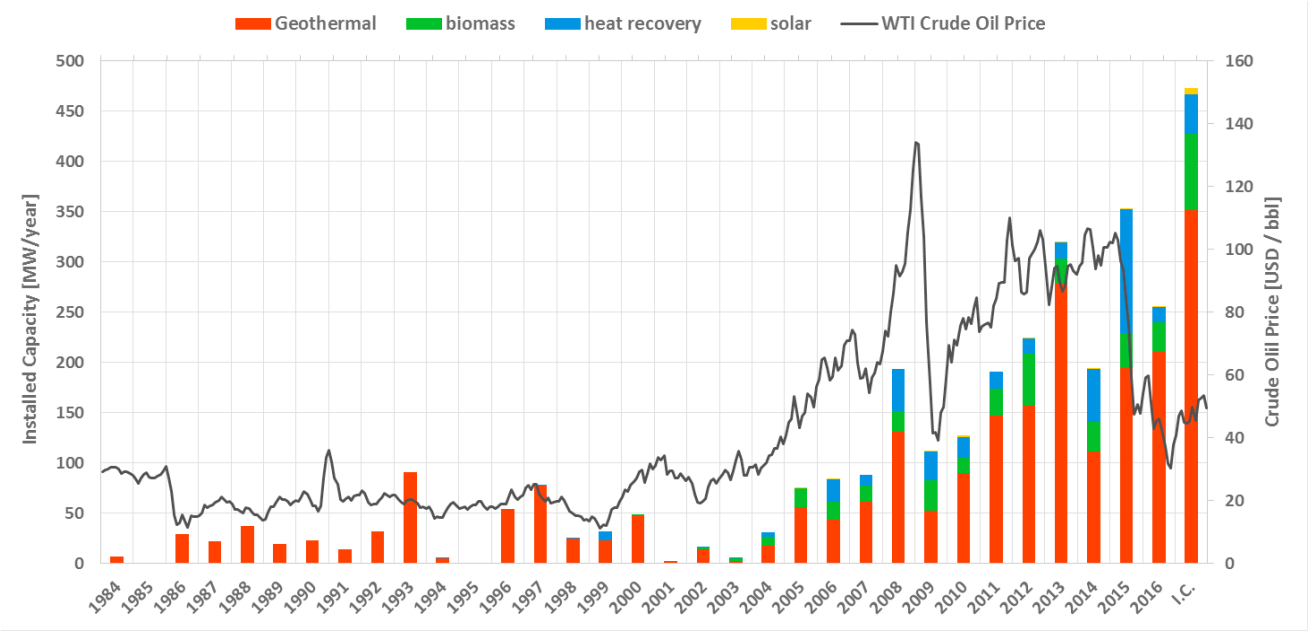

Figure 1. Installed ORC capacity per year and application [4]

As it can be seen in Figure 1, ORCs can use biomass combustion, geothermal reservoirs, waste heat recovery or thermal-solar energy as the cycle heat source, reflecting that this technology can take advantage of the less conventional renewable energy sources, making them even more attractive in the power production industry. From 2009 on, the geothermal energy exploitation by ORCs experienced an important growth, being

[1] The given data is not 100% accurate, as some manufacturers refused to provide information related to their projects to limit competitors' advantages.

coincident with the entrance of companies such as Exergy or TAS in the market [4]. These companies made significant investments on geothermal ORCs, seeing them as a safe bet.

The dominant role that geothermal energy has among the rest of heat recovery energy sources implies that countries with the largest geothermal reservoirs have the greatest share of the total installed capacity. These are: USA, Turkey and New Zealand. Other countries, such as Germany, Canada, Australia or Italy, bet for the biomass combustion, mainly because of the high incentives they receive for promoting the use of this energy source [4].

By the end of 2016, the ORC installed capacity represented 2701 MW of the world installed capacity. From that power, approximately 74.8% was produced from geothermal energy reservoirs, while the share of thermal-solar energy power production was so low that it could be neglected [4]. This tendency has been the same through years, and future predictions state that it is not going to change. What is more, the application of the ORC technology in combination with solar power is currently without any precedent in some countries such as United Kingdom [7], while, in others such as India, it is limited to some pilot projects or laboratory scale researches [8]. The main reason is that the installation costs for using solar energy in combination with ORCs are high, and installing photovoltaic panels with batteries is still a more viable solution for investors [4].

So far, most of the developed ORC projects have been focused on the construction of large-scale power plants (from 15 MW to 20 MW), although during the last years more and more small-scale power plants are being installed [4]. The normal price for a large-scale system is between 1410 $/kW [9] and 1580 $/kW [10], while small ORC systems (including cycles with less than 500 kW power outputs) have a much higher cost per produced kW [4].

It is predicted that the installed capacity is going to increase more than 460 MW by 2017 [4]. A few large projects have already been announced, and others are already under construction. At the same time, more and more countries are promoting energy efficiency initiatives through institutional set up to help to proliferate the development of the ORC technology, in an effort to mitigate the climate change [11].

3 Rankine power cycle description

The fundamentals of ORCs are the same as the ones of conventional steam Rankine cycles, with the only difference that, instead of using H_2O as the working fluid, organic working fluids are employed. A detailed explanation of the functioning of Organic Rankine Cycles, a brief introduction to the cycle components and, finally, a description of the most common ORC configurations and layouts are presented in this chapter.

3.1 Why organic working fluids?

Historically, the preferred methods for power production have been related to Gas Brayton or Steam Rankine power cycles, fueled by natural gas or other fossil fuels. These power cycles are linked to high-temperature heat sources, allowing for high thermal efficiencies. However, the development of renewable energies such as solar, biomass or geothermal energy during the last years, has introduced the difficulty of producing power at high efficiencies from the most conventional power cycles, due to the low-medium temperatures these new heat sources provide [1]. At this point, ORCs gain importance, since, as E. Macchi, M. Astolfi et al. stated in [1]:

"ORCs are the unrivalled technical solution for generating electricity from low-medium temperature heat sources of limited capacity".

The use of air/gas when the maximum temperature of the cycle is below 250 ºC / 400 ºC is hardly recommended because of the poor system performance. What is more, for temperatures below 250 ºC, the efficiency of the cycle can reach negative values, as the compression work is too high in comparison with the power that is produced in the expander [1]. The main advantages to take into consideration when comparing Rankine cycles with Brayton cycles for low-temperature heat recovery applications are related to the considerably lower compression work that Rankine cycles require, as the compression is carried out in the liquid phase in the formers [1].

The previously given reasons prevent the use of Brayton cycles for power production from low-medium temperature heat sources in detriment of Rankine cycles, but this does not explain why organic fluids are a better choice than water for running this kind of cycles. The reason is related to the three main constraints that water presents when it is used as the Rankine cycle working fluid [1]:

- Its thermodynamic properties make the use of multi-stage expansion necessary. As a consequence, turbines are expensive and the plant configuration is complex.
- The low maximum cycle temperature limits the degree of super-heating, meaning that the power output is also restricted.
- As water is a wet fluid, its vapor saturation curve in the T-s diagram has a negative slope, which means that the expansion is limited to an enthalpy drop that avoids entering the two-phase region, which may lead to droplet condensation and blade deterioration.

Also, for low power outputs (from few kW to few MW) the design of the steam expander is challenging, as the working fluid mass flow is small in comparison with the large expansion ratios it has to deal with. Under these conditions, lubrication is an issue, since water cannot effectively lubricate the contact surfaces in the expander, and important friction losses and blow-by may occur. One solution to this problem is to mix the water with lubricant, but this leads to cycle efficiency drops. Furthermore, the oil may suffer thermal decomposition if high temperatures are reached in the primary heat exchanger (PrHE) [6].

Considering that organic working fluids present lower critical pressures than water, they allow to work at lower evaporation and condensing temperatures. This thermodynamic advantage reduces the need of super-heating and guarantees “dry” expansion. Figure 2 shows in three different T-s diagrams the expansion processes for an isentropic, dry and wet fluid when the fluid conditions right before the expansion are saturated (1) or super-heated (1’). As it can be seen, the negative slope of the vapor saturation curve for wet fluids (water) makes the super-heating a requirement to avoid condensation during the

expansion. For isentropic working fluids, the degree of super-heating is not a requirement to guarantee that only vapour is presented after the expansion. Finally, dry fluids present a positive slope of the curve, meaning that, as it happened with isentropic working fluids, super-heating is not demanded to avoid problems in the turbine. However, dry fluids experience lower enthalpy drops through the expander as the degree of super-heating increases, since the constant pressure lines tend to approach each other as temperature increases. These lower enthalpy drops imply lower power outputs and higher temperatures at the outlet of the expander (a waste of heat which leads to greater cooling loads). This is the reason why some researches (see [1, 12, 13, 14] and [15]) hardly recommend high degrees of super-heating when the working fluid is "too dry", as it does not provide any cycle performance improvement, unless the surplus heat is used in a recuperator unit to preheat the fluid at the inlet of the primary heat exchanger.

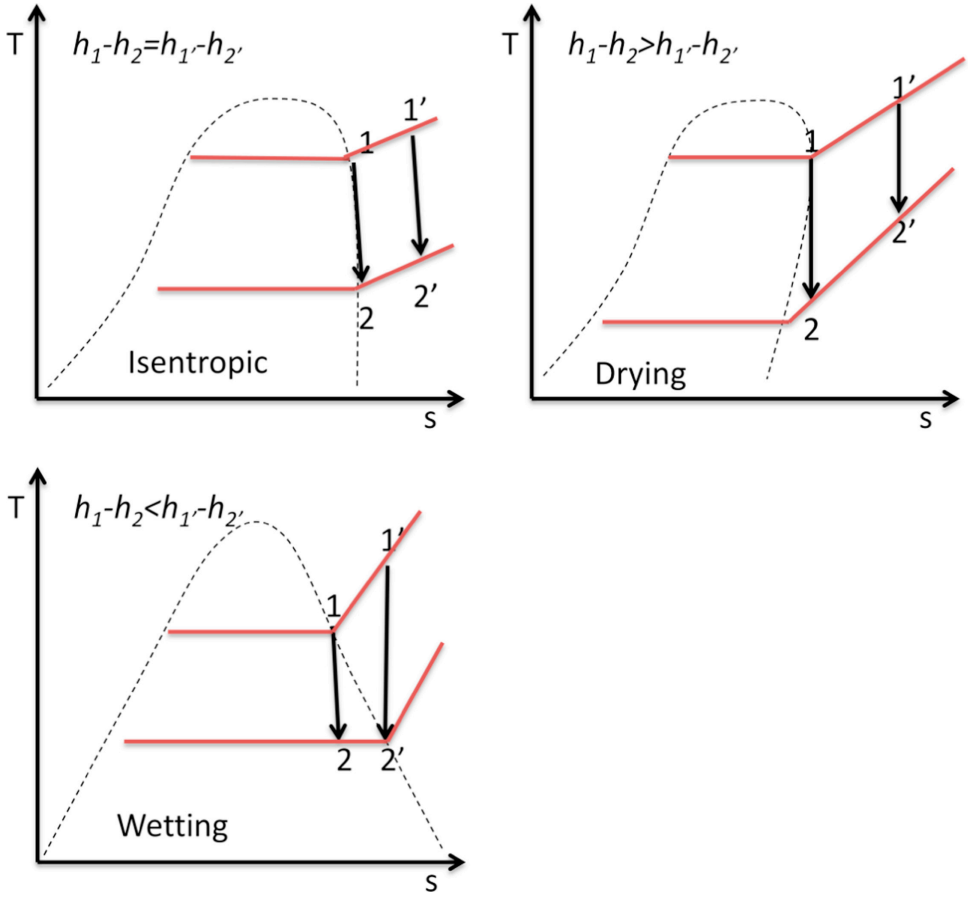

Figure 2. Expansion processes for isentropic, dry, and wet working fluids [12]

3.2 Cycle description and possible layouts

The most elementary ORC is the simple Rankine cycle, whose layout can be seen in Figure 3. It is a closed thermodynamic cycle, compound of four main components: the primary heat exchanger, the expander, the condenser and the pump. Starting from 4, the working fluid enters the primary heat exchanger in the liquid phase, where it absorbs heat from the hot source, being pre-heated, evaporated and, in some cases, super-heated. Once all the working fluid is in the vapour phase (5), it enters the expander component, normally a turbine, where it generates mechanical work while being expanded. This mechanical work is transformed into electric power by means of a generator. The working fluid may leave the expander (6) in a single-phase or two-phase state, depending on the amount of liquid content the turbine can handle without suffering blade erosion that may deteriorate its functioning. Then, it flows to the condenser, where the surplus heat is rejected and the working fluid is pre-cooled, condensed and, sometimes, further sub-cooled. Finally, the liquid working fluid is pumped back from 3 to the primary heat exchanger, closing the loop.

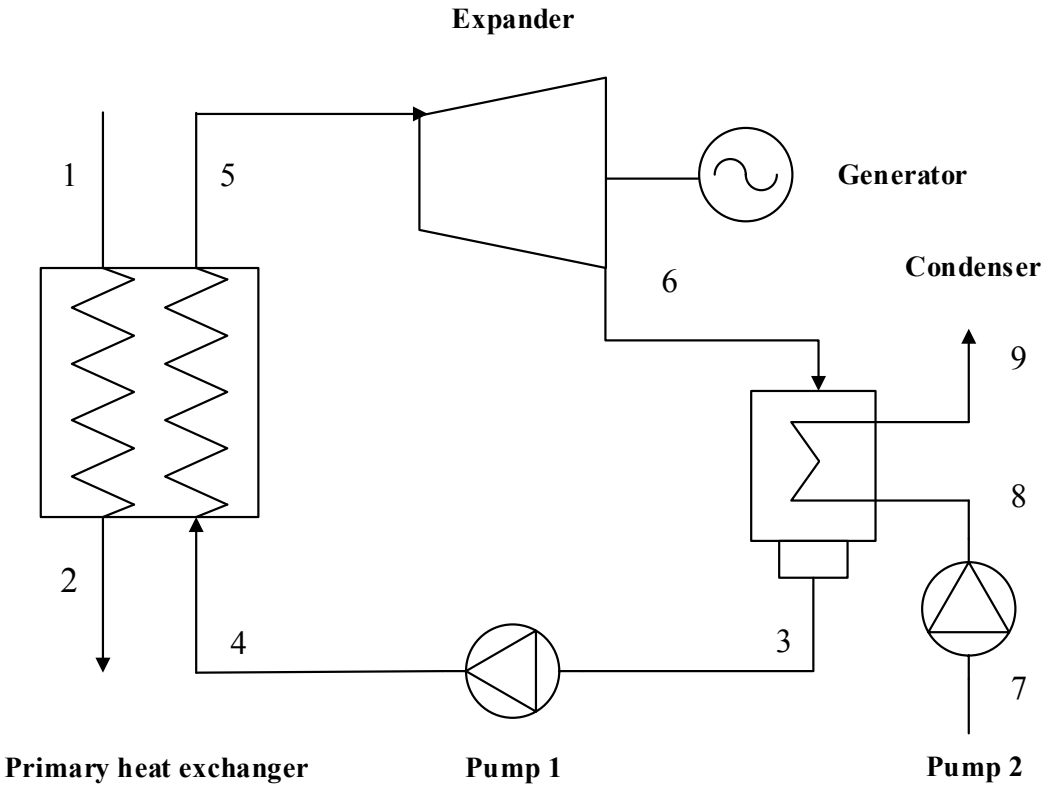

Figure 3. Simple ORC layout

Organic Rankine Cycles are characterized for having a flexible design, meaning that different innovative layouts can be implemented in an effort to improve the performance of the cycle. For example, using multiple pressure levels may lead to better temperature matches in the primary heat exchanger; reheating can increase the system power production while guaranteeing that condensation is avoided during the expansion; regeneration allows to make the most of the working fluid surplus heat at the outlet of the expander, among other alternatives. However, multiple pressure levels also require much more complex control systems and higher investment costs due to the larger heat transfer surfaces they entail, which are not justified in all cases [16]. Reheating does also require great investments, and, considering the nature of organic working fluids, super-heating the vapour to avoid condensation during the expansion is not necessary [17]. Finally, regeneration can be a good choice for increasing the efficiency of the system, although, as I. Encabo et al. [2] concluded after comparing both simple and regenerated cycles for a wide range of different working fluids, an economic analysis must also accompany the results to justify the implementation of this ORC layout.

Bearing in mind the last mentioned considerations and the objectives of the work, only the simplest layout will be considered in this project[2].

3.3 Cycle configurations

Organic Rankine Cycles flexibility does not simply lie on the different cycle layouts that can be implemented, but also on the different configurations we can find for each cycle layout. These include: subcritical cycles (saturated or super-heated) and transcritical cycles.

[2] B. Saleh et al. [15] stated that the thermodynamic ORC improvement related to the installation of a recuperator unit is low when compared to the extra cost it requires. Also, L. Tocci et al. advised in [22] that the simplest cycle layout is the best ORC choice when the aim is to minimize the cost. These assertions do also support the decision of excluding the study of a recuperated ORC from the scope of the work.

3.3.1 Subcritical cycles

This cycle configuration is characterized by the isothermal phase change during the evaporation. It compromises two different configurations: if the working fluid is saturated vapour at the outlet of the primary heat exchanger, the cycle is called “subcritical saturated cycle”, while, if the vapour enters the turbine as super-heated vapour, the cycle is then a “subcritical super-heated cycle”.

A great limitation that subcritical Organic Rankine Cycles have is that the isothermal evaporation provokes a high exergy destruction during the heat exchange process due to temperature differences. Some solutions to this problem were proposed by A. Schuster et al. [18], who suggested to work with transcritical cycles, or F. Haberle et al. [19], who studied the use of mixtures to avoid the isothermal evaporation and to improve the match between temperature profiles.

3.3.2 Transcritical cycles

Transcritical cycles main characteristic is that the heat addition from the hot source to the working fluid takes place at a pressure that is above the critical pressure of the working fluid. Therefore, the working fluid is heated up in a gliding temperature with a continuous phase change [17].

The principal advantage that this configuration has is that the gliding temperature profile of the working fluid allows for a much better temperature match with the heat source, and this leads to better heat transfer processes that result into higher thermal efficiencies. However, working under transcritical conditions does also imply increased power consumptions to pump the liquid fluid from the condensing pressure up to the transcritical one. This higher power consumption is dependent on the type of working fluid that is used in the cycle, as it can be neglected in some cases (for high molecular mass working fluids) or, on the other side, account for a big share of the produced power (for low molecular mass working fluids) [2].

Even though many research studies are focused on the development of transcritical cycles, their use in the industry is almost non-existing. Nowadays, only 4 projects are being run (3 of them in USA and another one in Italy) [4]. The reason is that it does not seem to be an attractive economic investment, as the higher efficiencies that can be achieved do not make up for the higher costs that working at high pressures entails [4]. Furthermore, high operating pressures require the use of more resistant materials and more complex pumps, which lead to higher investment costs.

One of the main challenges that transcritical cycles present is that the analysis of the heat transfer processes requires the study of 5 different flow regimes (Deteriorated Heat Transfer, Improved Heat Transfer, Normal Heat Transfer, Pseudo-Boiling and Pseudo-Film Boiling), which may cause the heat transfer coefficient to increase or dramatically deteriorate [20]. As experiments at supercritical pressures are very expensive, companies do not publish their results, leading to a lack of information in the open literature. All the transcritical heat transfer correlations that can be found in the literature are based on experimental data, with the drawback that they are only accurate within a particular data set. Some authors claim that the already existing correlations are not always precise, and they may show deviations up to $\pm$ 30% [20]. I. L. Pioro et al. [21] compared some of the already existing correlations, finding great differences between the obtained heat transfer coefficients values and concluding that no correlation can predict in a correct way the magnitude of the heat transfer coefficients for transcritical working fluids. Furthermore, the lack of equations is not just a problem when it comes to calculate the heat transfer coefficients at supercritical conditions, but also when calculating the pressure drops in the system heat exchangers. No satisfactory analytical nor numerical method has yet been developed, because of the difficulty of dealing with the severe variations of the working fluid properties at supercritical pressures.

For these reasons, transcritical cycles have not been considered in this work, as no enough information required for the simulations is available in the open literature.

3.4 ORC system components

Once the ORC has been presented as a whole, delving into the components that are part of it becomes necessary to guarantee the right design of the cycle depending on its applications and specifications. Considering the size of the technology market, this chapter is of special importance to determine the most suitable types of components for this work and to discard those ones that would not guarantee a good performance of the cycle.

3.4.1 Expander

Choosing the right expander is vital when designing an ORC, since it determines the power plant power output. There is a wide range of different prototypes and models in the market, and the selecting decision is directly linked to the size of the power plant and working fluid properties.

We can divide expanders in two main categories:

- Volumetric expanders: These positive displacement expanders are used in small-capacity ORCs [1]. In this type of machines, a fixed volume of fluid is trapped, expanded and discharged in a continuous cycle, transforming the fluid thermal energy into mechanical energy, which is further converted into electric power by means of a generator. Their design is very challenging and they are costlier than turbomachinery [17].

- Turbomachinery: Turbines are compound of a sequence of stators and rotors, each pair of them forming a turbine stage. The fluid is accelerated and expanded in the stator and then it is deflected in the rotor. During this process, the change of momentum of the fluid results into a torque applied to the shaft of the expander. The shaft drives an electrical generator, which transforms the mechanical energy into electrical power. They can be axial turbines, radial inflow turbines or centrifugal turbines [17].

Choosing a non-suitable turbine model for the cycle can cause its performance deterioration. For a power production lower than 20 kW, volumetric expansion turbines are preferred, while, for power productions higher than 70 kW, turbomachinery is a better choice. The reason is that when the power out of the turbine exceeds 70 kW, the rotational velocity decreases, preventing the bearing failure and allowing for the coupling with an electric generator (which is a challenge when velocity is high) [22]. If a volumetric expander wants to be installed in an ORC with a power production higher than 70 kW, it should be considered that greater volumes and sizes are going to be involved, implying higher costs and higher leakage losses (which diminish the plant efficiency). For the 20 kW - 70 kW range, both turbines perform more or less the same way [22].

Therefore, considering that the power outputs we are going to deal with in this work are expected to be higher than 100 kW, the axial turbine is the type of expander that is going to be modelled.

3.4.2 Heat exchangers

Heat exchangers are the ORC components in which the thermal energy transfer processes between the hot source and the working fluid (primary heat exchanger) and between the working fluid and the cold sink (condenser) take place.

Many different heat exchangers can be found in the market, and their design depends on their applications [23]. For Rankine cycles, the heat exchangers are indirect contact heat exchangers, meaning that heat is continuously transferred through a dividing wall, and there is no direct contact between the interacting fluids.

During the design of ORCs, special attention must be given to the design of the heat exchangers, since their cost represents an important share of the total investment of the plant. The types of heat exchangers that are normally preferred for Rankine cycles are shell-and-tube heat exchangers and plate heat exchangers. The formers provide a considerable high flexibility in design because they allow for many different geometries, while the second ones have been recently improved and, nowadays, their design allows for high efficiency condensation processes of high-density vapors such as ammonia,

propylene, and other refrigerants [23]. Both heat exchangers will be modelled in this work.

- Shell-and-tube heat exchanger

This kind of heat exchanger (Figure 4) is built of a bundle of round tubes mounted in a cylindrical shell. One fluid flows through the tubes, and the other one across them, through the shell. As it was before stated, this type of heat exchanger allows for many different designs, depending on the heat duty, pressure drops and corrosion specifications, accommodation of asymmetric flows, etcetera [23]. They allow to work at high pressures and temperatures (up to 100 MPa and 1100 ºC), to operate with heavy fouling (which may be desirable when geothermal water is used as the heat source and fouling effects can damage the heat exchanger), and to use toxic and flammable working fluids [23].

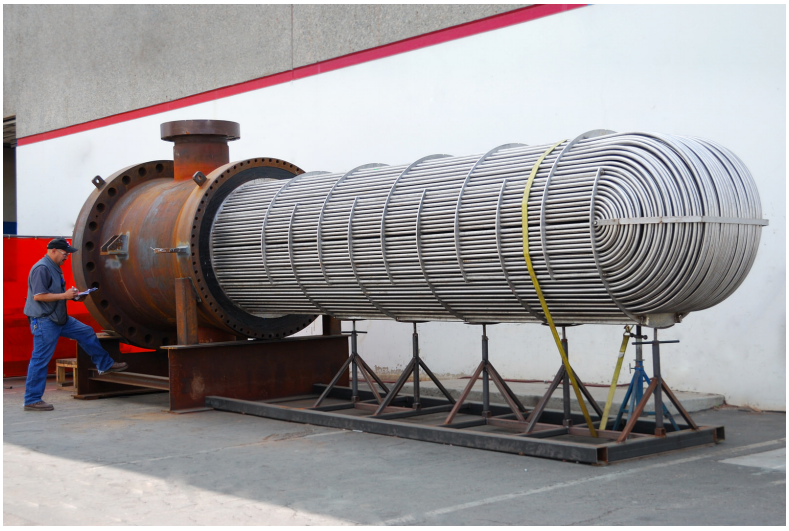

Figure 4. Industrial shell-and-tube heat exchanger [8]

The high-pressure fluid normally flows through the tubes, while the low-pressure fluid flows through the shell [24]. For this reason, in this work, the working fluid will be evaporating and condensing in the tubes while the hot and cold fluids will flow through the shell. Different configurations are also possible.

- Plate heat exchanger

This kind of heat exchanger is built of thin plates, which normally have corrugations or waved surface patterns, sealed with rubber junctions. Apart from avoiding the mixing of the fluids that are exchanging the heat, the rubber junctions stablish the channels through which the fluids flow. All plates are put together and compressed by means of two rigid metallic sheets, allowing for a parallel flow distribution, in which one fluid flows through the even plates and the other one through the odd ones [25] (see Figure 5).

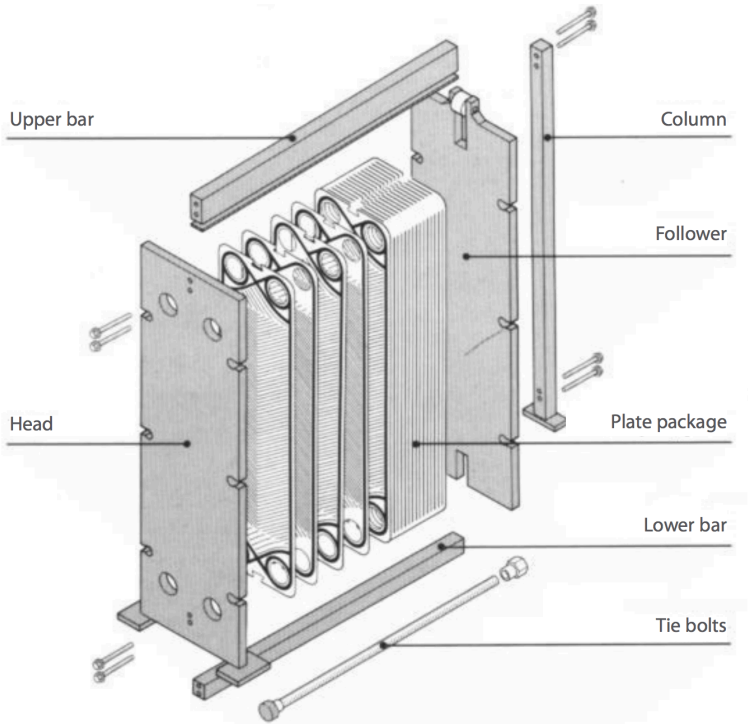

Figure 5. Exploded view of a plate heat exchanger [26]

Plate heat exchangers provide high heat transfer coefficients, which imply compact designs and reduced costs [23]. However, the limitation that plate heat exchangers present is that they do not allow for operating at high pressures (the highest working pressure is established at 3 MPa, although they are normally operated below 1 MPa) [23], neither at high temperatures (the maximum operation temperature is 150 ºC) [23]. For these reasons, they are not commonly used as primary heat exchangers in ORCs. Instead, plate heat exchangers are normally used in applications in which the heat transfer surface needs

to be modified with time, or in those ones that require the use of fluids with high propensity to cause corrosion problems, since their design allows for cleaning[3].

Both described heat exchangers may present different designs depending on the applications they are used for. For example, shell-and-tube heat exchangers admit many different combinations of diameters, lengths and number of tubes to guarantee the achievement of the most efficient heat transfer processes. Also, many shell and tube shapes are available in the market, with a variable number of baffles and nozzles. Regarding plate heat exchangers, the size and number of plates play an important role when designing them, but also the Chevron angle, the packing of the plates, among others. Both heat exchangers do also allow for an advanced modification which includes fins, but this is more expensive and requires more complex designs. A deeper analysis of the geometry design parameters of the presented heat exchangers can be found in Chapter 4.

3.4.3 Pumps

The pumps that are normally used in ORCs are centrifugal, which makes it possible to work at variable velocities and at various number of stages. Depending on the configuration, design of the cycle, operation conditions and kind of fluid, the pumps power consumption can represent a different share of the produced power. When the cycle operates under transcritical conditions, the design of the pumps gets complex, and their efficiency becomes one of the main parameters to optimize to guarantee the best performance of the plant [2].

[3] During the last years, numerous studies have been focused on the development of plate heat exchangers in order to allow for their use at higher operating temperatures and pressures because of the interesting design advantages they provide in comparison with other type of heat exchangers. S. Kakaç et al. already stated in [37] that, in special cases, plate heat exchangers can bare up to 25 bar and 260 ºC. Nowadays, new advanced materials allow for their use in high-temperature applications.

3.4.4 Generator

As the design of the generator is not going to be investigated in this work, we will not focus on its performance and specifications in detail. In spite of this, it is important to point out that cycle turbines are normally operated at the grid frequency; however, when they are used in ORCs, the turbine optimal velocity will be within a wide range of values depending on the working fluid [1]. Normally, in large-scale power plants, turbomachinery shafts rotate at low velocities, and generators can be assembled to them by means of a gear box. However, for low-scale power plants, turbomachinery optimal velocities tend to be much higher, and the generator can be adapted to these velocities up to certain limit (once this limit is exceeded, mechanical losses start increasing in a fast way).

3.4.5 Working fluid

The thermodynamic and transport properties of the working fluid determine the optimal Rankine cycle layout and optimal design of each one of its components. Hence, working fluid properties are closely related to the system cost and the cycle performance.

Choosing the most suitable Rankine cycle working fluid is a complex process, due to the great amount of different working fluids that can be found in the market, which can be further increased if mixtures are also considered [2]. Recognizing the impact of working fluid properties on the design of the cycle is vital to determine which working fluids may lead to the best performance when used in the system, and under which conditions. Not taking into consideration these properties may have a major negative impact on the cost, cycle performance and safety requirements [16]. The main fluid properties that should be analyzed when designing Rankine cycles are:

- Molecular weight: Heavy substances show lower enthalpy drops across the expansion process and lower sound velocities than light working fluids. This implies that turbines operating with heavy fluids can handle the expansion in a reduced number of stages, with lower loads (entailing more compact and cheaper expansion devices) [16].

- Molecular complexity: The higher the working fluid molecular complexity is, the higher the volume ratio becomes for a fixed pressure ratio (hence, more expansion stages are required in the turbine). This is especially important for small and micro ORCs, for the ones the turbine cost represents the greatest share of the overall system cost and less expansion stages are preferred. On the other side, the most complex substances entail dry expansion processes that lead to no liquid problems at all, extending the lifetime of the expander [16].

  The molecular complexity determines whether the fluid is dry, isentropic or wet, which, at the same time, has a great impact on the cost of the plant considering that wet fluids require larger heat exchanger surfaces to reach a sufficiently high degree of super-heating at the inlet of the expander.

- Critical properties: The critical temperature of the working fluid determines the volume and size of the system. High critical temperatures are normally related to large systems dimensions and high costs [16].

Other fluid properties, such as toxicity or flammability, may not have such an important direct impact on the cycle performance and cost, but they must also be analyzed when selecting the Rankine cycle working fluid, as, in case the system experiences a failure, personnel safety must always be guaranteed.

3.4.6 Other components

Other important components that are part of ORCs but whose design is considered out of the scope of this project are the non-condensable gases remover and the instrumentation and piping elements.

Decreasing the condensing pressure can lead to better overall power plant performances, since it entails higher power productions. However, the amount of non-condensable gases presented in the condenser increases when the condensing pressure is reduced, causing a raise of the turbine back-pressure, which leads to poor power generation [1]. Since daerators (components which are normally installed in conventional steam Rankine

cycles) cannot be installed in ORCs because of the environmental and economic problems related to the venting of organic fluids to the atmosphere, non-condensable gases removers need to be used instead. This results into higher investment costs, which may be balanced with the resulting increased power outputs. In order to avoid the use of non-condensable gases removers in this work, a condensing pressure constraint to limit the vacuum in the condenser will be defined.

Regarding the instrumentation and piping of the plant, it represents an important share of the total cost, which can reach values up to 25% - 30% [1]. For this work, it will be assumed that the required piping and control systems are going to be the same for all study cases, meaning that their impact on the results can be neglected when comparing the different simulated scenarios.

4 Heat exchangers geometry

The necessity of designing more and more cost-efficient Rankine cycles has led to a progressively increasing number of research studies focused on the heat exchangers design, with the objective of maximizing the heat transfer effectiveness and, at the same time, reducing their cost. These studies do not only cover the already existing designs, but also analyze and propose new innovative models, such as helical coils heat exchangers [27] or brazed plate heat exchangers [28]. However, as these components are still under development and research, finding suitable and reliable correlations that allow for their computation is not possible yet. For this reason, the most conventional heat exchangers were preferred for this project, since the correlations that are required to study their design can easily be found in the literature.

Most of authors consider that shell-and-tube and plate heat exchangers are the best heat exchanger choices for modelling ORCs ([29, 30, 31, 32], among others). Based on this, we decided to resort to these types of heat exchangers to construct our model.

Once the types of heat exchangers that are going to be implemented in this work have been determined, it is important to analyze the parameters that may affect the heat transfer process effectiveness and their related cost. Therefore, studying the heat exchangers geometry is a key step to take when the performance and/or overall cost of Rankine cycles wants to be optimized. The main geometry parameters of the selected heat exchangers are presented in this chapter.

4.1 Shell-and-tube heat exchanger

Figure 6 shows the simplest layout for a shell-and-tube heat exchanger. Its main components are the shell, the tubes and the baffles. Their geometry specifications can be found in the literature, which are normally given by the manufacturers as a range of maximum and minimum standardized values (see Table 1).

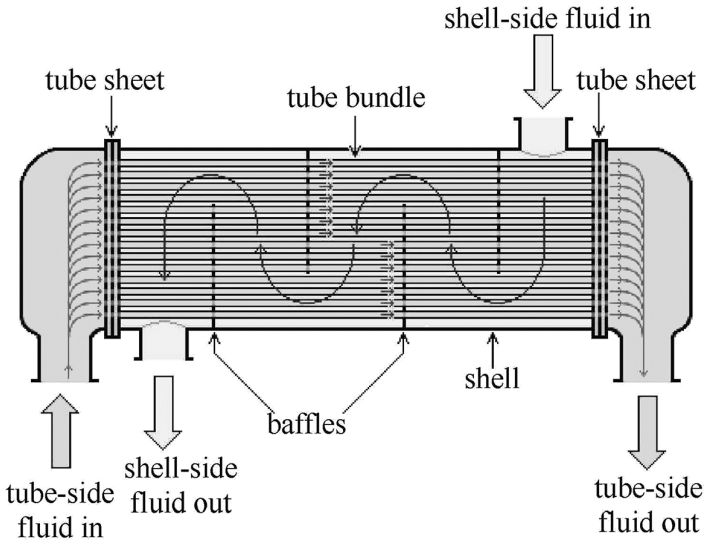

Figure 6. Shell-and-tube heat exchanger with one shell pass [33]

The number of tube passes in the shell depends on the type of shell-and-tube heat exchanger. The Tubular Exchanger Manufacturers Association (TEMA) is a set of standards that defines the heat exchanger style by means of a designated system of notations that corresponds to the different kinds of available front heads, shell types and rear heads [34]. From all the mechanical configurations that TEMA allows to build, only the E-Type shell is suitable for most duties and applications. For this reason, this type of shell is the most commonly used in industry applications [35]. Following the advices, the shell-and-tube heat exchanger simulated in this work will also be an E-Type shell.

Table 1. Geometry and operating considerations for the shell-and-tube heat exchanger design [36, 37, 38]

Parameter	**Lower boundary**	**Upper boundary**
d_o	3.5 cm	51 cm
t	3 mm	15 mm
u_{tube}	0.9 m/s	2.6 m/s
P_T	$1.25 \cdot d_o$	$1.5 \cdot d_o$
D_s	$1/15 \cdot L_t$	$1/5 \cdot L_t$
B	$0.4 \cdot d_s$	$0.6 \cdot d_s$
L_b	$0.25 \cdot d_s$	$0.35 \cdot d_s$
N_p	1	-

The tube layout (φ) can take values of 30º (triangular pitch) or 90º (square pitch). Figure 7 shows the cross section of the shell-and-tube heat exchanger for these two tube layouts.

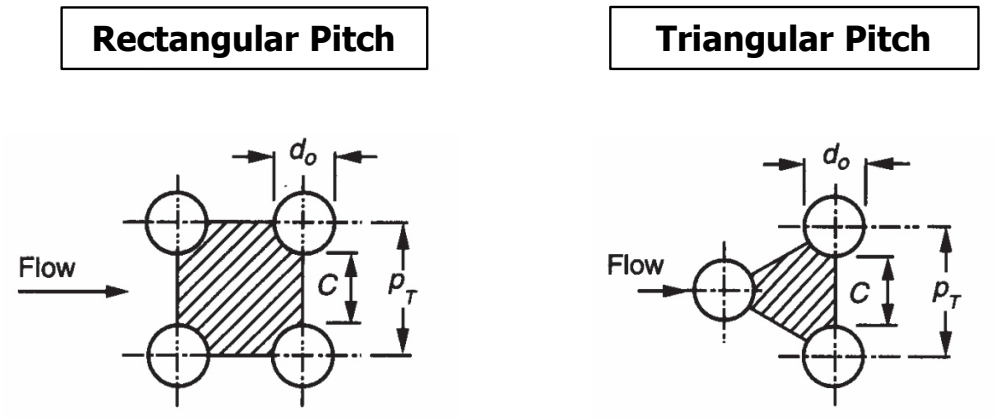

Figure 7. Square and triangular tube layouts [39]

From all parameters given in Table 1, the required number of tubes can be calculated:

$$N_T = 4 \cdot \frac{\dot{m}_{wf} \cdot N_p}{u_{tube} \cdot \rho_{wf} \cdot d_i^2 \cdot \pi} \qquad (4.1)$$

Where the inside diameter (d_i) can be obtained from:

$$d_i = d_o - 2 \cdot t \qquad (4.2)$$

Once the number of tubes is known, it is possible to determine the shell diameter as follows [37]:

$$D_s = \sqrt{\frac{4 \cdot N_t \cdot \mathrm{CL} \cdot {P_T}^2}{\pi \cdot \mathrm{CTP}}} \qquad (4.3)$$

Where CTP is the Tube Count Constant, which accounts for the clearance space between the shell and tubes, and depends on the number of passes [37]:

$$\text{CTP} = \begin{cases} 0.93\ (1\ \text{pass}) \\ 0.9\ (2\ \text{passes}) \\ 0.85\ (3\ \text{passes}) \end{cases} \qquad (4.4)$$

And CL takes into consideration the tube layout [37]:

$$\text{CL} = \begin{cases} 1\ (\text{for the rectangular pitch}) \\ 0.87\ (\text{for the triangular pitch}) \end{cases} \qquad (4.5)$$

Both the baffle length and the space between baffles are directly related to the shell diameter through constant values given from design (see Table 1).

Finally, the number of baffles can easily be calculated from the distance between baffles and the tube length:

$$N_b = \frac{L_t}{\text{B}} - 1 \qquad (4.6)$$

Normally, calculating the number of baffles yields to non-integer values, so it has to be approached to the next integer (not to the closest one). For this reason, once the number of baffles is obtained and corrected, the distance between baffles must be re-calculated.

The shell-and-tube heat transfer area can be calculated as a function of the heat exchanger geometry parameters:

$$A = N_s \cdot N_t \cdot \pi \cdot d_o \cdot L_t \qquad (4.7)$$

4.2 Plate heat exchanger

Plate heat exchangers geometry allows for an infinite number of different models and sizes that may make it hard to determine their optimum design, although manufacturing standardized values can be used to stablish geometry boundaries that may simplify the

problem. Available commercialized plate designs and their operating limits can be seen in Table 2.

Table 2. Geometry and operating considerations for the plate heat exchanger design [37]

Parameter	**Lower boundary**	**Upper boundary**
t	0.5 mm	1.2 mm
$\dot{V}_{ch}$	$1.4 \cdot 10^{-4}$ m^3/s	$3.5 \cdot 10^{-3}$ m^3/s
b	2 mm	5 mm
L_h	0.5 m	3.5 m
β	25º	70º

There are different types of plate patterns depending on the shape of their corrugations, although the most conventional ones are Chevron plates [25] (see Figure 8). Chevron plates present corrugations that are oriented with certain angle with respect to the flow direction, entailing the existence of contact points between plates (which improve the mixing of streams and increase the turbulence level). The transition to turbulent flow has a major impact when determining the H.E heat transfer coefficient, which improves with the increasing turbulence [25]. However, this is normally accompanied by greater fluid pressure drops. Therefore, determining the optimum value of the Chevron angle is important to guarantee a good balance between the heat transfer efficiency and the pressure drop.

The main limitation with respect to plate heat exchangers dimensions are defined by the maximum and minimum pressures and temperatures the plates can bear (see Section 3.4.2).

Setting the optimum plate corrugation height is also important, since it determines the hydraulic diameter, which has a great influence on the calculations of the heat transfer coefficients and pressure drops[4].

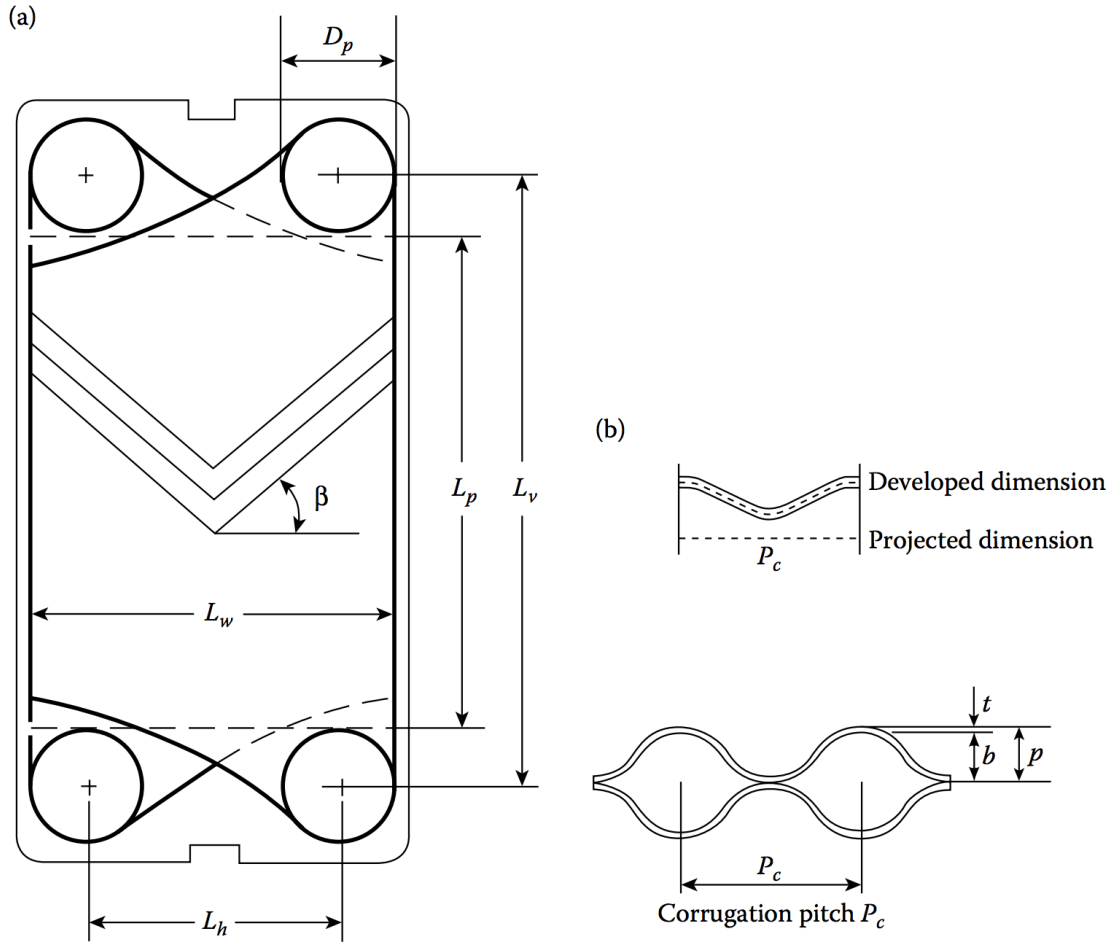

Figure 8. *Basic geometric characteristics of a Chevron plate*[5] *(a) and developed and projected dimensions of a Chevron plate cross-section (b) [37]*

[4] Sometimes, the hydraulic diameter is calculated as the relationship between the corrugation height and the increased area factor. This area factor is the existing relationship between the real heat exchange surface of the plate and the projection of the plate in a parallel plane. Considering that the value of this parameter is close to 1, we will assume (for simplicity) that the real heat exchange surface and the projected area are the same.

[5] We are going to consider that the effective plate height and width are the same as the total plate height and width (plate ports are neglected) in order to simplify the calculations.

The number of channels per pass can be calculated by relating the fluid mass flow with the volume flow per channel:

$$N_{ch} = \frac{\dot{m}}{\rho \cdot \dot{V}_{ch}} \qquad (4.8)$$

Considering that all plates must be designed with the same number of channels, it is important to apply Equation 4.8 to both fluids that are interfering in the heat transfer process, in order to make sure that both of them fulfill the volume flow limits specifications given in Table 2.

Once the right number of channels per pass has been determined, the number of plates can be obtained as [37]:

$$N_t = 2 \cdot N_{ch} \cdot N_p + 1 \qquad (4.9)$$

Where the integer "2" is included in the formula considering that only half of the plates are destined for each working fluid.

From all calculated geometry parameters, the heat transfer area of the plate heat exchanger can be calculated as:

$$A = L_p \cdot L_h \cdot N_t \qquad (4.10)$$

5 Thermodynamic fundamentals

In this chapter, the thermodynamic basis that is required for the cycle simulation is going to be presented. These thermodynamic fundamentals are essential not only for computing and solving all states of the cycle, but also for defining the thermodynamic objective function, which is also introduced in this chapter.

5.1 First and second laws of thermodynamics

The first and second laws of thermodynamics for open systems are given by the following equations:

$$\frac{dE}{dt} = \sum_{i} \dot{Q}_i - \dot{W} + \sum_{in} \dot{m}_{in} \cdot h_{in} - \sum_{out} \dot{m}_{out} \cdot h_{out} \qquad (5.1)$$

$$\frac{dS}{dt} = \sum_{i} \frac{\dot{Q}_i}{T_i} + \sum_{in} \dot{m}_{in} \cdot s_{in} - \sum_{out} \dot{m}_{out} \cdot s_{out} + \dot{\sigma} \qquad (5.2)$$

Considering that the system that is computed in this work operates under steady-state conditions:

$$\frac{dE}{dt} = 0, \quad \frac{dS}{dt} = 0 \qquad (5.3)$$

5.2 System exergy and irreversibilities

The exergy of a system at a given thermodynamic state is defined as the maximum useful work that can be obtained from the system when it is brought from this mentioned state to equilibrium with the surroundings. In other words, it represents the amount of energy that is available for being used as work. If the second and first laws of thermodynamics are combined, it is possible to formulate an equation for the system exergy:

$$0 = \sum_i \dot{Q}_i \cdot \left(1 - \frac{T_o}{T_i}\right) - \dot{W} + \sum_{in} \dot{m}_{in} \cdot e_{in} - \sum_{out} \dot{m}_{out} \cdot e_{out} - \dot{I} \qquad (5.4)$$

Where e (the exergy of the open system) can be computed as a function of enthalpy and entropy:

$$e = (h - h_o) - T_o \cdot (s - s_o) \qquad (5.5)$$

T_o, h_o, and s_o are the temperature, enthalpy and entropy of the surrounding conditions respectively, evaluated at the ambient conditions.

When real systems move from their thermodynamic state to equilibrium with the surroundings, certain amount of exergy is destroyed. This is the phenomenon of irreversibility. As the irreversibilities of the system increase, the amount of work that can be obtained is reduced. Considering that exergy can be defined as the system ability to produce work, and that entropy can be described as the system inability to produce work, both exergy and entropy can be related by means of the following equation:

$$\dot{I} = T_o \cdot \dot{\sigma} \qquad (5.6)$$

Where $\dot{I}$ is the rate of exergy destruction and $\dot{\sigma}$ is the rate of entropy generation.

5.3 Thermodynamic objective function

When carrying out the thermodynamic optimization of Rankine cycles, many different objective functions can be used. The most common ones are the net power output, the first-law efficiency and the second-law efficiency. However, not all authors resort to these objectives functions. For example, F. Angulo-Brown [40] turned to the so-called "ecological function", which is defined as $\dot{W} - T_o \cdot \dot{\sigma}$, while V. Holubec et al. [41], to a trade-off function proportional to $\eta \cdot \dot{W}$. Therefore, setting the thermodynamic objective

function is arbitrary, although it is always a combination of net power, rate of entropy generation and efficiency [42].

R. Agromayor et al. stated in [43] that the three most commonly used thermodynamic objective functions (net power output, first-law efficiency and second-law efficiency) are equivalent in terms of optimization results, since they all entail maximizing the power output from a fixed heat source. Optimizing the second-law efficiency has the benefit of giving insight about how much potential for improvement is left. Following their advices, the second-law efficiency will be chosen as the thermodynamic objective function in this work.

The second-law efficiency of the system can be formulated as:

$$\eta_{II,cycle} = \frac{\dot{W}_{net}}{\dot{E}_{in}} \qquad (5.7)$$

The recovery efficiency in the primary heat exchanger must be considered when defining the second-law efficiency of the whole power plant, as not all the energy that is available from the heat source can be used. This recovery efficiency is given as:

$$\eta_{recovery} = \frac{\dot{E}_{in}}{\dot{E}_{max}} \qquad (5.8)$$

Where $\dot{E}_{max}$ is the maximum amount of exergy that can be recovered.

Therefore, the plant second-law efficiency, and hence the thermodynamic objective function of this work is defined as:

$$\eta_{II} = \eta_{II,cycle} \cdot \eta_{recovery} = \frac{\dot{W}_{net}}{\dot{E}_{max}} \qquad (5.9)$$

From the given formulas, the first-law of thermodynamics and equations of state can be used to calculate all the states of the cycle. Once this is done, all the cycle irreversibilities

can be computed to find a solution for the thermodynamic objective function. The way these formulas are applied to the different system components to solve the cycle will be presented in Section 9.4.

6 Heat transfer area and pressure drop calculations

The design of the heat exchangers must be carried out in order to determine the required heat transfer area to meet certain thermal duties specifications. This heat transfer area has a major importance when determining the cost of the system, and it is dependent on the H.E heat transfer coefficients. Determining the pressure drop that all fluids experience in the heat exchangers is also of importance. This chapter summarizes all the correlations that are required to determine the H.E heat transfer coefficients and pressure drops[6].

6.1 Heat transfer area

For calculating the required heat exchangers heat transfer area, the Logarithmic Mean Temperature Difference (LMTD) method is going to be used. The main used formula is:

$$\dot{Q} = U \cdot A \cdot \Delta T_{LMTD} \qquad (6.1)$$

Where:

$$\Delta T_{LMTF} = \frac{T_{hot,in} - T_{cold,out} - T_{hot,out} + T_{cold,in}}{\ln \frac{T_{hot,in} - T_{cold,out}}{T_{hot,out} - T_{cold,in}}} \qquad (6.2)$$

As Equation 6.1 reflects, the heat transfer area is a function of the heat transfer coefficient, which has to be calculated by means of empirical correlations. This is not an easy task, since literature provides a wide range of correlations that may differ from one another. All single-phase flow correlations are well defined, and numerous experimental studies

[6] For simplicity, we assumed that fluid properties are constant at all points of each cross-section area of all computed H.E nodes. This means that the factor $\phi = \left(\frac{\mu}{\mu_w}\right)^{0.14}$ that takes the fluid properties variations with respect to the wall into consideration, has a value equal to 1, and it is not going to be included in the formulations.

linked to theoretical correlations show their reliability. However, when it comes to analyze the evaporation and condensing processes (i.e processes that involve two-phase behaviors), calculating the heat transfer coefficients gets more complex. Many studies related to this problem have been carried out, and the number of associated published papers keeps on increasing year by year. However, no correlation that accurately fits all experimental data has yet been found, because of the difficulty of determining which one of the convective or boiling/condensation effects is prevailing in the heat exchange process. All the presented correlations have been studied during the literature review in order to make sure that they have already been used by other authors in the field.

6.1.1 Shell-and-tube heat exchanger heat transfer coefficients

The shell-and-tube heat exchanger can be modelled as the primary heat exchanger or as the condenser of the Rankine cycle.

For calculating the heat transfer coefficients of this type of heat exchangers, it is necessary to divide them in three different regions, since the required correlations for the single-phase regions (pre-heating, super-heating, pre-cooling and sub-cooling), and the two-phase regions (evaporation and condensation) are different.

The overall heat transfer coefficient can be defined as [37]:

$$\frac{1}{U_{overall}} = \frac{1}{\alpha_{fl}} \cdot \frac{d_o}{d_i} + \frac{d_o}{\lambda} \cdot \ln\left(\frac{d_o}{d_i}\right) + \frac{1}{\alpha_{wf}} \qquad (6.3)$$

Where the heat transfer coefficient of the working fluid flowing through the tubes (α_{wf}) is computed in different ways depending on its phase state. Regarding the shell side, the same correlation will be used for all H.E sections, as the heating/cooling water does not experience any phase change during the heat transfer process.

- Shell-side

The convective heat transfer coefficient for the fluid flowing through the shell can be calculated by means of Mc Adams correlation [37]:

$$\alpha_{fl} = \frac{k_{fl}}{d_e} \cdot \left(0.36 \cdot \left(\frac{d_e \cdot G_s}{\mu_{fl}} \right)^{0.55} \cdot Pr^{\frac{1}{3}} \right) \qquad (6.4)$$

Where:

$$G_s = \frac{\dot{m}_{fl}}{A_s} \qquad (6.5)$$

The mass velocity is a function of the shell characteristic area, which can be defined as [44]:

$$A_s = \frac{d_s}{P_T} \cdot (P_T - d_o) \cdot L_b \qquad (6.6)$$

The hydraulic diameter (equivalent diameter) is a factor that relates the fluid crossing area and the wetted perimeter. Hence, its value is dependent on the tube layout [44]:

$d_e = 4 \cdot \frac{P_T^2 - \pi \cdot \frac{d_o^2}{4}}{\pi \cdot d_o}$ for a tube layout = 90º (square pitch) (6.7)

$d_e = 4 \cdot \frac{P_T^2 \cdot \sqrt{3}/4 - \pi \cdot \frac{d_o^2}{8}}{\pi \cdot \frac{d_o}{2}}$ for a tube layout = 30º (triangular pitch) (6.8)

- Tube-side (working fluid)

The expression that needs to be used when calculating the working fluid heat transfer coefficient depends on the phase the working fluid is at each H.E section:

- Single-phase flow: Pre-heating and super-heating sections (primary heat exchanger) and pre-cooling and sub-cooling sections (condenser)

Gnielinski correlation can be used to calculate the convective heat transfer coefficient when the working fluid is in the vapour or liquid phase ($x \leq 0$ or $x \geq 1$) [37].

$$\alpha_{sp,wf} = \frac{k}{d_i} \cdot \frac{\left(\left(\frac{f}{8}\right) \cdot (Re - 1000) \cdot Pr\right)}{1 + 12.7 \cdot \sqrt{\frac{f}{8}} \cdot \left(Pr^{\frac{2}{3}} - 1\right)} \qquad (6.9)$$

Where f (Darcy friction factor) depends on the flow regime (laminar or turbulent):

$$f = \frac{16}{Re} \quad \text{for } Re \leq 2300 \qquad (6.10)$$

$$f = (0.79 \cdot \ln(Re) - 1.64)^{-2} \quad \text{for } Re > 2300 \qquad (6.11)$$

The Prandtl number expression is:

$$Pr = \frac{c_p \cdot \mu}{k} \qquad (6.12)$$

and the Reynolds number is calculated as:

$$Re = \frac{4 \cdot \dot{m}_{wf}}{\mu \cdot d_i \cdot \pi} \qquad (6.13)$$

Different correlations must be defined for boiling and condensation regimes:

- Two-phase flow - Evaporation

Gungor-Winterton correlation is used to calculate the working fluid heat transfer coefficient during the evaporation process. Its formula is dependent on the vapour quality

at each computed node, the boiling number and the liquid convective heat transfer coefficient, among others. This correlation states [45, 46, 47]:

$$\alpha_{tp,wf} = \alpha_{l,wf} \cdot \left(1 + 3000 \cdot Bo^{0.896} + 1.12 \cdot \left(\frac{x}{1-x}\right)^{0.75} \cdot \left(\frac{\rho_l}{\rho_v}\right)^{0.41}\right) \qquad (6.14)$$

Where the boiling number is [47]:

$$Bo = \frac{q}{h_{lg} \cdot G_{eq}} \qquad (6.15)$$

and:

$$G_{eq} = \frac{\dot{m}_{wf}}{\pi \cdot \frac{d_i^2}{4} \cdot \frac{N_t}{N_p}} \cdot \left(1 - x + x \cdot \left(\frac{\rho_l}{\rho_v}\right)^{\frac{1}{2}}\right) \qquad [7](6.16)$$

The liquid convective heat transfer coefficient can be calculated by means of Gnielinski correlation (Equation 6.9). However, in order to follow exactly the same procedure given by C. Zhang et al. in [46], Dittus-Boelter correlation was preferred.

$$\alpha_{l,wf} = \frac{k_l}{d_i} \cdot 0.023 \cdot Re_l^{0.8} \cdot Pr_l^{0.4} \qquad (6.17)$$

The Reynolds number for the liquid working fluid can be calculated as a function of the vapour quality:

$$Re_l = \frac{G \cdot d_i \cdot (1-x)}{\mu} \qquad (6.18)$$

[7] Even though A. Lakew et al. [45] and C. Zhang et al. [46] and do not specify how to calculate the mass flow velocity that is required to compute the Boiling number formula, J. R. García-Cascales et al. includes in [52] the impact of the vapour quality on this parameter in a plate heat exchanger. For this reason, we decided to add this impact to the original correlation.

- Two-phase flow - Condensation

The working fluid condensation and evaporation do not yield the same heat transfer coefficients, and different correlations from the ones we have already presented must be defined to study the heat transfer process when the shell-and-tube heat exchanger is used to reject the surplus heat. Shah correlation [48] can be used as a good approach to compute the working fluid condensation heat transfer coefficient:

$$\alpha_{tp,wf} = \alpha_{l,wf} \cdot \left((1-x)^{0.8} + 3.8 \cdot \frac{x^{0.76} \cdot (1-x)^{0.04}}{{p_r}^{0.38}} \right) \qquad (6.19)$$

Where p_r is:

$$p_r = \frac{P_{sat}}{P_{crit}} \qquad (6.20)$$

Therefore, as a summary, the heat transfer coefficient for the shell-and-tube heat exchanger will be calculated as follows:

- For the super-heating, pre-heating, pre-cooling and sub-cooling sections:

$$\frac{1}{U_{overall}} = \frac{1}{\alpha_{sp,fl}} \cdot \frac{d_o}{d_i} + \frac{d_o}{\lambda} \cdot \ln\left(\frac{d_o}{d_i}\right) + \frac{1}{\alpha_{sp,wf}} \qquad (6.21)$$

- For the evaporation and condensing sections:

$$\frac{1}{U_{overall}} = \frac{1}{\alpha_{sp,fl}} \cdot \frac{d_o}{d_i} + \frac{d_o}{\lambda} \cdot \ln\left(\frac{d_o}{d_i}\right) + \frac{1}{\alpha_{tp,wf}} \qquad (6.22)$$

Where $\alpha_{sp,fl}$ is given in Equation 6.9 and $\alpha_{tp,wf}$ value depends on whether the shell-and-tube heat exchanger is used as the primary heat exchanger (Equation 6.14) or as the condenser of the cycle (Equation 6.19).

The conduction resistance of the pipes has the same value in all sections, since it does not depend on the properties of the fluids, but only on the geometry design of the tubes and on the thermal conductivity of the material they are made of.

6.1.2 Plate heat exchanger heat transfer coefficients

Once again, we need to divide the heat exchanger in three different regions for being able to compute the evolution of all heat transfer coefficients.

For calculating the overall heat transfer coefficient, the following equation needs to be solved:

$$\frac{1}{U_{overall}} = \frac{1}{\alpha_{wf}} + \frac{\delta}{\lambda} + \frac{1}{\alpha_{fl}} \qquad (6.23)$$

- Working fluid-side

We need to divide it in:

- Single-phase flow. Pre-heating, super-heating, pre-cooling and sub-cooling sections

More than 5 different correlations were found for the single-phase plate heat exchangers calculations. Among all of them, the most well-known correlations were developed by Okada, Ono et al. [49], Kumar [50] and Wanniarachchi and Ratman [51]. Considering that Okada's correlation is only valid for water, and that Wanniarachchi's and Ratman's correlation considers too many geometry parameters that are out of the scope of this work, Kumar's correlation was chosen as a good approach to the single-phase convective heat transfer coefficient, as it includes two constants (called Kumar constants) that take into account the Chevron angle value and the flow conditions (by means of the Reynolds number) [37]. Appendix B shows the values of these Kumar constants in Table A. Therefore, from Kumar, the heat transfer coefficient correlation for single-phase flows in plate heat exchangers is defined as:

$$\alpha_{sp} = \frac{k}{d_h} \cdot C_h \cdot Re^n \cdot Pr^{\frac{1}{3}} \qquad (6.24)$$

Where the hydraulic diameter can be approached to:

$$d_h = 2 \cdot b \qquad (6.25)$$

Reynolds number needs to be calculated for one single channel, meaning that not only the number of plates, but also the number of passes per plate and the number of channels per pass must be considered. The mass velocity can be calculated as [37]:

$$G_{ch} = \frac{\dot{m}_{total}}{N_c \cdot b \cdot L_w} \qquad (6.26)$$

And, finally, the Reynolds number:

$$Re = \frac{G_{ch} \cdot d_h}{\mu} \qquad (6.27)$$

- Two-phase flow - Evaporation

To compute the two-phase working fluid heat transfer coefficient during evaporation in the plate heat exchanger, the Yan-Lin correlation can be used [52]:

$$\alpha_{tp,wf} = \frac{k_l}{d_h} \cdot 1.926 \cdot Pr_l^{\frac{1}{3}} \cdot Bo^{-0.3} \cdot Re^{0.5} \cdot \left(1 - x + \left(\frac{\rho_l}{\rho_v}\right)^{0.5}\right) \qquad (6.28)$$

Where:

$$Re_{eq} = \frac{G_{eq} \cdot d_h}{\mu_l} \qquad (6.29)$$

And the boiling number can be calculated as stated in Equation 6.15.

- Two-phase flow - Condensation

For the condensing section, a different correlation from the one given for the evaporation process needs to be used. The chosen one is the Yan-Lio-Lin correlation [46, 52], which depends on the working fluid vapour quality:

$$\alpha_{tp,wf} = \frac{k_l}{d_h} \cdot 4.118 \cdot Re_{eq}^{0.4} \cdot Pr^{\frac{1}{3}} \qquad (6.30)$$

Where:

$$Re_{eq} = \frac{G_{eq} \cdot d_h}{\mu_l} \qquad (6.31)$$

and:

$$G_{eq} = G \cdot (1 - x + x \cdot \left(\frac{\rho_l}{\rho_v}\right)^{\frac{1}{2}} \qquad (6.32)$$

- Cooling and heating fluids

Considering that all the plates that compound the plate heat exchanger are identical, the geometry parameters that need to be included in the heat transfer correlations calculations for the interacting fluids are exactly the same. Therefore, Equation 6.24 can be applied to both the working fluid and the heating/cooling fluid when they are in the single-phase state.

Therefore, as a summary, the heat transfer coefficient for the plate heat exchanger must be calculated as:

- For the pre-heating, super-heating, pre-cooling and sub-cooling sections:

$$\frac{1}{U_{cond}} = \frac{1}{\alpha_{sp,wf}} + \frac{\delta}{\lambda} + \frac{1}{\alpha_{fl}} \qquad (6.33)$$

- For the evaporation and condensing sections:

$$\frac{1}{U_{cond}} = \frac{1}{\alpha_{tp,wf}} + \frac{\delta}{\lambda} + \frac{1}{\alpha_{fl}} \qquad (6.34)$$

Where α_{fl} is calculated from Equation 6.24 and $\alpha_{tp,wf}$ value depends on whether the plate heat exchanger is used as the primary heat exchanger (Equation 6.28) or as the condenser of the cycle (Equation 6.30).

The conductivity resistance of the plates is only a function of their thickness and thermal conductivity of the material, so its value is the same for all the different flow regimes.

Once the overall heat transfer coefficient has been obtained for all the different H.E sections, it is possible to determine the area that is destined for each one of these sections by applying Equation 6.1. Finally, the total H.E heat transfer area of both the primary heat exchanger and the condenser can be calculated as the sum of all sections areas:

$$A_{PrHE} = A_{pre-heating} + A_{evaporating} + A_{super-heating} \qquad (6.35)$$

$$A_{cond} = A_{pre-cooling} + A_{condensing} + A_{sub-cooling} \qquad (6.36)$$

These equations must be consistent with Equations 4.7 and 4.10, in which the heat transfer areas were given as a function of the H.E geometry parameters[8].

[8] In our code, the heat transfer area is calculated by means of Equation 6.1, in combination with Equations 6.35 and 6.36. Once the total H.E surface is known, Equations 4.7 and 4.10 can be used to compute the geometry parameters that were not defined a priori, as they were not required to compute the heat transfer coefficients correlations. This way, the heat exchanger areas given from Chapter 4 and Chapter 6 formulas are consistent.

6.2 Pressure drop calculations

Pressure drop calculations are different for each type of heat exchanger, and also for each section in which they can be divided.

6.2.1 Shell-and-tube heat exchanger pressure drops

- Shell-side

The shell fluid velocity fluctuates because of the constricted area between adjacent tubes [39]. Also, the baffles positioning and dimensions have a great impact on the pressure drop that the fluid flowing through the shell experiences. For simplicity, the formulation that is going to be used to calculate the shell-side pressure drop assumes that the velocity of the fluid through the shell is fully developed, remaining constant, which yields an estimate (this was also considered for the shell-side convective heat transfer coefficient calculations).

The pressure drop in the shell can be calculated by means of [44]:

$$\Delta p_s = f \cdot \frac{d_s \cdot (N_b + 1) \cdot {G_s}^2}{2 \cdot \rho \cdot d_e} \cdot N_s \qquad (6.37)$$

Which takes into consideration the number of times the bundle is crossed $(N_b + 1)$ and G_s is given by Equation 6.5.

Regarding the friction factor, it can be calculated as [44]:

$$f = \exp(0.576 - 0.19\, ln(Re_s)) \qquad (6.38)$$

Even though this approximation can be considered accurate enough, it does not consider the pressure losses which are due to the contractions and expansions that the fluid suffers when entering and leaving the shell through the nozzles and when entering and leaving the tube bundles. A more accurate model is described in detail in [53] (the Delaware

method) which accounts for these secondary losses. This model has not been implemented in our code, as it includes more geometry parameters whose inclusion would have made the computational problem much more complex.

- Tube-side (working fluid)

The pressure drop in the tubes can be obtained from [37]:

$$\Delta p_1 = 4 \cdot f \cdot \frac{L_t \cdot N_p}{d_i} \cdot \left(\frac{G^2}{2 \cdot \rho} \right) \qquad (6.39)$$

Where f is given from Equation 6.10 or Equation 6.11, depending on the flow regime.

This tubes pressure drop does not take into consideration the additional pressure drops that the fluid experiences during a return due to the sudden expansions and contractions (consequence of the change of direction in the passes). As the expression to calculate these secondary pressure losses is simple and does not require the implementation of complex models, it has been included in the calculations [37]:

$$\Delta p_2 = 4 \cdot N_p \cdot \frac{G^2}{2 \cdot \rho} \qquad (6.40)$$

Finally, the total pressure drop in the tube side is:

$$\Delta p_{total} = \Delta p_1 + \Delta p_2 = 2 \cdot N_p \cdot \frac{G^2}{\rho} \cdot \left(f \cdot \frac{L_t}{d_i} + 1 \right) \qquad (6.41)$$

6.2.2 Plate heat exchanger pressure drops

As plate heat exchangers allow for a wide variety of different designs and plates arrangements, developing suitable pressure drops correlations for all kinds of H.E design is still a challenge [37]. C. Tribbe and H. Müller-Steinhagen [54] stated that the geometry of the plates has a great influence on the pressure drop, while some properties of the fluid,

such as the liquid viscosity, could be neglected when the heat rate is low, as their influence on the fluid pressure drop is small. The pressure drop correlations that are presented in this section can be considered to be suitable for a preliminary sizing of the plates. For both interacting fluids, the same formula can be used.

The pressure drop due to channel friction can be obtained from [37]:

$$\Delta p_{ch} = 4 \cdot f \cdot \frac{N_p \cdot L_p}{d_h} \cdot \frac{{G_{ch}}^2}{2 \cdot \rho} \qquad (6.42)$$

Where the friction factor f considers the Kumar constants given in Appendix B[9]:

$$f = \frac{k_p}{Re^m} \qquad (6.43)$$

As the fluids also flow through the ports of the plates, the associated pressure drop should be considered. However, this would require the definition of a new degree of freedom (the diameter of the port). For simplicity, and considering that the pressure drop in the port is low when compared to the channel friction pressure drop, the total pressure drop in the plate heat exchanger will be calculated as:

$$\Delta p_{total} = 1.1 \cdot \Delta p_{ch} \qquad (6.44)$$

[9] Although the Kumar constants values that are needed to calculate the friction factor are given for single-phase flows, the working fluid pressure drop in the plate heat exchanger is expected to be so low that the difference between using a more accurate pressure drop correlation for the two-phase flow would be negligible. The reason is that the cooling/heating water mass flow rate is always higher than the working fluid mass flow, and the pressure drop limitation for the water side is always the one that determines the design of the heat exchanger. This was checked after having run a few simulations.

7 Cost modelling and techno-economic optimization

Even though the basic ORC has been adopted in the industry in a successful manner, optimizing both its cost and its performance at the same time is still a challenge in the engineering field. Numerous studies have been carried out with this objective, but most of them do not include the impact of each individual cycle component in the analysis. For this reason, there is still a lack of information in relation to the effect that the component modelling has on the ORC cost [55].

In order to find suitable results from the techno-economic optimization, the equipment cost, plant balance and investment cost of the heat source exploitation must be most certainly known [16]. In this chapter, different cost models are discussed, all component cost correlations are defined, and the techno-economic objective function is presented.

7.1 Cost correlations

7.1.1 Cost component correlations

Even though most of the authors that have studied the techno-economic optimization of ORCs agree on the importance of defining the right cost correlations for the models, the available data has high uncertainty. This is due to the fact that engineering companies (which we can consider the best and most trustful source of information) have strict politics to keep their economic data as concealed as possible. For this reason, three main models have been generalized and defined to keep certain consistency between the different published studies. These models were developed by D.W. Green [56], R. Turton et al. [57] and H. Loth et al. [58].

Green's model includes only one reference and cost variation exponent, meaning that it is not sufficiently accurate, and calculations may deviate from the real data if the component size is too different from the reference model size. On the other side, Loth's

model includes foundations, insulation and instrumentation costs, which are hard to find in the open literature.

Turton's model is considered the most accurate cost model, since it does not present great deviations when comparing the theoretical cost results with the ones that are found in the market. During the literature review process, it was found that Turton's model is the most embraced one [3, 24, 46, 59]. For these reasons, Turton's model is the one that is going to be used to compute the cost of all cycle components in this work.

The cost of each ORC component can be calculated as a function of its most important size factor, also called "Capacity Factor" (CF), which needs to be corrected by taking into consideration a pressure factor and a material factor, as it will be shown next.

Turton's main correlation is:

$$\log C_P = K_1 + K_2 \log_{10}(CF) + K_3 (\log_{10}(CF))^2 \qquad (7.1)$$

Where CF depends on the kind of component the correlation is applied to. CF values for each one of the system components can be found in Table 3.

Table 3. Capacity Factors for the different ORC components, [57, 59]

Component	**Capacity Factor (CF)**
PrHE	Heat transfer surface, A [m^2]
Condenser	Heat transfer surface, A [m^2]
Turbine	Power output, W [kW]
Pump	Power consumption, W [kW]
Generator	Electrical power, W [kW]

The basic cost (C_P) needs to be corrected to heed the operating pressure and manufacturing materials. This should be done as follows [46, 59]:

$$C_{BM} = C_P \cdot F_{bm} = C_P \cdot \left(B_1 + B_2 \cdot F_m \cdot F_p\right) \qquad (7.2)$$

Where F_m and F_{bm} values are extracted from [57] and [46], and they depend on the design of the component.

To define the material factor (F_m), carbon steel was selected as the manufacturing material for all components. G. Li stated in [32] that this material is suitable for heat source temperatures up to 290 ºC, and that more advanced manufacturing materials would be needed just in case of operating at higher temperatures. As this temperature level is not going to be exceeded in none of the proposed scenarios, it can be assumed that carbon steel is suitable for avoiding problems related to high thermal stresses in the Rankine cycle components computed in this work[10].

Finally, F_p can be calculated as:

$$\log F_p = C_1 + C_2 \log_{10}(p) + C_3(\log_{10}(p))^2 \qquad (7.3)$$

All constants' values ($K_1, K_2, K_3, B_1, B_2, C_1, C_2$ and C_3), which are cost coefficients, are presented in Table 4. In order to select the right values of these coefficients, the following considerations must be taken into account [57]:

- For the primary heat exchanger, in case the evaporation pressure is found between 5 and 140 bar, values for C_1, C_2 and C_3 must be modified to 0.03881, -0.11272 and 0.08183, respectively.

- For the pump, in case the pressure moves between 10 and 100 bar, C_1, C_2 and C_3 should take the values -0.3935, 0.3957 and -0.00226, respectively.

[10] As it was stated in Section 3.4.2, new plate heat exchangers manufacturing materials allow for operating at considerably high temperatures and pressures. However, Turton's manual does not include the most advanced materials yet, making it not possible to compute the cost of these components when studying the application of medium- or high-temperature heat sources.

Table 4. Cost constants values for the different Rankine cycle components [46, 57]

Equipment	K_1	K_2	K_3	C_1	C_2	C_3	B_1	B_2	F_m	F_{bm}
Plate H.E	4.6656	-0.1557	0.1547	0	0	0	0.96	1.21	1.0	-
Shell-and-Tube H.E	4.8306	-0.8509	0.3187	0	0	0	1.63	1.66	1.30	-
Turbine	2.2476	1.4965	-0.1618	-	-	-	-	-	-	3.30
Pump	3.3892	0.0536	0.1538	0	0	0	1.89	1.35	1.5	-

Even though Turton's correlation is considered to constitute a good approach to the cost modelling of the different Rankine cycle components, defining the right cost correlation for the turbine is not easy, since there are many different parameters that influence its design and, therefore, its cost. For power plants operating at low loads, the expander design is a problem that has not been solved yet [60]. The main difficulty when trying to set the turbine cost is that not all authors agree upon a general nor a specific cost correlation.

Some authors propose to study the turbine cost correlation as a function of its number of stages and size, not taking into consideration the material nor the pressure factor [3]. However, considering that the ORC industry deals with many different solutions and includes a wide range of different types of turbines (some companies are even developing their own models), an agreement with respect to the turbine design does not exist yet. For this reason, Turton's turbine cost correlation [57] has been chosen to estimate the expander cost, since it does not dig deep into the turbine design. This assumption is also based on different literature research studies, in which we found that most of the authors resort to Turton's turbine cost correlation, stating that it can be accurate enough when the system is not designed for high power production [24, 31, 46, 59].

The generator is the only one component whose cost correlation is not defined by Turton. However, it can be easily obtained by means of the following equation [46]:

$$C_{p,gen} = 60 \cdot \left(W_{gen}\right)^{0.95} \qquad (7.4)$$

Finally, the total investment cost can be calculated as the sum of the cost of all cycle components.

$$C_{tot} = C_{BM,PrHE} + C_{BM,cond} + C_{BM,pump} + C_{BM,turb} + C_{BM,gen} \qquad (7.5)$$

Other factors such as the Capital Recovery Cost (CRC) can also be considered to make the cost analysis more realistic, although they require assuming the interest rate and the plant life time. For this reason, they are not going to be included in the cost modelling. However, the Chemical Engineering Plant Cost Index (CEPCI) needs to be heeded in order to adjust the system overall cost from 2001 (year of publication of the resource from the one we extracted the cost constants values) to 2018. Therefore, the cost must be corrected as follows [46]:

$$C_{tot,2018} = C_{\mathrm{tot},2001} \cdot \frac{CEPCI_{2018}}{CEPCI_{2001}} \qquad (7.6)$$

Where $CEPCI_{2001}$ = 397 [46] and $CEPCI_{2018}$ = 562.1 [61].

7.1.2 Working fluids

Defining the cost correlations for the system components requires to relate them with reference models by means of material and pressure factors. However, for working fluids, no comparison with other pure substances is required, since each working fluid has its own defined cost, which is set by the market law of supply and demand.

Depending on the class the working fluid belongs to, its cost will move in a wide range of values. More specifically, there is an important cost difference between flammables and non-flammable working fluids. Non-flammable substances present a 12 times lower cost than the flammable ones and, even though security and firing systems, and the required authorizations, are more complex, these additional costs may not be high enough to cover the product cost difference [16]. However, this depends on the politics each country has with respect to the use of toxic or flammable working fluids (Europe, for

example, has banned the use of extremely dangerous working fluids, regulated by the Seveso II-III Directive) [16].

Even though most literature studies focus the ORC techno-economic optimization on finding the optimum design of the expander and heat exchangers, the cost of the working fluid can represent a share of more than 10% of the total installation cost [16], meaning that the fact of not including it on the cost analysis can lead to non-realistic results. However, authors do not agree on this assertion, and no article threating the working fluid cost impact on the overall system cost could be found in the open literature. The reason is that it requires the estimation of the plant volume and a preliminary sizing of all cycle components and piping, which is difficult to analyze in early stages. Also, studies presented in [47, 59, 62] and [63] point out that the working fluid cost contribution to the overall system investment cost of small-scale ORCs is slight, and can be neglected because of the small size of the system. For the mentioned reasons, the working fluid cost will not be included in this work.

7.1.3 Other costs

When it comes to analyze the investment cost that is required for setting up an ORC power plant, fixed and variable costs can be included. A. Bejan et al. [64] proposed an analysis of all the expenses that are part of the total system investment (including equipment, installation, instrumentation, land, service facilities, licenses, research…). When the exploitation cost of the heat source is high, the equipment cost may be considered negligible [16]. This is the case of geothermal exploitations, whose expensive campaigns and costly drilling activities (which represent more than a half of the total share) guide the techno-economic optimization to maximize the thermodynamic efficiency, in an effort to counteract the great investments they require with high power outputs.

Since this work is only going to cover the exploitation of a geothermal heat source, its associated drilling cost is not going to be considered, as it will not have any impact on the conclusions when comparing the different suggested scenarios. The same basis applies to extra costs such as land, required licenses or inflation costs.

7.2 Techno-economic objective function

As M. Astolfi et al. pointed out in [16], there are three different models that can be used as a basis to carry out the cost optimization of a power plant. These models are:

- Capital budgeting analysis or investment appraisal: It is the most general model, since it is based on the investment cost and rate of return (which allows to compare completely different power plants). However, it requires making electricity price assumptions, which are strongly dependent on the power plant location. This means that this model entails uncertainties and variations that may lead to wrong conclusions and/or results.

- Levelized cost of electricity (LCOE): This model does not require the definition of the electricity price, although it considers the cost of the fuel (in case it is used) and the Operation and Maintenance (O&M) costs.

- Specific Cost of the Plant (SCP): The total cost is analyzed by means of an index that is obtained from the quotient between the total cost and the plant power output.

From the proposed models, the first one was discarded due to the numerous assumptions that need to be made and that may deviate the results from their real trend. LCOE and SPC models are based in the same principles, with the only difference that the LCOE model includes fuel and O&M costs, while the SCP model does not. As the heat source that is going to be studied in this work is hot water from a geothermal reservoir, no fuel requirements must be considered, and, since the O&M costs are a function of the working fluid selection and design of the plant, including them as part of the analysis would require making assumptions of which not enough information is provided in scientific literature.

Therefore, the objective function that has been chosen to guide our calculations is the Specific Cost of the Plant[11]:

$$SIC = \frac{C_{tot}}{\dot{W}_{tot}} \qquad (7.7)$$

The design of the cycle will be focused on achieving the highest possible power output while reducing the costs to minimums. This means that the optimum Specific Investment Cost of the plant does not necessarily imply the lowest investment cost.

7.3 Other objective functions

By carrying out a literature research, it was found that many different objective functions can be applied to execute the Rankine cycle techno-economic optimization. Based on previous works, M. M. Hettiarachi et al. [65] proposed the optimization of the overall heat transfer area per unit of power (m^2/kW), so did J. Wang et al. in [66]. On the other side, Y. Feng et al. [67] proposed the optimization of the heat exchangers surfaces alone, considering that their cost represents the highest share of the system cost. Other authors, such as E. Cayer et al. [62] and S. Quoilin et al. [68], optimized the relative cost per unit of power (€/kW). Even though many different approaches have been proposed by field experts, no information with respect to which one of them is more meaningful could be found.

Rankine cycles have a great potential in the electricity market, although the high cost they entail in relation to the power that can be obtained from them makes this technology less competitive with respect to other energy sources, such as wind or solar energies in some conditions [22]. In this context, optimizing the plant Specific Investment Cost (SIC)

[11] In the literature, it is more common to refer to "Specific Investment Cost" (SIC) instead of "Specific Cost of the Plant" (SCP). To be consistent with literature, the former will be preferred for this report.

becomes a useful tool, as it makes it possible to evaluate and compare their competitiveness with other power production systems.

8 Optimization

In this section, some concepts that are fundamental to carry out the problem optimization are presented. All optimization processes require choosing at least one objective function, selecting a set of independent variables that control the value of the objective function, and defining constraints that limit the values the degrees of freedom can take. Therefore, the optimization problem needs to find the values of the variables that minimize or maximize the objective function while meeting the specified constraints. This can be formulated as [43]:

$$\min f(x) = \begin{cases} lb \leq x \leq ub & (8.1) \\ c_{ineq}(x) \leq 0 & (8.2) \\ c_{eq} = 0 & (8.3) \end{cases}$$

Where f is the objective function, x is the vector of degrees of freedom, lb and ub are the lower and upper bounds vectors for the degrees of freedom respectively, c_{ineq} is the vector of inequality constraints and c_{eq} is the vector of equality constraints.

8.1 Objective functions

The objective function is the output of the simulation that we want to optimize. For the work that is being carried out in this Master Thesis, two different objective functions need to be defined: one for the thermodynamic optimization and another one for the techno-economic optimization. These two objective functions are discussed in Section 5.3 and Section 7.2 respectively, and their optimum value is obtained when their global minimum solution is reached[12].

[12] The thermodynamic optimization aim is to maximize the Rankine cycle second-law efficiency. Considering that most MATLAB optimization algorithms are designed to minimize the objective function value, a minus sign needs to be added to the objective function when maximizing the performance of the plant, meaning that the problem optimization has to be defined as: "$\max f(x) = -\min f(x)$"

8.2 Degrees of freedom

The degrees of freedom are the independent variables whose values must be specified to determine a unique solution of the optimization problem. For example, the enthalpy at the inlet of the turbine and the outlet diameter of the shell-and-tube H.E tubes are degrees of freedom in this work.

The heat exchangers design allows for defining a great number of variables whose value may have an important impact on both the cost and the performance of the cycle. Considering that the computational time that is required to find the objective function optimum solution increases as the number of degrees of freedom increases, some assumptions needed to be made in order to avoid time-consuming simulations. This means that the set of degrees of freedom that was selected for this work can be modified to make it more or less computational expensive.

8.3 Constraints

Constraints are the conditions that the solution of the optimization problem must satisfy. These constraints can be of two types: inequality constraints or equality constraints.

Inequality constraints stablish certain limitations that cannot be violated when solving the optimization problem, such as the temperature jump limitation of the cooling water. On the other side, equality constraints are equations that need to be satisfied to make the objective function solution feasible. This means that equality constraints are much more difficult to handle in nonlinear programming, as they require that the solution point lies exactly on multiple curved surfaces at the same time. Therefore, as the number of equality constraints increases, the required computational time to find a feasible solution increases as well. Increasing the number of inequality constraints does also lead to costlier computational times, although they provide more flexibility to some extent.

8.4 Upper and lower bounds

Upper and lower bounds have the same computational role as inequality constraints, but they are specifically used to set the limits of the degrees of freedom. Considering that bounds are much easier to handle than constraints, defining the right degrees of freedom can help to reduce the computational cost of the program. Therefore, when laying out the problem, the definition of the degrees of freedom and constraints can determine the computational cost.

8.5 Optimization algorithms

There are many different algorithms that can be used to optimize a problem, and each one of them has its own characteristics and is meant for a specific application. This means that the optimization algorithm should not be randomly chosen, but that the one that best adapts to the nature of the problem must be selected.

One of the main concerns when designing our optimization model was the computational time that was required to find the optimum solution to a problem with such a great amount of degrees of freedom and constraints. Considering all the scenarios that wanted to be covered in this work, minimizing the required computational time became one of the main objectives during the first stages of the project, in an effort to avoid undesirable delays.

Two different types of optimization algorithms were considered for this work: gradient-based algorithms and direct-search algorithms. Gradient-based algorithms are preferred against the time-consuming direct-search methods when the computational time needs to be as short as possible. The main problem that gradient-based algorithms present is that the possibilities of finding local optimal solutions are greater than when direct-search algorithms are used. Therefore, when choosing the optimization algorithm, the decision of choosing between a fast-converging but little reliable algorithm, and a slow-converging but highly reliable algorithm must be made. Because of the reasons that were previously stated, gradient-based algorithms are preferred for this work.

In order to solve the gradient-based problem related to reaching local minimal solutions, all results were plotted in a set of organized graphs as soon as they were obtained. This way, it was easy to detect which solutions were not global minimums. When a local minimum solution was found, the vector of degrees of freedom was modified, and the simulations were run again until a logical value which followed the plotted tendencies was reached.

9 Case study and methodology

9.1 The starting case study

The starting case study is a low-temperature geothermal application with a 10 kg/s water stream at 120 ºC. This water stream can transfer heat to the Rankine cycle working fluid with the limitation of reaching a minimum temperature of 15 ºC at the outlet of the primary heat exchanger. The main assumptions and boundary conditions can be found in Table 5.

Table 5. Assumptions and boundary conditions for the starting case study [2, 17]

Hot source		
Fluid	[-]	H_2O
$\dot{m}_{in}$	[kg/s]	10
T_{in}	[ºC]	120
$T_{out,min}$	[ºC]	15
$T_{out,max}$	[ºC]	85
p_{out}	[bar]	3
$\Delta T_{PrHE,\min,pp}$	[ºC]	5
Cold source		
Fluid	[-]	H_2O
T_{in}	[ºC]	10
$\Delta T_{c,max}$	[ºC]	10
$\Delta T_{c,min}$	[ºC]	2
$\Delta T_{c,\min,pp}$	[ºC]	5
Ambient conditions		
p_{amb}	[bar]	1.013
T_{amb}	[ºC]	15
Pump		
Polytropic efficiency	[%]	70
Turbine		
Polytropic efficiency	[%]	80

Where ΔT_c is the temperature jump of the cooling fluid in the condenser and $\Delta T_{\min,pp}$ refers to the minimum pinch point temperature difference in the heat exchangers.

The system is operating under steady-state conditions, and heat losses and pressure drops in the pipes are neglected. Kinetic and potential energy variations are also neglected. The maximum temperature of the cycle is assumed not to drop with the geothermal reservoir exploitation.

The heat exchanger design process can be complex if all the geometry parameters given in Chapter 4 are set as degrees of freedom. Previous experience from the Specialization Project results showed that some H.E geometry parameters have a negligible impact on the optimization results, while others always reach exactly the same values when solving the optimization problem. For the mentioned reasons, all these H.E geometry parameters are going to be defined as assumptions, which are summarized in Table 6.

Table 6. Heat exchanger geometry assumptions

Shell and tube heat exchanger		
Pitch layout	[-]	Triangle
N_p	[-]	1
N_s	[-]	1[13]
L_b	[-]	$0.25 \cdot d_s$
B	[-]	$0.5 \cdot d_s$
Plate heat exchanger		
Chevron angle	[º]	45
b	[mm]	2
N_p	[-]	1
t	[mm]	5
Plates and tubes walls		
Material	[-]	Carbon steel
Thermal conductivity	[W/m·K]	16.5

Regarding the relationship between the baffle length and the space between baffles with the shell diameter, mean values of the upper and lower bounds given in Table 1 have been

[13] The number of passes and the number of shells were set to 1 for simplicity. In case these numbers are increased, the corresponding correction factors should be added to the calculations.

defined. Since both parameters must be re-calculated once the number of baffles is rounded (as it must be an integer), using mean boundary values makes sure that the re-calculated values are within the design constraints.

Carbon steel thermal conductivity is assumed to be constant with temperature. Considering that the material thermal resistances of the plates and tubes are negligible when compared to the convective thermal resistances that the fluids entail, any change in the manufacturing material conductivity is expected not to have a remarkable impact on the results.

Fouling resistances are time dependent and, as this work is focused on a steady-state system (in which variables are not time-dependent), they have been discarded from the study. Therefore, heat exchangers are supposed to be completely clean in all the scenarios that are proposed for this work.

9.2 Degrees of freedom and constraints

The designed MATLAB code includes 10 thermodynamic degrees of freedom, which are bounded to avoid unrealistic performances or unfeasible heat exchangers designs (see Table 7[14]).

Apart from these thermodynamic degrees of freedom, the heat exchangers design does also require the definition of a few more degrees of freedom (see Table 8). Depending on the system heat exchanger configuration, the number of degrees of freedom will move from 14 (when both the PrHE and the condenser are plate heat exchangers) up to 18 (when both cycle heat exchangers are shell-and-tube heat exchangers).

---

[14] For Table 7: $p_{min} = p_{sat}\ (T_o)$;
$h_{min} = h_{sat,liq}\ (T_o)$;
$h_{max} = h\ (T_{h1},\ p = 0)$.

Table 7. Degrees of freedom and bounds for the cycle[15]

	Degree of freedom	Lower bound	Upper bound
x_1	Heat source exit temperature	15 ºC	85 ºC
x_2	Temperature jump of the cooling fluid	2 ºC	10 ºC
x_3	Pressure at the inlet of the turbine	p_{min}	$0.9 \cdot p_{crit}$[16]
x_4	Pressure at the outlet of the turbine	p_{min}	$0.9 \cdot p_{crit}$
x_5	Enthalpy at the inlet of the turbine	h_{min}	h_{max}
x_6	Enthalpy at the inlet of the PrHE	h_{min}	h_{max}
x_7	Heating fluid pressure drop (PrHE)	0.1 %	15 %
x_8	Working fluid pressure drop (PrHE)	0.1 %	20 %
x_9	Working fluid pressure drop (condenser)	0.1 %	15 %
x_{10}	Cooling fluid pressure drop (condenser)	0.1 %	-

Table 8. Degrees of freedom and bounds for the H.E design [36, 37, 38]

Shell and tube heat exchanger			
x_I	Tubes outlet diameter	35 mm	510 mm
x_{II}	Wall thickness	3 mm	15 mm
x_{III}	Working fluid velocity in the tubes	0.9 m/s	2.6 m/s
x_{IV}	Pitch - outlet diameter relationship	1.25	1.5
Plate heat exchanger			
x_I	Volume flow per channel	0.5 m^3/h	12.5 m^3/h
x_{II}	Plate width	0.5 m	3.25 m

[15] Degrees of freedom from $x_1$to x_6 were defined as dimensionless variables and their value was normalized in an effort to reduce the computational time (taking values from 0 to 1).

[16] x_3 is up-bounded at $0.9 \cdot p_{critical}$ to avoid operating close to the critical point or under transcritical conditions (for the ones no heat transfer correlations were found in open literature).

Apart from the defined degrees of freedom and their bounds, some equality and inequality constraints had to be specified as well. These constraints are presented in Table 9.

Table 9. Optimization problem equality and inequality constraints

Inequality constraints:	
c_1	The working fluid has to be subcooled at the inlet of the pump to avoid cavitation.
c_2	The working fluid has to be saturated or superheated at the outlet of the evaporator (in order to avoid trilateral and partial evaporation cycles).
c_3	The working fluid has to be saturated or superheated at the outlet of the expander (in order to avoid vapour qualities lower than 1).
c_4	The pinch point in the evaporator has to be higher than the minimum temperature difference specified to avoid temperature crossing.
c_5	The pinch point in the condenser has to be higher than the minimum temperature difference specified to avoid temperature crossing.
c_6	The Specific Investment Cost cannot be negative.
Equality constraints:	
c_7	The calculated heating fluid pressure drop in the PrHE has to be equal to the one provided as a degree of freedom.
c_8	The calculated working fluid pressure drop in the PrHE has to be equal to the one provided as a degree of freedom.
c_9	The calculated working fluid pressure drop in the condenser has to be equal to the one provided as a degree of freedom.
c_{10}	The calculated cooling fluid pressure drop in the condenser has to be equal to the one provided as a degree of freedom.

The expressions that were used to compute these constraints can be found in Appendix C.

9.3 Fluid screening

REFPROP provides a list of 127 pure substances that can be used as working fluids in Rankine cycles. However, not all these pure substances are appropriate for the case studies that are going to be studied in this work. In order to discard unsuitable working fluids, a fluid screening process had to be carried out, based on the need of meeting the following 4 requirements:

1. The ODP has to be zero or close to zero[17].
2. The GWP must be lower than 2000[18].
3. The fluid critical temperature needs to be higher than the ambient temperature to make condensation possible.
4. The saturation pressure at ambient temperature has to be higher than 1 kPa to limit vacuum in the condenser.

From the 44 remaining working fluids, some of them were discarded because of the uncertainty related to their use in the industry. Also, preliminary results from the Specialization Project suggested that working fluids with a T_{max}/T_{crit} lower than 0.8 or higher than 1.15 present a too high Specific Investment Cost that cannot justify their use in the proposed Rankine cycle scenario. Therefore, special attention was mainly given to the most commonly used organic working fluids with a temperature ratio in a range of 0.8 and 1.15.

A final list of 18 working fluids was obtained as a result of the fluid screening selection (see Table 10). All of these remaining working fluids were considered for the starting case study analysis.

[17] The zero-ODP is a requirement to accomplish the Montreal protocol agreement [77].

[18] The GWP was set to 2000 to discard the worst greenhouse gases but, at the same time, not to ignore some of the most commonly used in the industry working fluids.

Table 10. List of remaining working fluids after the fluid screening selection

	Chemical name	Alternative name	Class	T_{max}/T_{crit}
1	Propane	R290	Alkane	1.0629
2	2-Methylpropane	Isobutane – R600a	Alkane	0.9640
3	Butane	R600	Alkane	0.9248
4	Pentane	R601	Alkane	0.8370
5	Propene	Propylene – R1270	Alkene	1.0772
6	Cis-2-butene	Cis-butene – C2-Butene	Alkene	0.9022
7	Propyne	-	Alkyne	0.9770
8	Cyclopropane	-	Cycloalkane	0.9871
9	Dimethylether	DME	Ether	0.9819
10	Chlorodifluoromethane	R22[19]	HCFC	1.0646
11	Difluoromethane	R32	HFC	1.1193
12	1,1,1,2-Tetrafluoroethane	R134a	HFC	1.0506
13	1,1-Difluoroethane	R152a	HFC	1.0174
14	1,1,1,3,3-Pentafluoropropane	R245fa	HFC	0.9204
15	1,1,2,2,3-Pentafluoropropane	R245ca	HFC	0.8784
16	2,3,3,3-Tetrafluoroprop-1-ene	R1234yf	HFO	1.0688
17	Trans-1,3,3,3-tetrafluoropropene	R1234ze	HFO	1.0279
And an inorganic working fluid:				
18	Ammonia[20]	R717	Inorganic	0.9697

[19] R22 does not meet all the fluid screening requirements, as it presents a too high ODP. However, as replacing R22 with other working fluids has become a need for new systems because of environmental regulations, it was found of interest to study its thermodynamic and cost performance in order to find which other working fluids would be suitable candidates to substitute it.

[20] Ammonia was included in the list even though it is an inorganic working fluid. The reason is that its good thermal properties have made it one of the most preferred working fluids in the industry.

9.4 Component modelling

The basis of the simulation software is the same as the one R. Agromayor et al. developed in [17], which includes the thermodynamic fundamentals (first and second laws of thermodynamics) that are needed to compute all the cycle states and to optimize the results. In this work, all the cycle components have been modelled by means of the first law of thermodynamics, which, in combination with the degrees of freedom, allow to compute all the states of the Rankine cycle. Once these states are known, correlations related to heat exchangers pressure drops and heat transfer coefficients (see Chapter 6) can be computed. The application of the second-law efficiency makes it possible to obtain all the cycle irreversibilities and to compute the thermodynamic objective function (see Chapter 5). Finally, cost correlations given in Chapter 7 are used to calculate the cycle SIC (i.e the techno-economic objective function)[21].

9.4.1 Heat exchangers

The heat duty in both the primary heat exchanger and the condenser can be calculated by means of the first law of thermodynamics:

$$\dot{Q} = \dot{m}_{hot} \cdot \left(h_{hot,in} - h_{hot,out}\right) \qquad (9.1)$$

$$\dot{Q} = \dot{m}_{cold} \cdot \left(h_{cold,out} - h_{cold,in}\right) \qquad (9.2)$$

During the computation, both heat exchangers must be discretised for two reasons:

[21] Reference [17] does not cover the heat exchangers design, neither its influence on the heat exchangers pressure drops nor heat transfer processes. This means that even though the thermodynamic fundamentals that were computed in this work for solving the Rankine cycle are the same as the ones [17] resorted to, our model considers heat transfer and pressure drop correlations that the reference does not include. Cost correlations were also added to our code, as [17] does not cover the cost of the system.

1. The pinch point location is unknown a priori. The temperature difference is computed in each node to find it.

2. Heat transfer coefficients and pressure drops calculations require the definition of the different heat exchanger sections in which the working fluid is in a different state (liquid phase, vapour phase or two-phase). Discretizing the heat exchangers allows to compute the vapour quality at each node and hence, to determine the fluid state, which is needed to resort to the right correlations.

Heat transfer coefficients and pressure drops are calculated after the states at the inlet and outlet of both heat exchangers are known. The heat transfer coefficient of the two-phase working fluid in the evaporator depends on the Boiling number, which, at the same time, is dependent on the heat flux. The heat flux can only be calculated if both the heat duty and the area are known, but the area is dependent on the overall heat transfer coefficient. This means that the heat transfer coefficient and the area of the primary heat exchanger depend on each other, but none of them is known a priori. In order to solve this problem, the MATLAB function *fzero* had to be included in the code. This function guesses a heat flux value, computes the overall heat transfer coefficient and checks if Equation 9.3 is true. In case it is not, the process is repeated in an iterative loop until suitable values for the heat flux and the overall heat transfer coefficient are obtained. Then, the heat transfer area can be calculated by relating the heat duty and the heat flux (Equation 9.4). This process is followed at each computed node.

$$\dot{q} - U_{PrHE} \cdot \Delta T_{LMTD} = 0 \qquad (9.3)$$

$$A = \frac{\dot{Q}}{\dot{q}} \qquad (9.4)$$

Once the required heat transfer surfaces are known, their associated cost can be computed.

Heat exchangers give rise to two different sources of irreversibility: pressure drops due to friction and the temperature differences between the interacting fluids when

exchanging the heat. Equations 9.5 and 9.6 are computed in the code to find the rate of exergy destruction in both cycle heat exchangers.

$$\dot{I}_{H.E} = \dot{m}_{hot} \cdot \left(e_{hot,in} - e_{hot,out}\right) - \dot{m}_{cold} \cdot \left(e_{cold,out} - e_{cold,in}\right) \qquad (9.5)$$

$$\dot{I}_{H.E} = \dot{m}_{cold} \cdot T_o \cdot \left(s_{cold,out} - s_{cold,in}\right) - \dot{m}_{hot} \cdot T_o \cdot \left(s_{hot,in} - s_{hot,out}\right) \qquad (9.6)$$

9.4.2 Expander and pump

The outlet states of both the expander and the pump can be calculated when the inlet state conditions and the component outlet pressure are known. At this point, resorting to the polytropic efficiency ordinary differential equation is necessary, which can be solved by means of the *ODE45* function in MATLAB.

$$\frac{dh}{dp} = \frac{1}{\rho} \cdot \eta_{polytropic} \qquad (9.7)$$

Once the inlet and outlet states are known, the first law of thermodynamics can be used to compute the expander power production and the pumps power consumption.

$$\dot{W}_{exp} = \dot{m} \cdot (h_{in} - h_{out}) \qquad (9.8)$$

$$\dot{W}_{pump} = \dot{m} \cdot (h_{out} - h_{in}) \qquad (9.9)$$

Results from Equation 9.8 allow to compute the cost of the expander and the electric generator, while the pumping power obtained from Equation 9.9 makes it possible to calculate the cost of the pumps.

The rate of exergy destruction of the expander and pumps can be computed according to Equations 9.10 and 9.11 respectively.

$$\dot{I}_{exp} = \dot{m} \cdot (e_{in} - e_{out}) - |\dot{W}|_{exp} = \dot{m} \cdot T_o \cdot (s_{out} - s_{in}) \qquad (9.10)$$

$$\dot{I}_{pump} = \dot{m} \cdot (e_{out} - e_{in}) - |\dot{W}|_{pump} = \dot{m} \cdot T_o \cdot (s_{out} - s_{in}) \qquad (9.11)$$

9.5 Solution algorithm

The cycle is solved in a sequential manner, meaning that, starting from the PrHE, the inlet and outlet states of each component are modelled one by one. Figure 9 shows the flow-sheet of the cycle optimization algorithm.

When the main MATLAB script is executed, all the input data from Table 5 and Table 6, and the degrees of freedom from Table 7 and Table 8 (with their corresponding bounds and constraints given in Table 9) are supplied to the cycle simulation main function.

This main function includes a series of "sub-functions" that allow to compute all the states of the cycle, heat transfer areas, pressure drops, cost components, and the second-law efficiency and Specific Investment Cost of the plant. All thermodynamic properties at each state are provided by means of REFPROP library function calls.

Once this is done, all constraints are evaluated and the objective function is computed. Then, the MATLAB algorithm checks if the constraints tolerance is violated. If it is, new values are assigned to the degrees of freedom and the cycle simulation starts again, following the same previously described steps. In case the constraints tolerance is within the limits, the optimality of the objective function is checked. If the objective function change is below the established tolerance (which depends on the defined objective function), the simulation stops, the results are saved in MATLAB, Excel and .txt files, and the diagrams of interest are plotted. If the objective function change is higher than the set tolerance, new values for the degrees of freedom are guessed by the Sequential Quadratic Programming algorithm within the MATLAB function *fmincon*, and the simulation starts again.

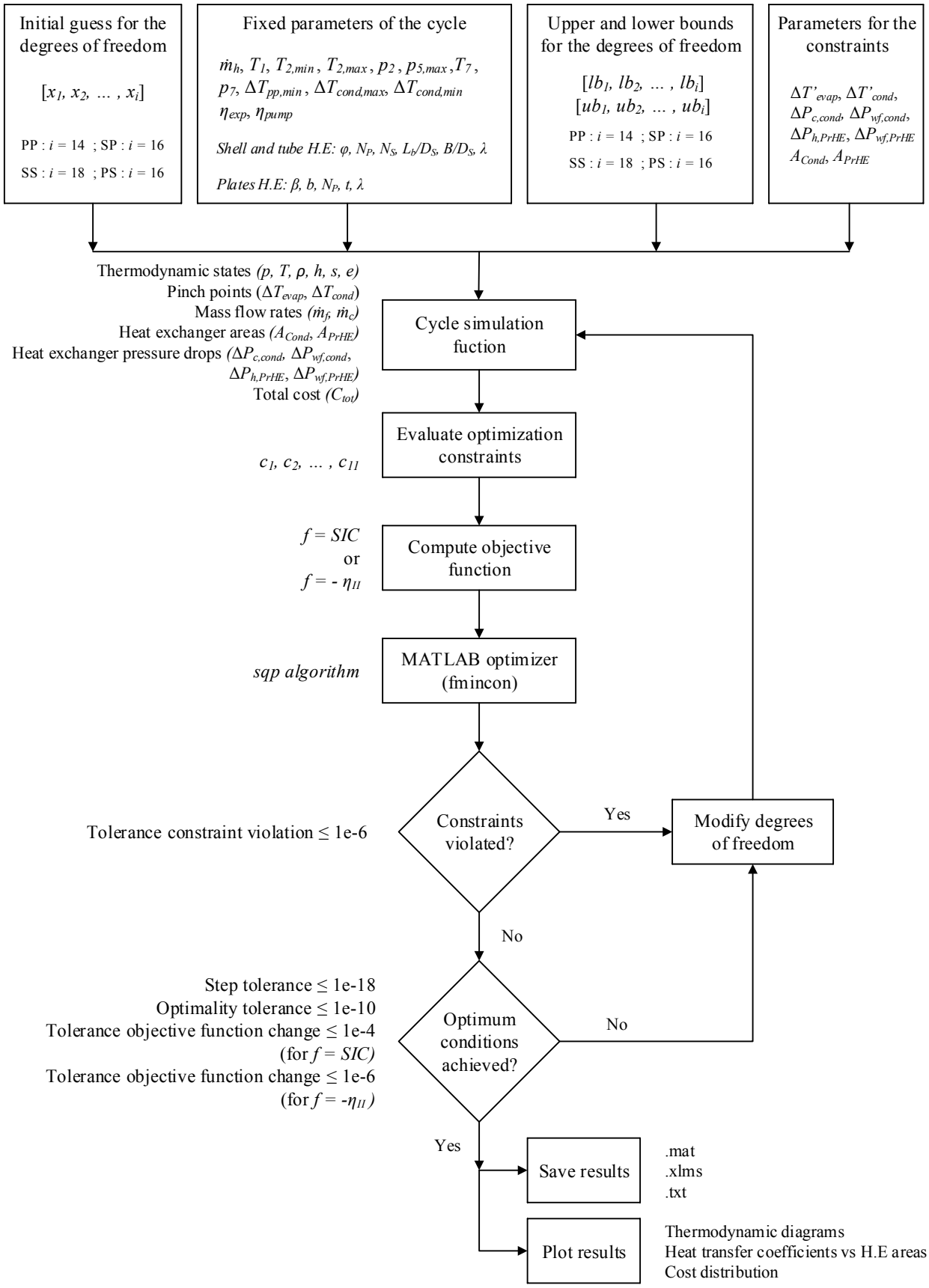

Figure 9. Cycle optimization algorithm flow-sheet

10 Results and discussion

10.1 Validation of the model

As it was stated in Section 1.6, the model validation is the main limitation that had to be faced when accomplishing this work. Even though a literature study was carried out in an effort to find any already existing model that could be used to carry out the validation, we finally came to the conclusion that it was not possible.

In this section, the reasons and challenges that have prevented the validation process from being carried out are going to be presented.

10.1.1 Validation challenges

The model that was constructed for this work requires the use of many different correlations in order to find the solution of two different and not-directly related objective functions: the system Specific Investment Cost and the cycle second-law efficiency. This means that cost correlations, heat transfer coefficient correlations, the laws of thermodynamics and pressure drop correlations had to be combined to develop the MATLAB code. Apart from this, the code allows for designing two different types of heat exchangers in detail, whose geometry parameters have a great impact on the results.

When carrying out a model validation, it is important to find a reference model with similar characteristics, allowing for a suitable comparison of the results. Considering all the variables and concepts that were combined for developing this work, it was not possible to find any model so detailed as ours in open literature.

- Cost correlations

We found in the literature that many different methods can be used with the aim of estimating the cost of installing a Rankine cycle, but only a few authors discuss the accuracy and validity of the results. Due to the lack of information related to the cost of

real installed Rankine cycle systems, each author resorts to different correlations, making it even harder to execute the validation process. Some authors use standard correlations, others, combine these standard correlations with their own-defined formulas, and others apply correlations extracted from different sources [69]. Most of authors turn to Turton's cost correlations, although Turton does not provide information for estimating the cost of the generator. Also, considering the great amount of different multiplying factors that can be applied to the cost correlations, differences between estimations for the same case study can be even wider (S. Lemmens [69] states that the accuracy obtained from the best techniques moves from 10% to 30%).

Furthermore, not all authors set the Specific Investment Cost of the plant as the objective function to carry out the techno-economic optimization. Most authors prefer to study the system cost with relation to the net energy output, instead of net power output. As in those cases results are expressed in €/kWh (instead of €/kW), it is not possible to use energy production based models for executing the validation, unless the yearly operating hours are given (which was not the case).

Important deviations can also be found with respect to monetary units. Some authors use dollars, while others resort to euros. Not only a ratio of conversion must be applied in case of carrying out the validation based on a model that resorts to a different monetary unit, but also the updated CEPCI must be included. The main problem related to this consideration is that, depending on the rate of change, results may experience large deviations from time to time.

- Heat transfer coefficients

With respect to the heat transfer processes, choosing suitable heat transfer coefficient correlations for each side of the heat exchangers consists on making modelling assumptions, due to the large increasing amount of available correlations that can be found in the literature. This choice compromises not only the design of the heat exchanger, but also the thermodynamic performance of the cycle.

Authors such as F. Táboas et al. [70] studied how heat transfer results may deviate when using different heat transfer correlations for computing the same heat exchange processes, concluding that deviations of more than 20% can be reached when applying 5 different heat transfer coefficient correlations to a single-phase heat transfer process in a plate heat exchanger. Disagreements are normally due to the definition of the different factors that correlations require for the heat transfer coefficient calculations. Among these factors, geometrical design parameters and thermodynamic working fluid properties are the most important ones.

Furthermore, apart from the great amount of different correlations that can describe the same heat transfer processes, the model of this work includes 4 different heat exchangers configurations.

- Assumptions and boundary conditions

Our model requires the definition of more than 30 input values (assumptions and bounds), in order to find the optimum solution of a set of 14 degrees of freedom or more. This means that, in case the model results want to be compared with literature data, more than 50 inputs should be provided to the cycle computation. None of the studies that were found in open literature gives such a detailed information of their developed models, making it impossible to simulate similar case studies. This is of main importance considering that criteria such as the evaporation and condensing pressures, or any of the H.E geometry design parameters, have a great impact on the results, meaning that small changes of their value lead to great results deviations.

The working fluid selection is also a degree of freedom that needs to be taken into consideration when executing the model validation. Considering that fluid transport properties are fundamental for determining the efficiency of the heat transfer processes and the size of the system components, this fact reduces the list of possible studies that could be used for executing the model validation even more.

10.1.2 Conclusions for the model validation

From all the given reasons, it was finally concluded that validating the model that was developed for this work is not possible. In order to guarantee the highest reliability of the results, an effort was made to find the original literature sources of all correlations, and correcting all possible mistakes derived from their use in other works. Also, the obtained results will be compared with the ones found in the literature, in order to find out if their tendency is similar. Therefore, each one of the listed conclusions presented in Chapter 11 will be accompanied by a brief comparison with literature studies. This is in agreement with the only one study related to systems cost validation that could be found in the literature (carried out by S. Lemmens in [69]). After having executed an exhaustive analysis for its model validation, this author concluded that exact outcomes are not as important as the proportional comparison, meaning that results are always relative when talking about industrial processes cost estimates.

10.2 Different heat exchanger configurations results

Considering the great amount of different types of heat exchangers that might be used to build a Rankine cycle and the different configurations that their combination allows for, we decided to study the four different configurations that could be implemented in the cycle with the shell-and-tube and the plate heat exchangers. This way, finding out which heat exchanger configuration and which working fluids give the best results for the given starting case study can help to determine the most likely configuration to reach the lowest SIC for any other considered case study.

10.2.1 General results

The two different types of heat exchangers that were presented in Section 3.4.2 can be combined in 4 different ways. These 4 configurations have been implemented and simulated by means of the MATLAB code developed in this Master thesis, including all the associated correlations and formulas that are required to solve the cycle. All simulations were run for the initial case study presented in Section 9.1, and for the 18

working fluids that remained after the fluid screening selection process. The defined objective function is the SIC of the plant. The obtained results for all working fluids can be found in Appendix D (Table B), while results for isobutane and C2-Butene are shown in Table 11, as they will be further studied in this section.

Table 11. Different H.E configurations results for isobutane and C2-Butene (SIC optimization)

Working fluid (Class)	**T_{max}/T_{crit} [K/K]**	**Conf.**	**SIC [$/kW]**	**η_{II} [%]**	**Evaporator area [m^2]**	**Condenser area [m^2]**	**Power output [kW]**
Isobutane (Alkane)	0.964	PP	4112.97	32.52	119.17	184.70	234.08
		SP	4485.26	28.69	169.05	161.28	206.48
		PS	6553.39	19.59	261.32	178.57	141.08
		SS	7309.21	18.77	121.43	309.07	135.15
C2-Butene (Alkene)	0.902	PP	4365.78	28.72	106.55	185.25	206.78
		SP	4382.23	25.92	135.17	120.66	186.47
		PS	5739.46	20.36	48.24	218.40	146.63
		SS	7322.22	17.21	156.80	244.13	123.88

Figure 10 shows the SIC results for each one of the different simulated working fluids and heat exchanger configurations, as a function of the T_{max}/T_{crit} relationship. As it can be seen, for all the possible heat exchanger configurations we can implement in the Rankine cycle, the working fluids reaching the lowest SICs are those ones that present a T_{max}/T_{crit} between 0.97 and 1.02. Among all of them, ammonia gives the best results.

The SIC increases with the T_{max}/T_{crit} for values higher than 1.02, although this rise is not too remarkable. What is more, R32, with a T_{max}/T_{crit} = 1.119, presents one of the 5 lowest SICs, which is even lower than the one obtained for cyclopropane for the PP and SP configuration cases. This means that this working fluid presents one of the best results even though its temperature ratio is not within the defined limits of 0.97 and 1.02. The reason is that it is a wet working fluid, and the expansion allows for a low degree of super-heating at the outlet of the expander, which leads to small pre-cooling surfaces that imply important condenser cost savings. The same basis applies to ammonia, whose wet nature turns it into the best working fluid choice for all the different H.E configurations.

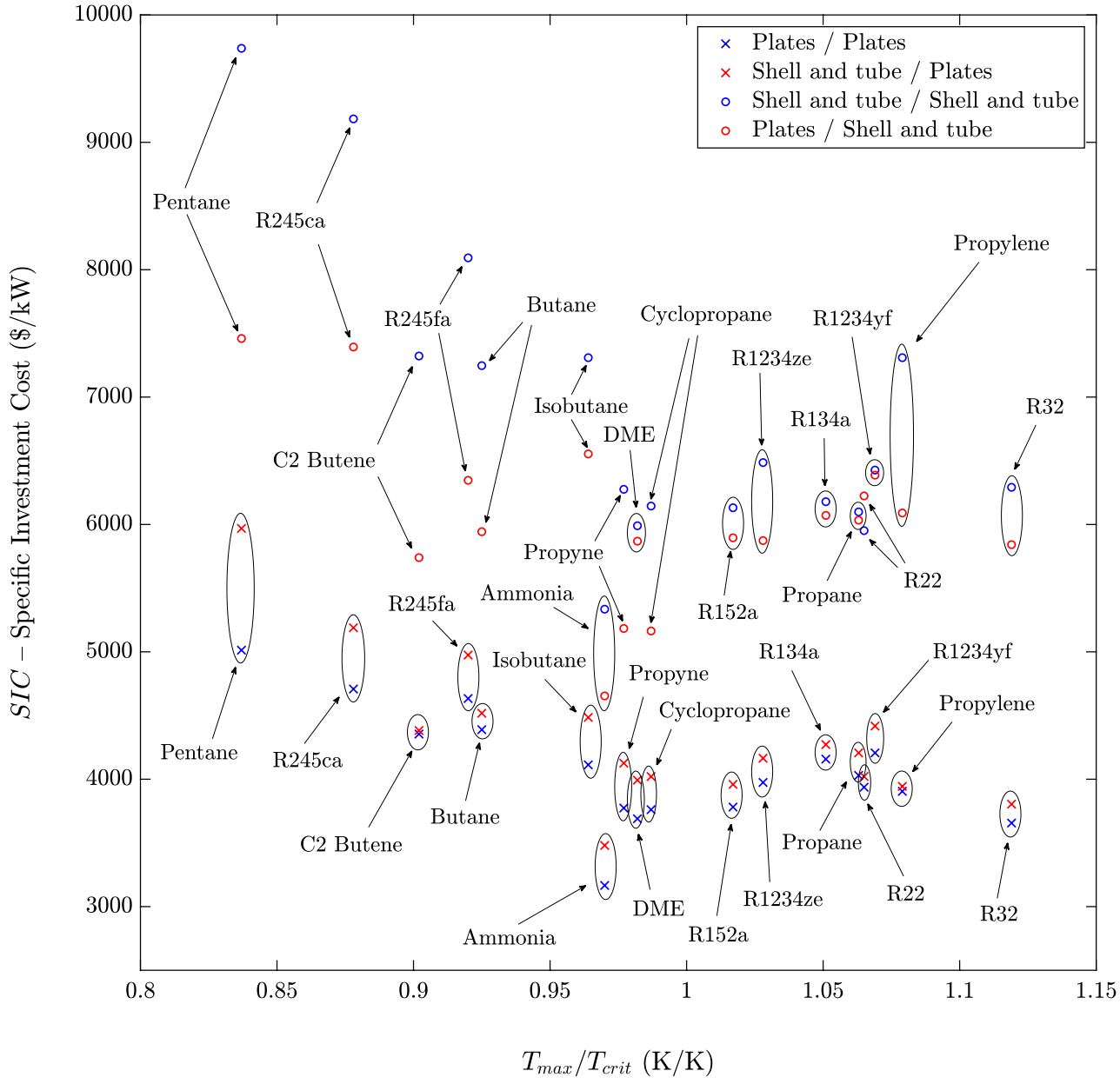

Figure 10. SIC vs T_{max}/T_{crit} for all the different studied heat exchanger configurations and working fluids

It has to be pointed out that a maximum working pressure limitation had to be set during the simulations ($0.9 \cdot p_{crit}$) in order to avoid transcritical cycles or to operate too close to the critical pressure. All working fluids with a T_{max}/T_{crit} higher than 1.02 tend to reach the maximum allowed pressure, so we can expect the results to improve as the maximum

allowed pressure limitation is increased. This means that it is likely that all these working fluids reach better SIC results when operating under transcritical conditions, although limitations in our model did not allow to check it.

On the other side, working fluids with a T_{max}/T_{crit} lower than 0.97 present a high SIC that tends to increase as the temperature ratio is lower. The reason is that, for this kind of working fluids, meeting the constraints implies operating at pressures much lower than the critical one and with low pressure ratios, leading to reduced power outputs and lower densities and temperatures that entail larger heat transfer surfaces because of the deteriorated working fluid HTC. This effect worsens as the working fluid critical temperature increases.

Among the low-temperature-ratio working fluids, isobutane and butane are remarkable cases, as their SICs are considerably high even though their temperature ratio is not much lower than 0.97. The reason is that these working fluids are dry, meaning that high degrees of super-heating are reached at the outlet of the expander, even if the super-heated vapour temperature at the outlet of the primary heat exchanger is not too high. This has a negative impact on the required condenser pre-cooling surface, which leads to large and costly condenser areas. This consideration, together with the better results that have been previously described for ammonia and R32 (wet working fluids), confirm that, among the working fluids with a similar T_{max}/T_{crit}, wet working fluids allow to reach lower SICs than isentropic and dry working fluids.

By comparing the different H.E configuration results, it can be clearly observed that the PP configuration gives the lowest SICs for all the simulated working fluids, mainly because of the small heat transfer surfaces that both the PrHE and the condenser require. Also, due to the high overall heat transfer coefficients that plate heat exchangers present, increasing the working fluid degree of super-heating does not lead to a notable increase of the heat transfer areas, allowing for higher power productions able counteract the slight higher cost of the components.

For all working fluids, the best heat exchangers configuration is the PP, followed by the SP, the PS and, finally, the SS. If we compare the best and the worst configurations (PP

and SS respectively), the greatest deviation (200%) is observed for R245ca, while the lowest one is reached for R134a (lower than 50%). When comparing PP and PS configurations, the results deviations move from 31.5% (C2-Butene) up to 60% (R32). Finally, SIC deviations between the two best configurations are not so big, and they tend to increase as the working fluid critical temperature increases. This highlights how important the evaporation pressure limitation is for the primary heat exchanger cost, and hence, the system SIC, and the different impact it has on the results depending on the kind of heat exchanger that is used as the cycle evaporator. SIC deviations between SP and PP configurations reach a maximum for pentane (19.03%), and a minimum for C2-Butene and propylene (lower than 1%).

In order to analyse how the cycle behaves when resorting to one H.E configuration or another, particular cases for two different working fluids are going to be presented. These working fluids are C2-Butene and isobutane, and they were chosen as the object of the analysis because of the noticeable differences that could be seen when looking at their T-s diagrams. The objective of this analysis is then to show that the behaviour of the cycle is not only dependent on its configuration, but also on the working fluid choice.

10.2.2 Specific case: C2-Butene

Figure 11 shows the T-s diagrams for the 4 different simulated heat exchangers configurations when C2-Butene is used as the working fluid. As it can be seen, the degree of super-heating is almost negligible in all cases, with exception of the PP configuration.

For those configurations using the shell-and-tube heat exchanger as the PrHE, increasing the degree of super-heating implies appreciable larger heat transfer surfaces, which, in most of the cases, are not compensated by the resulting increased power outputs. For the PS configuration, using a plate PrHE entails high heat transfer coefficients whose associated heat transfer areas can justify the increased vapour temperature at the outlet of the mentioned component. However, its combination with the shell-and-tube condenser brings up with a problem: even though the required increased PrHE super-heating heat transfer surface is low, the higher turbine inlet temperature does also imply an increased

turbine outlet temperature, and hence, more heat must be rejected in the pre-cooling section of the condenser. This fact, together with the lower overall heat transfer coefficient that drives the heat exchange process in the shell-and-tube condenser, entails large condenser surfaces that cause prominent increments of the SIC (despite of the higher cycle power output).

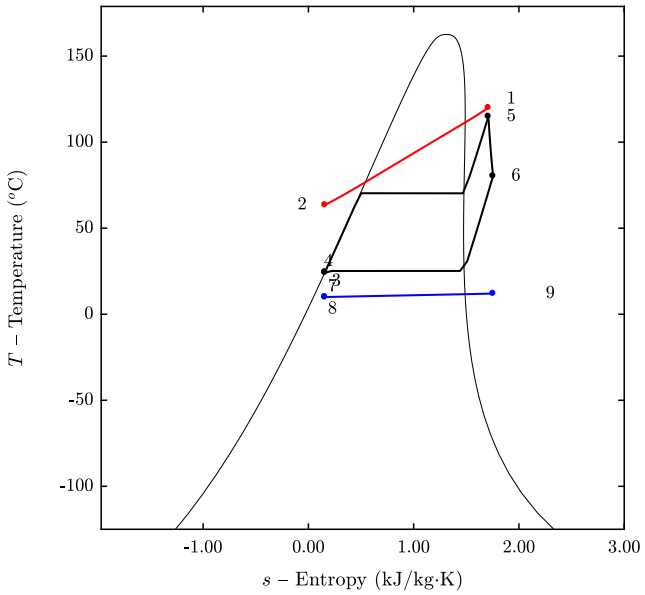

PP. Degree of super-heating= 44.68 ºC

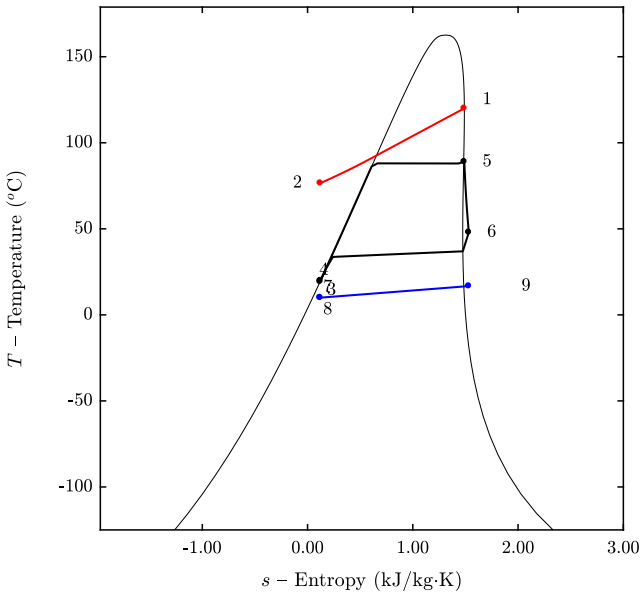

PS. Degree of super-heating = 1.02 ºC

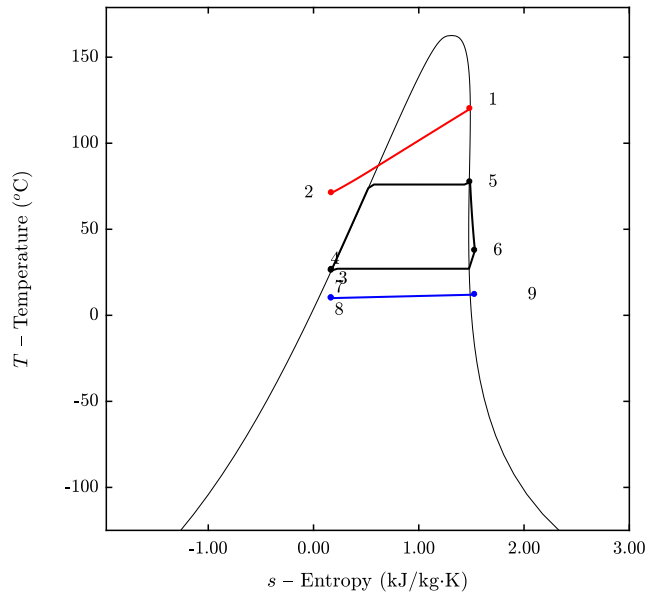

SP. Degree of super-heating = 1.44 ºC

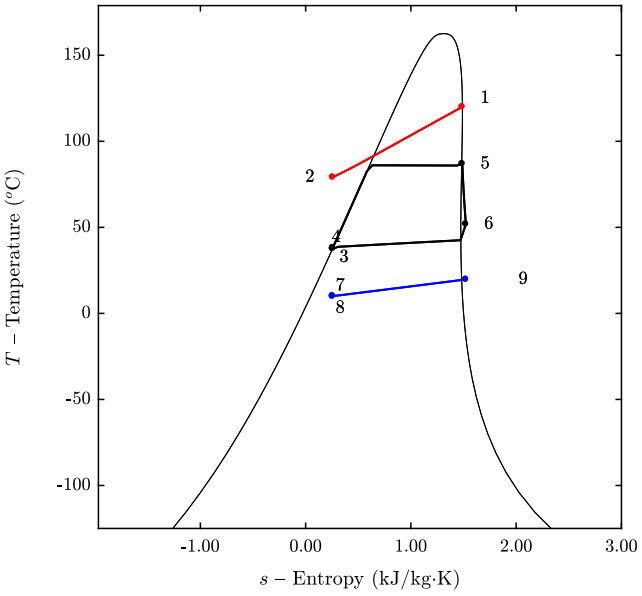

SS. Degree of super-heating = 0.99 ºC

Figure 11. C2-Butene T-s diagrams for the 4 different heat exchanger configurations

10.2.3 Specific case: Isobutane

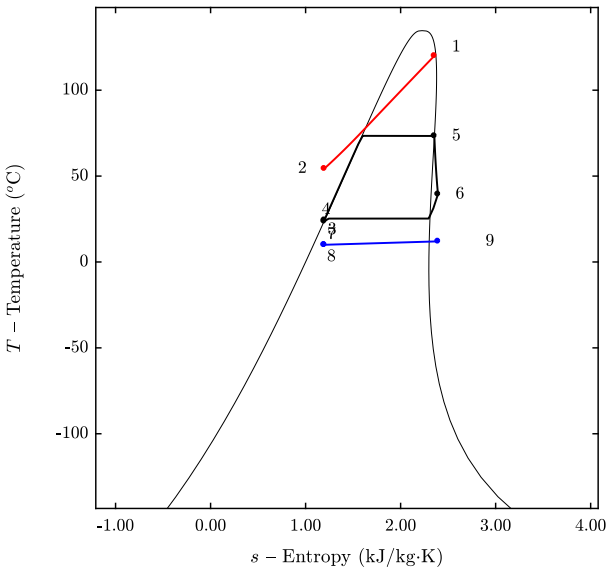

PP. Degree of super-heating= 0 ºC

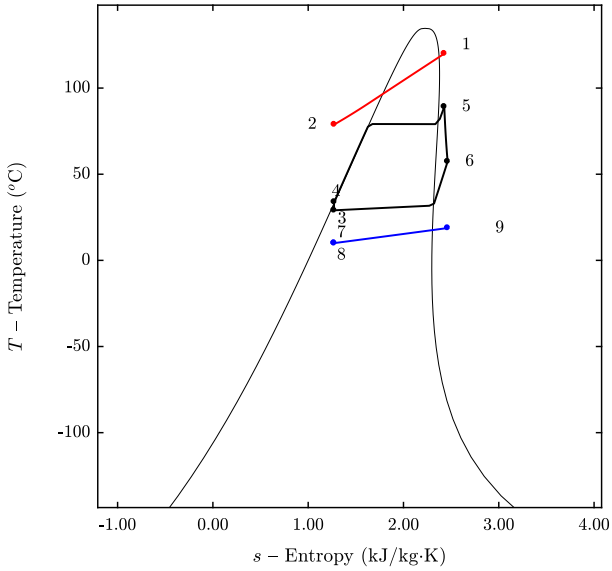

PS. Degree of super-heating = 25.18 ºC

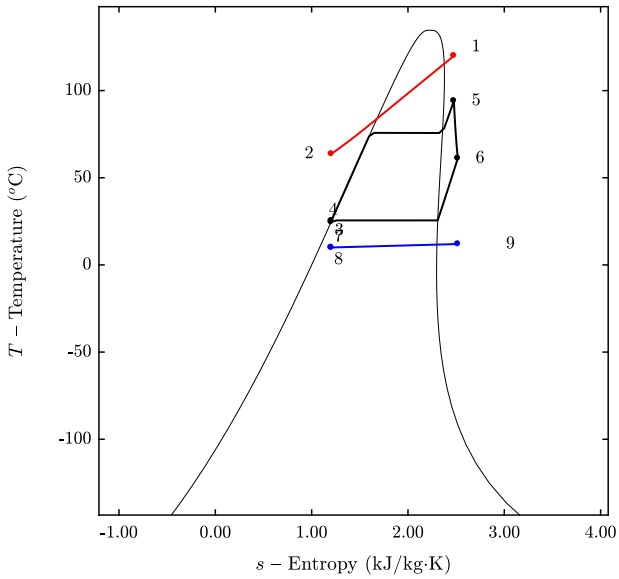

SP. Degree of super-heating = 18.47 ºC

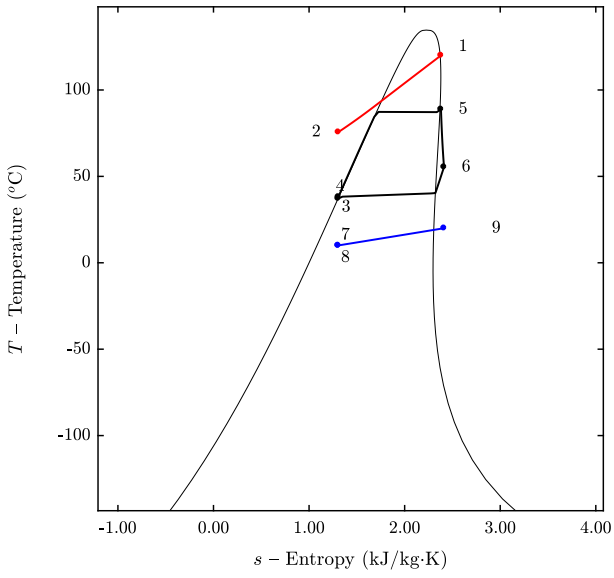

SS. Degree of super-heating = 1.65 ºC

Figure 12. Isobutane T-s diagrams for the 4 different heat exchanger configurations

The behaviour that C2-Butene shows for the different H.E configurations is not the same as the one the rest of working fluids present. DME, isobutane and pentane, among others, do not reach the best SIC results when the degree of super-heating at the inlet of the turbine is high. The reason is that the heat transfer coefficients these working fluids

present are not high enough to guarantee a low increase of the primary heat exchanger surface when the temperature of the working fluid out of this component rises.

Figure 12 shows the T-s diagrams for the different simulated heat exchanger configurations when isobutane is used as the cycle working fluid. As it can be seen, there are important differences between the PP configuration T-s diagram and the rest of H.E configurations T-s diagrams. Among these differences, the most remarkable ones are that no degree of super-heating is reached at the outlet of the PrHE and that the hot source outlet temperature is much lower than for the rest of configurations. By analyzing the results, we found that the optimum evaporation pressure for the PP configuration is the lowest one among all the different configuration results, while its cycle power output is the highest one. Also, isobutane mass flow reaches its highest value when used in the PP Rankine cycle. These assertions lead to the conclusion that, for isobutane PP case, the higher power production that can be achieved by increasing the evaporated working fluid mass flow leads to better SIC results than the fact of increasing the power output by increasing the degree of super-heating.

When both heat exchangers are of the shell-and-tube type (SS configuration), the condensation pressure tends to increase in order to find smaller heat transfer surfaces caused by the increasing temperature differences between the cooling water and the working fluid. Because of the much lower HTC that isobutane presents in the shell-and-tube condenser, its LMTDs are the highest ones among all the studied H.E configurations. This means that the expansion process is limited in SS cycles, leading to poor power outputs. The same condensing pressure tendency applies for the PS configuration, although, in this case, the greater condenser sizes that the increasing LMTD entails, can be slightly compensated with certain degree of super-heating to increase the power output, as the plate PrHE has a better overall heat transfer coefficient that allows for not so large heat transfer areas when increasing the vapour outlet temperature.

Therefore, for both analyzed working fluids, the degree of super-heating is dependent on the balance between the required heat transfer area and the power production. The vapour temperature out of the primary heat exchanger keeps on increasing until the increased net power output cannot compensate the higher cost that larger heat exchangers entail. From

the results, the point at which this balance is found is closely related to the working fluid properties, meaning that it is not possible to predict the cycle behaviour a-priori only by considering the cycle heat exchangers configuration.

We have aforementioned that C2-Butane and isobutane do not show the same results nor tendencies when analysing their performance under different H.E configurations. However, there is something that can be observed in both Figure 11 and Figure 12: the temperature jump that the cooling water experiences is much higher when the condenser is a shell-and-tube heat exchanger than when it is a plate heat exchanger. The reason is that the pressure drop that the cooling water experiences in the shell is much higher than the one it suffers in the channels of the plates (for the same cooling load). Considering that pressure drop limitations were set when running the simulations to avoid too poor cycle performances, the shell-and-tube condenser tends to resort to low cooling water mass flows to meet the defined constraints. On the other side, the pressure drop that the sink water experiences through the channels when the condenser is made of plates, does not constitute a limitation, and its mass flow tends to reach the highest value that the volumetric flow constraint allows for. For isobutane case, the sink temperature jump is 10 ºC (the maximum allowed), with a cooling water mass flow lower than 42 kg/s for both PS and SS configurations, while, for the PP and SP configurations, the temperature jump that the water presents finds the minimum value (2 ºC), and the mass flow reaches values of 301.81 kg/s and 257.96 kg/s respectively. Considering that the mass flow is one of the parameters that has the greatest impact on the heat transfer coefficient calculations (because of its direct influence on the Reynolds number), the fact of working with low mass flows causes important overall heat transfer coefficient drops, leading to larger condenser surfaces[22].

[22] It has to be considered that we are assuming water as the cooling fluid and that the pumping power is not affecting the system performance much (hence, great cooling flows can be used). In addition, we are also assuming that there is infinite access to water and high mass flows are not a problem. In many geothermal applications there is little, or no water at all, available for the cooling. In these cases, air-cooled-condensers with a much higher associated fans power consumption need to be used, and the cooling mass flows and temperature jumps are expected to be different.

- Isobutane primary heat exchanger

In order to analyse how the heat transfer coefficients evolve along the cycle heat exchangers, Figure 13 shows the primary heat exchanger heat transfer coefficients evolution for isobutane case and for the 4 different H.E configurations.

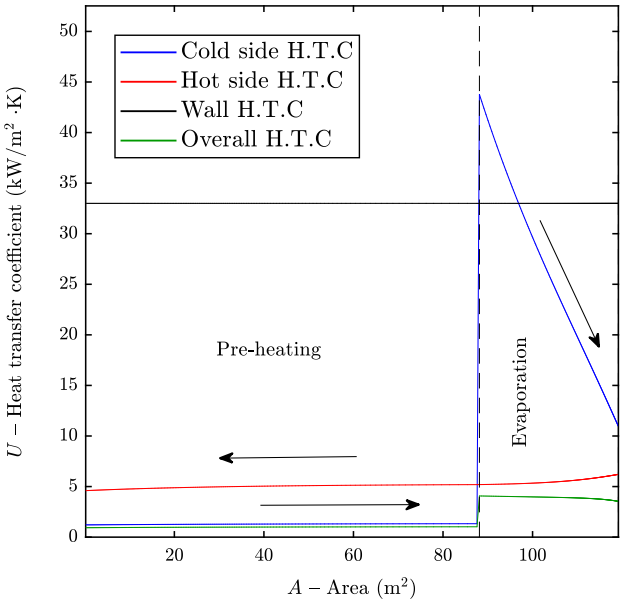

PP. PrHE area = 119.17 m²

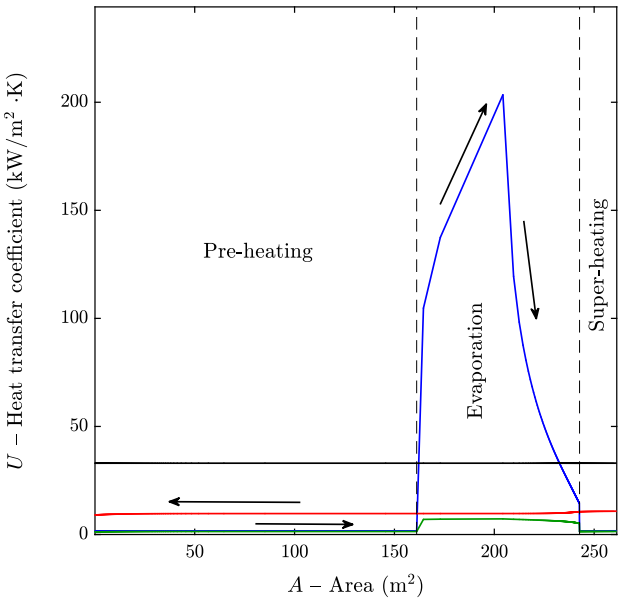

PS. PrHE area = 261.32 m²

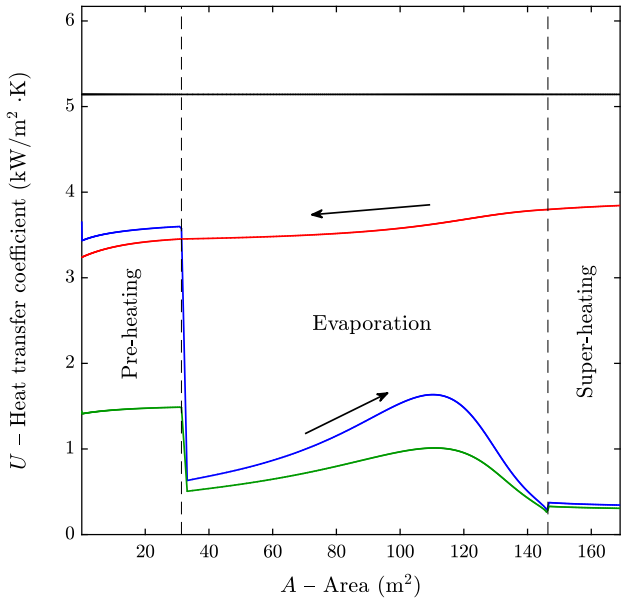

SP. PrHE area = 169.05 m²

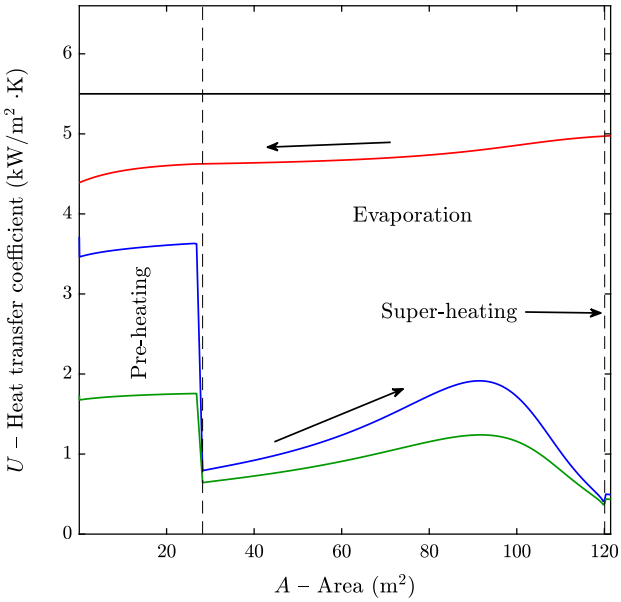

SS. PrHE area = 121.43 m²

Figure 13. Primary heat exchanger heat transfer coefficients evolution for the 4 different heat exchanger configurations (isobutane case)

As it can be seen in the figure, the shape of the HTCs evolution is dependent on the type of heat exchanger that is used. In order to make the HTCs analysis easier, the PrHE analysis will be divided in three different sections:

- Pre-heating section: When the PrHE is made of plates, the overall HTC in the pre-heating section is lower than when a shell-and-tube primary heat exchanger is preferred, meaning that the former requires larger pre-heating surfaces (87.59 m^2 and 164.52 m^2 for the PP and PS configurations respectively, and 33.17 m^2 and 28.30 m^2 for the SP and SS configurations respectively).

- Evaporation section: The overall HTC considerably increases in the evaporation section when resorting to the PP and PS (plate primary heat exchangers) configurations, leading to smaller evaporation areas than the ones that the SP and SS configurations require.

- Super-heating section: The extra heat transfer surface that is required for the super-heating process depends on the working fluid HTC and on the degree of super-heating that needs to be reached. For example, the PS configuration requires smaller areas to reach higher degrees of super-heating than the SP configuration (14.67 m^2 and 25.18 ºC against 20.27 m^2 and 18.47 ºC). The reason is that plate heat exchangers present a much higher overall HTC in the super-heating section than the shell-and-tube heat exchangers (approximately 1600 W/m^2K against 350 W/m^2K).

Something that is also visible in Figure 13 is that the working fluid constitutes the limiting thermal resistance only in the pre-heating and super-heating sections when using plate primary heat exchangers, being coincident with the sections that require the largest heat transfer surfaces. For being able to generalize these results, the HTC evolution in the plate PrHE was checked for the rest of working fluids, and they all showed the same tendency as isobutane.

On the other side, the working fluid acts as the fluid limiting the heat transfer process in all sections of the PrHE for the SS configuration, something that is again shared by all working fluids.

Regarding the SP configuration, isobutane limits the heat transfer process in the evaporation and super-heating sections, while, in the pre-heating section, its HTC value is slightly higher than the one obtained for the heat source. As this difference is so small, it can be considered that the working fluid and the hot-side fluid share the HTC impact on the heat transfer process. When taking a look at the rest of working fluids, most of them (such as DME, pentane, R245ca or R245fa) show the same tendency as isobutane, although others like R1234yf, propane or propylene do not. For these last mentioned working fluids, the hot source fluid and the working fluid do also share the impact on the overall PrHE heat transfer coefficient, although this time the working fluid HTC is a bit lower than the heat source heat transfer coefficient. For both SS and SP configurations, the evaporation surface represents a high percentage of the total PrHE surface.

Even though configurations PP and PS resort to the same kind of primary heat exchanger, important differences can be found for the HTCs evolution and heat exchanger areas. For instance, in the pre-heating section, the overall heat transfer coefficient for the PP configuration is around 1000 W/m^2K, while, as it was before stated, it has a mean approximated value of 1600 W/m^2K in the PS case (the difference is even more remarkable in the evaporation section). The reason is that the PS configuration tends to work at higher evaporation pressures (16.91 bar against 12.27 bar) to reach higher power outputs that can counteract the larger condenser areas that the shell-and-tube condenser requires. This is also the reason why the PS configuration shows the need of reaching certain degree of super-heating at the outlet of the PrHE, while the PP configuration does not. Therefore, the cycle parameters determine the HTCs and, at the same time, the H.E technology determines the optimal cycle parameters.

- Isobutane condenser

Figure 14 shows the evolution of the HTCs in the condenser for the 4 different possible configurations. Once again, it can be seen that the kind of installed heat exchanger

determines the shape and tendency of the heat transfer coefficient evolution along the component, mainly due to the differences in geometry and also to the different empirical correlations. The working fluid limits the heat transfer process in all the condenser sections, no matter the kind of H.E configuration that is implemented. This is mainly due to the enormous cooling water mass flow that is used to condense the working fluid, which yields to high HTCs.

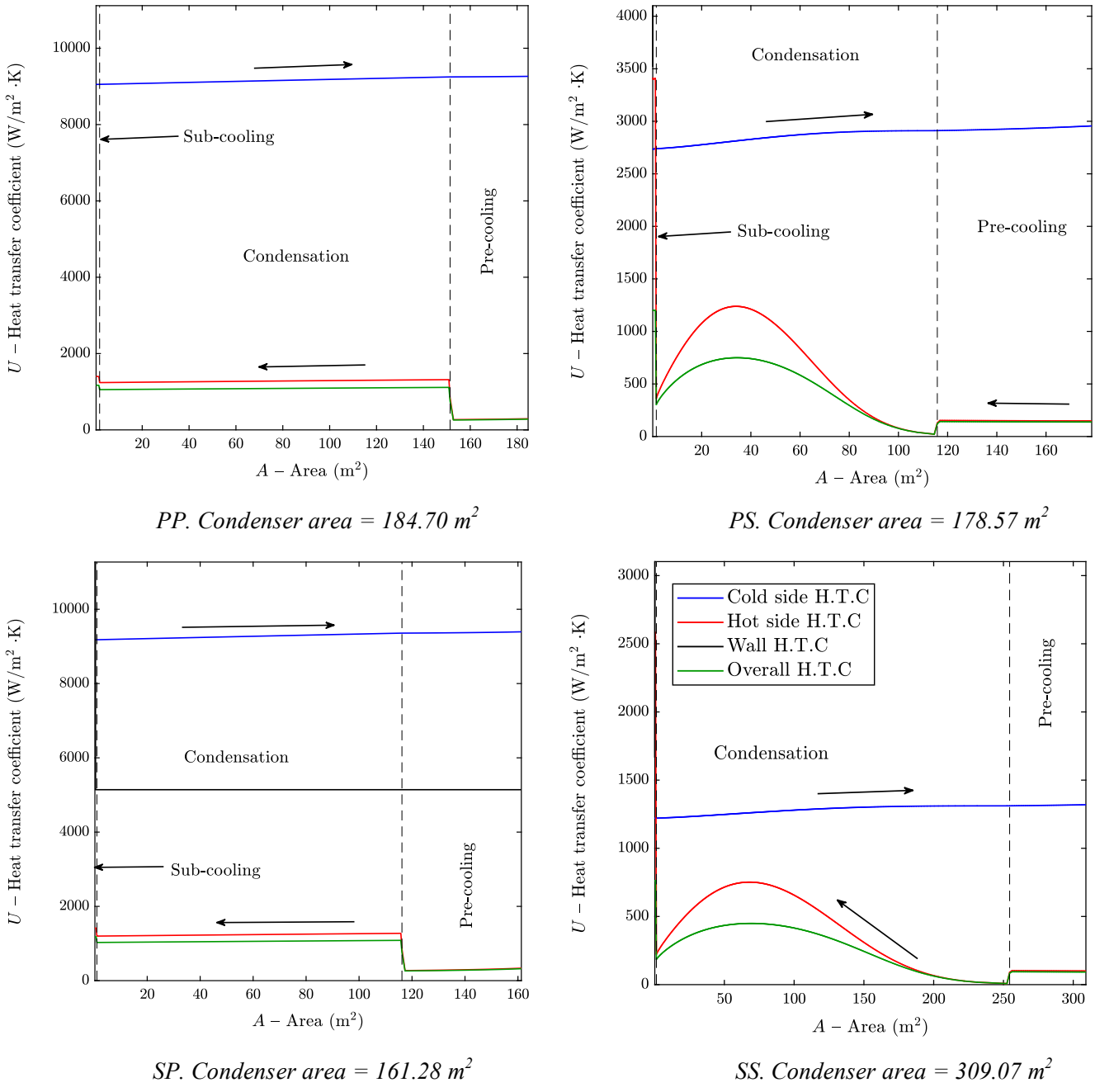

PP. Condenser area = 184.70 m²

PS. Condenser area = 178.57 m²

SP. Condenser area = 161.28 m²

SS. Condenser area = 309.07 m²

Figure 14. *Condenser heat transfer coefficients evolution for the 4 different heat exchanger configurations (isobutane case)*

In case of using a condenser made of plates, the overall HTC keeps an almost constant value along the entire condenser, with the exception of the pre-cooling section, in which the poor thermal conductivity of the vapour leads to low heat transfer coefficients. For the shell-and-tube condenser, the working fluid heat transfer coefficient experiences more visible variations when moving from one section to another. In the pre-cooling section, it is low and keeps a constant value until isobutane starts condensing. During the condensation process, the working fluid heat transfer coefficient reaches a peak, and then it decreases again until all the fluid is in the saturated liquid state. The considerably higher heat transfer coefficient that the working fluid presents in the liquid state leads to an almost negligible required sub-cooling surface, which is almost imperceptible in all plots.

The heat sink heat transfer coefficient increases as it absorbs the heat that the working fluid rejects (i.e. it increases with temperature), although this fact has a low impact on the overall heat transfer coefficient considering that the cooling water does never limit the heat transfer process. In spite of this, it is important to point out that the cold side HTC value experiences a much greater variation along the condenser for the PS and SS configurations because of the higher temperature jump it suffers, and that this heat transfer coefficient is much lower than the one obtained when plate heat exchangers are used as the cycle condenser. The reason for this last assertion is the lower cooling water mass flow that is required to meet the H.E pressure drop constraints, which results into lower HTCs. Even though the cold side heat transfer coefficient does not have a great impact on the heat transfer process, it determines how close the overall and the working fluid HTCs are. This means that the higher the cold water heat transfer coefficient is, the more important the working fluid heat transfer coefficient becomes for the heat exchange process. For this reason, in order to improve the overall plate condenser HTC, special attention should be paid to the working fluid thermal properties, while, for shell-and-tube condensers, there is still a margin to improve the overall heat transfer coefficient by improving the cold side HTC (although the effect is minor).

When comparing the SS and the PS configurations, it can be observed that the condenser heat transfer area is much higher in the first case than in the second one, even though the same type of heat exchanger is used. Despite of this, the pre-cooling surface that the PS configuration requires is higher than the one the SS configuration needs. The reason is

that higher working fluid temperatures at the inlet of the turbine do also imply higher temperatures at the outlet of the same component, and hence, at the inlet of the condenser (in the first case, the temperature of the working fluid when entering the pre-heating section is 84.24 ºC, while it only reaches a value of 55.39 ºC in the second one). For this reason, in order to bring the super-heated vapour to the saturated conditions, the PS configuration needs to reject more heat than the SS configuration, entailing larger pre-heating areas. We need to remember that the heat transfer coefficient in the PrHE was higher for the PS configuration than it was for the SS case, meaning that the heat could be better used to evaporate a higher amount of working fluid. This higher working fluid mass flow leads to higher HTCs in both the condenser and the PrHE, leading to the lower condensing surfaces that can appreciated in Figure 14.

Higher condensing pressures imply greater LMTDs and entail higher heat transfer coefficients that lead to smaller condenser heat transfer areas. In spite of this, increasing the condensing pressure does also limit the power production in the turbine. For this reason, the condensing pressure values that are reached when optimizing the SIC of the plant are set in order to find a balance between the higher power output that can be achieved when decreasing the condensing pressure and the larger condenser surface that is required when the condenser LMTDs and HTCs are reduced.

For those configurations that resort to the shell-and-tube condensers, the condensing pressure reaches in both cases (PS and SS) slightly higher values than 5 bar, while for the configurations that use plate condensers, the condensing pressure is around 3.5 bar. Considering that the heat transfer coefficient is much lower in the first two cases because of the heat exchanger design, the cycle SIC solution tends to reach increased condensing pressures in order to reduce the condenser surface by increasing the LMTDs, even though the turbine power experiences important drops. For the SP and PP configurations, increasing the power output can counteract the effect of reducing the heat transfer coefficients and LMTDs when decreasing the condenser pressure. The consequence is that the power outputs that are achieved for the PS and SS cycles do not surpass values of 150 kW in none of the cases, while, for the PP and SP cycles, power outputs higher than 200 kW can be achieved. This is something important to have into consideration when designing the expander component.

10.2.4 Component cost distribution

In relation with the component cost distribution, Figure 15 shows in a few bars plots the SIC share of the different Rankine cycle components, for all the simulated working fluids and heat exchangers configurations. As it can be observed, for all working fluids, the SIC reaches the lowest values for the PP configuration, followed by the PS, SP and, finally, the SS configuration. This is consistent with the results that were plotted in Figure 10, and reflects that the fact of resorting to shell-and-tube heat exchangers in Rankine cycles entails high SICs. The effect is much more remarkable when the shell-and-tube heat exchanger is set as the cycle condenser than when it is used as the PrHE.

By taking a look at the first two mentioned heat exchangers configurations (which employ plate condensers), it can be observed that their associated SICs are very similar. The slightly increased SIC that results from the use of a shell-and-tube PrHE is only a consequence of the increased cost of the same component, as the Specific Investment Cost of the rest of components remains almost constant.

The shell-and-tube condenser SIC has a meaningful importance in PS and SS configurations, as it represents a great percentage of the overall SIC of the system. While the cost distribution is more or less balanced between the turbine and the condenser when resorting to PP or SP configurations, in all PS and SS studied cases, the turbine does not represent a high percentage of the overall SIC, which is mainly covered by the condenser cost. For these last two mentioned H.E configurations, the condenser SIC represents more than 50% of the overall SIC, while for PP and SP configurations, there is no working fluid showing a condenser cost share higher than 40%.

The expander Specific Investment Cost is similar for all working fluids and heat exchangers configurations, although it is important to point out that this does not mean that its cost is the same. What is more, PP and SP configurations show a much higher turbine cost than the two other configurations (because of the much higher net power outputs the formers allow to achieve), although their cost/power relationship is almost the same. Table 12 summarizes the results obtained for the turbine cost and its associated Specific Investment Cost when butane is set as the system working fluid, affirming that,

even though this component can be considerably costly, a high net power output can counteract this effect when optimizing the Specific Investment Cost of the plant, making the most expensive turbines more attractive to reach low overall SICs.

In relation to the pumps cost, it represents a very low percentage of the overall SIC, although in cases such as R22, R1234yf, propylene, propane and R32 cycles, the SIC of these components reaches higher cost shares. For example, for propylene PS configuration, the pumps cost is 41 706.73 $ (with an associated SIC of 338.84 $/kW), while, for the same configuration, when pentane is the cycle working fluid, the pumps cost is 11 309.57 $, with a SIC of 118.09 $/kW. These 5 mentioned working fluids have the lowest critical pressure among all the studied ones, and they tend to operate at high pressures. These higher operating pressures imply higher power consumptions, but they do also entail higher power outputs that tend to reduce the SIC values of all components. By taking a look at the backwork ratio[23] (BWR), it increases with the T_{max}/T_{crit} relationship, meaning that, for working fluids operating at evaporation pressures close to the critical one, the pumping power consumption gains importance over the turbine power production and hence, the related pump SIC increases (for example, The BWR for propylene is 0.299, while it is only 0.024 for pentane).

Table 12. Turbine cost and SIC for different H.E configurations when butane is used as the working fluid

Configuration	Net power output [kW]	Turbine cost [$]	Turbine SIC [$/kW]
PP	208.59	238977.32	1622.13
SP	205.30	237040.00	1634.74
PS	139.22	181334.19	1844.20
SS	125.15	171734.60	1942.91

Finally, the generator SIC tendency when moving from one H.E configuration to another is exactly the same as the one the turbine SIC follows, because of being dependent on the turbine power production. Still, its contribution to the overall SIC is almost negligible.

[23] The backwork ratio is the relationship between the pumps power consumption and the turbine power output.

Once all the proposed heat exchangers configurations were analyzed for the 18 listed working fluids, the 5 working fluids giving the best results and the best heat exchangers configuration were chosen for carrying out the rest of the study presented in this work. These working fluids are: ammonia, DME, propylene, R32 and R152a. Also, benzene and pentane were included in the analysis in order to be able to generalize the results, as these two working fluids present much higher critical temperatures than the 5 previously mentioned ones.

Even though it was showed that the PP configuration gives the lowest SIC results when implemented in the cycle, the operational pressure and temperature limitations that these heat exchangers present (see Section 4.2) limit the flexibility of the power plant when it comes to exploit heat sources different from the geothermal one (such as waste heat recovery heat sources or other heat sources that provide heat at higher temperatures or pressures). For this reason, and with the aim of making our model more flexible and adaptable to different applications, the SP configuration was preferred to carry out the rest of the analysis.

When it comes to study how the different cycle parameters may affect the system efficiency or its cost, we can focus the study on a sensitivity analysis of many different factors. In the next sections, the study will be focused on how the heat source inlet temperature and its mass flow, and the sink inlet temperature, can affect both the thermodynamic cycle behaviour and the Specific Investment Cost of the plant. In order to do so, 5 different heat source inlet temperatures are going to be simulated (120 ºC, 150 ºC, 175 ºC, 200 ºC and 250 ºC), in combination with 3 heat source mass flows (10 kg/s, 25 kg/s and 50 kg/s), and 3 different cooling water inlet temperatures (5 ºC, 10 ºC and 15 ºC). This means that 475 different scenarios are going to be studied.

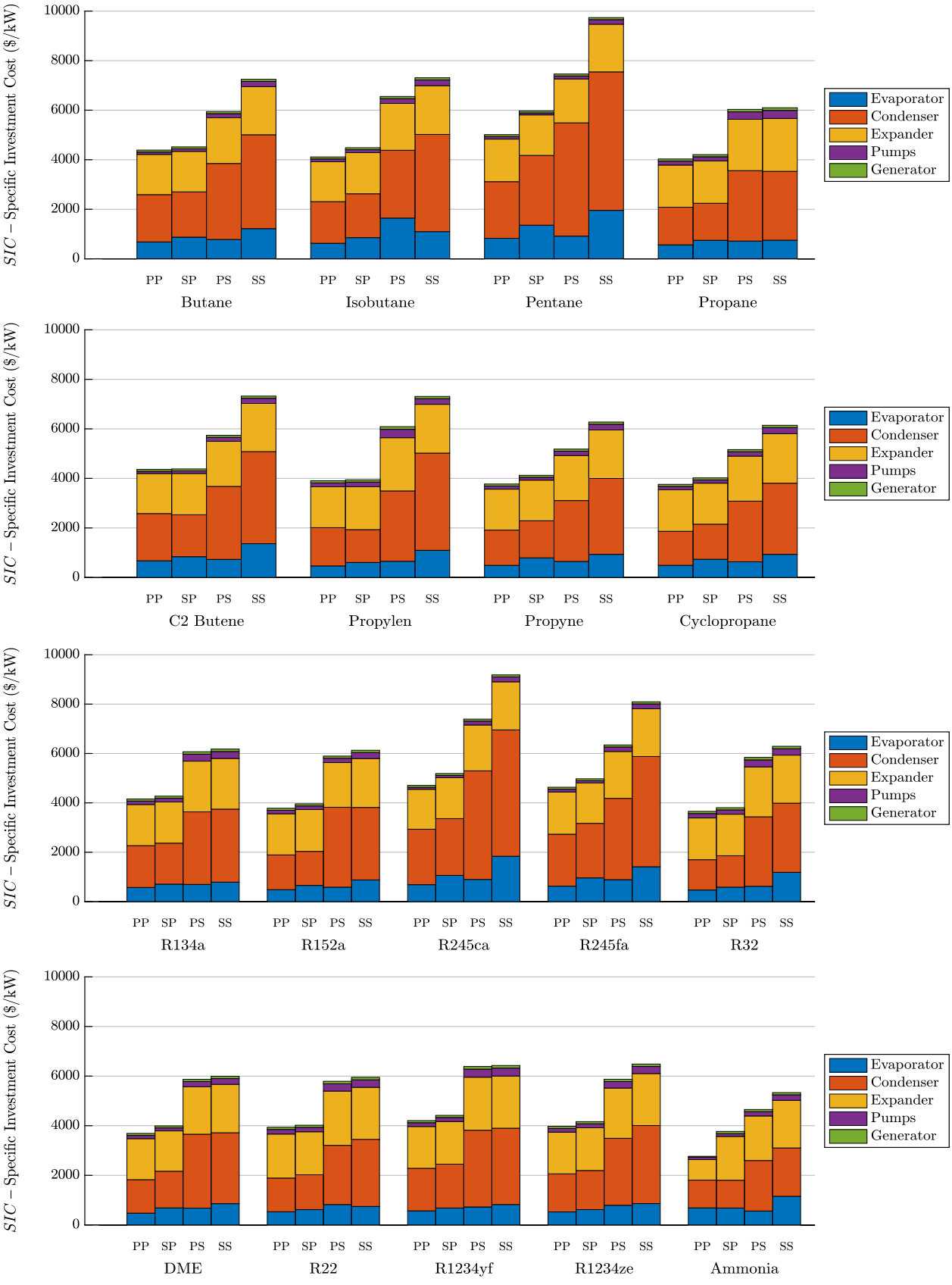

Figure 15. SIC component share for the different simulated working fluids and heat exchangers configurations

10.3 SIC optimization

Appendix E includes in Tables C, D, E, F and G, the obtained results for all the considered study cases when the SIC is set as the objective function. From these tables, diverse plots and graphs have been extracted with the objective of making the results analysis much more visual.

Figure 16 shows the SIC evolution as a function of the hot water and the cooling water inlet temperatures. All the represented data below to a 10 kg/s heat source case study, as the tendency that all results present for the rest of simulated heat source mass flows is the same. As it can be seen in the mentioned figure, increasing the heat source inlet temperature leads to lower SICs (Figure 17 allows for a better appreciation). However, the opposite happens when increasing the heat sink inlet temperature (as it can be better seen in Figure 18). When the sink inlet temperature is reduced, the working fluid allows the end of the expansion to reach lower condensing pressures, meaning that the cycle power output rises, leading to lower SICs (even though the condenser requires larger surfaces that imply higher costs).

Heat source inlet temperature variations from 250 ºC down to 120 ºC can cause SIC growths of more than 2400 $/kW for ammonia, more than 2000 $/kW for R32 and more than 2500 $/Kw for R152a. On the other side, increasing the sink inlet temperature from 5 ºC to 15 ºC supposes a SIC rise of more than 600 $/kW, 475 $/kW and 545 $/kW for the aforementioned working fluids. Considering that sink temperature changes are likely to happen because of the weather conditions variations between summer and winter, while a reduction of the heat source inlet temperature is only expected to happen as time passes and the heat source is exploited (specially for the case of geothermal reservoirs), we may expect that, in the short term, the condensing temperature will determine the SIC most important variations, while, in a long term, the heat source inlet temperature may have a much greater impact on the SIC of the plant.

By looking at the results from Figure 16, Figure 17 and Figure 18, it can be seen that the inlet sink temperature has a greater impact on the SIC results for ammonia, R152a and DME when the heat source inlet temperature is low than when it reaches its maximum

value. For ammonia, the SIC rise that arises when moving from a cooling temperature of 5 ºC to 15 ºC is around 608 $/kW for a heat source inlet temperature of 120 ºC, while it decreases as the heat source inlet temperature increases, reaching a SIC rise of only 76.83 $/kW at 250 ºC for the same heat sink temperature variation. For DME case, the difference moves from 446.40 $/kW at 120 ºC to 104.55 $/kW at 250 ºC and, for R152a, from 494.37 $/kW to 120.41 $/kW.

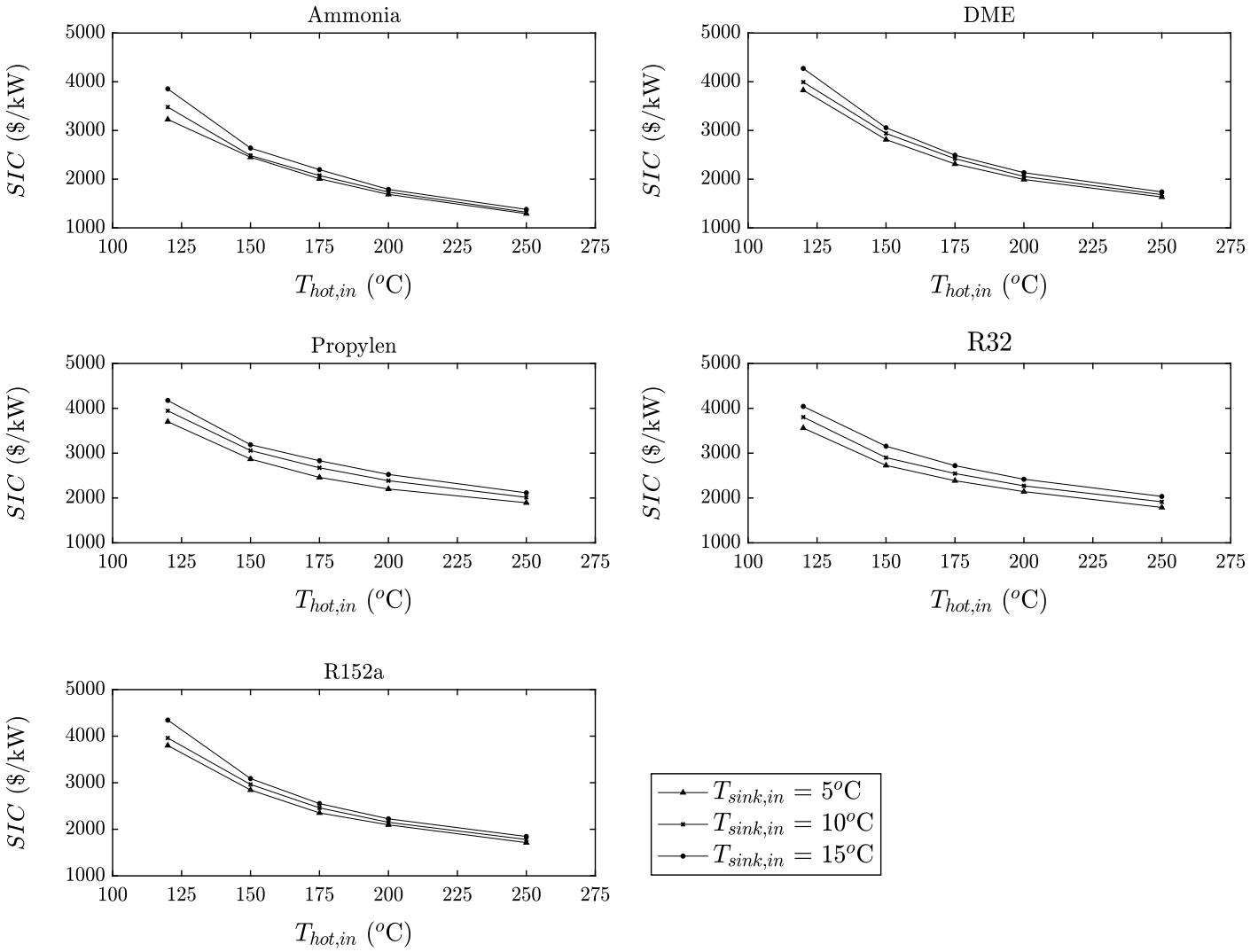

Figure 16. SIC evolution with the heat source and heat sink inlet temperatures ($\dot{m}_{hot}$ = 10 kg/s)

For R32 and propylene cases, even though higher sink water temperatures show a decreasing impact on the SIC of the plant as $T_{hot,in}$ rises, at 250 ºC it is still giving large SIC variations when it moves from 5 ºC to 15 ºC (245.46 $/kW for R32 and 221.40 $/kW for propylene). This means that the cooling water temperature has a greater

impact on the SIC of those cycles that resort to working fluids with higher T_{max}/T_{crit} relations. The main reason is that, as these working fluids present higher BWRs, the cycle net power output and power consumption are more susceptible to condensing and evaporation temperature changes.

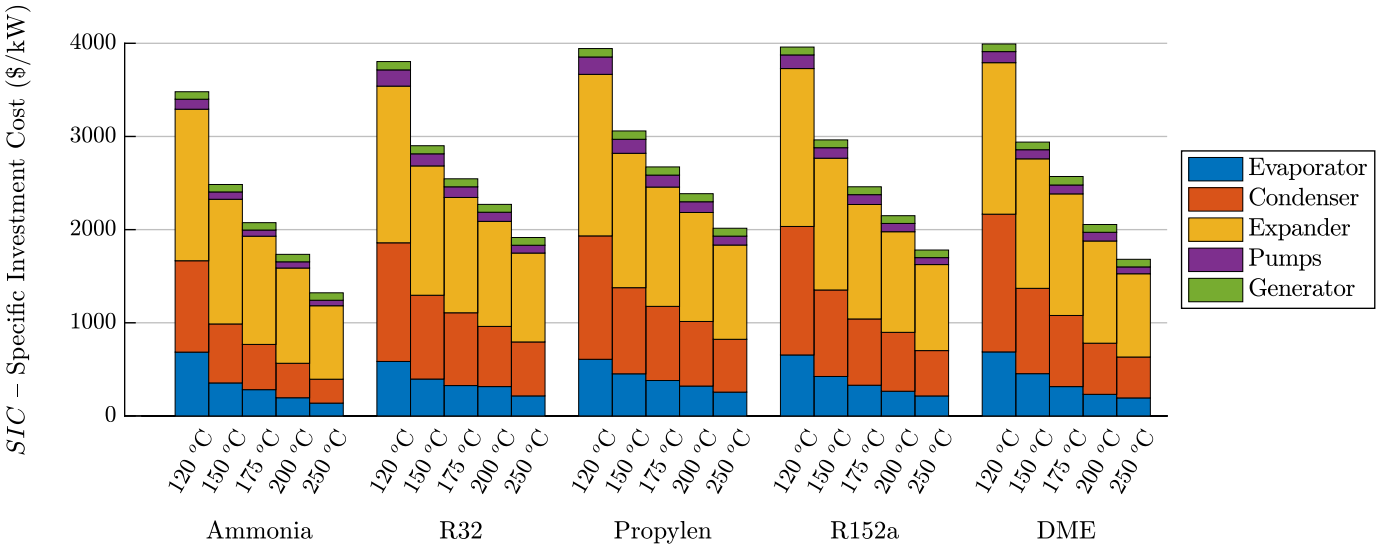

Figure 17. SIC evolution with the heat source temperature (bar graph)

($T_{sink,in}$ = 10 ºC, $\dot{m}_{hot}$ = 10 kg/s)

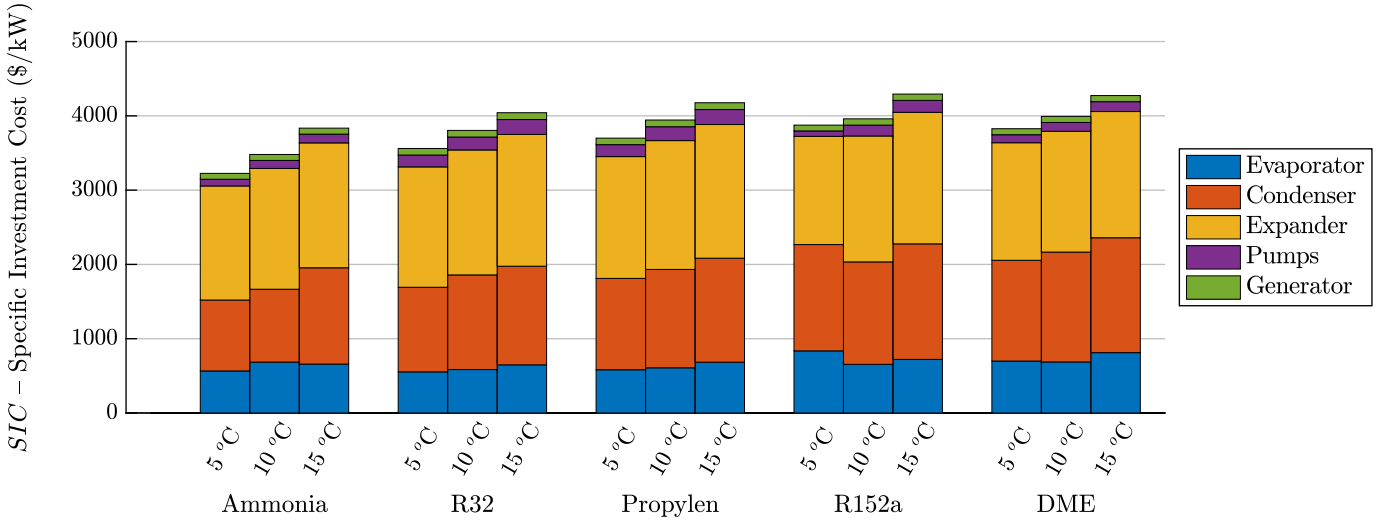

Figure 18. SIC evolution with the cold sink temperature (bar graph)

($T_{hot,in}$ = 120 ºC, $\dot{m}_{hot}$ = 10 kg/s)

We have before stated that all the different heat source mass flow scenarios give the same tendency results. However, it is important to point out that, even though the SIC tendency is the same, the SIC values are not; as the heat source mass flow increases, the SIC drops.

This is due to the fact that the increased amount of hot water that flows through the PrHE allows for a higher heat recovery, entailing larger heat exchanger surfaces whose associated greater cost can be counteracted by a higher power production to reduce the SIC. This does not mean that the cost of the plant decreases, but that the relationship between the cost of the cycle components and the power output does.

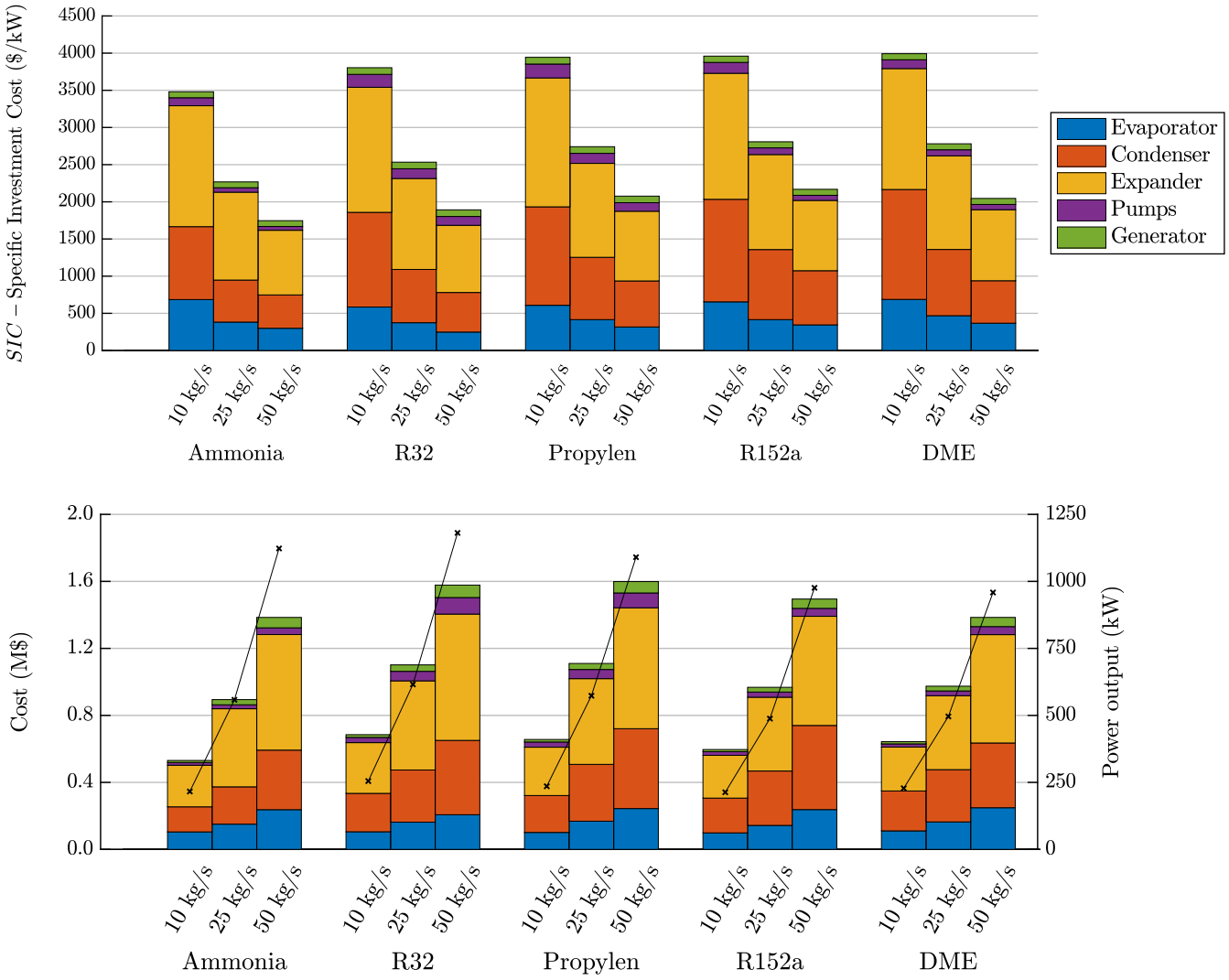

Figure 19. SIC, cost and power output evolution for different heat source mass flows ($T_{hot,in}$ =120 ºC, $T_{sink,in}$ = 10 ºC)

Figure 19 clearly shows how the SIC of the plant can be reduced by half when moving from the highest temperature heat source scenario (250 ºC) to the one with the lowest temperature (120 ºC), while the cycle cost is doubled. This effect is counteracted by an

increasing power output. For example, for a $T_{sink,in}$ of 15 ºC and a $T_{hot,in}$ of 120 ºC, ammonia cycle cost increases in more than 1.08 M$ when increasing the hot water mass flow from 10 kg/s up to 50 kg/s, while the power output rises from 191.236 kW to 987.95 kW, allowing for a SIC reduction of 1997.58 $/kW. This highlights the fact that constructing a large-scale Rankine cycle power plant is more expensive than installing a small-scale one, although the cost per produced kW can make it a more attractive choice for investors.

Table 13 shows the cost of the largest- and smallest-scale power cycles that can be designed for each one of the studied working fluids. The lowest power output cycles are achieved for a $T_{hot,in}$ of 120 ºC, a $T_{cold,in}$ of 15 ºC and a $\dot{m}_{hot}$ of 10 kg/s, while the highest ones are found for values of 250 ºC, 5 ºC and 50 kg/s respectively. As the table shows, for all working fluids, moving from the smallest-scale to the largest-scale Rankine power cycle has a high associated extra cost. However, the SIC in all cases is balanced and lessen by a considerably increased power output.

Table 13. Power output, cost and SIC for the largest- and smallest-scale Rankine cycle power plants

Working fluid	**Power output [kW]**	**Cycle cost [M$]**	**SIC [$/kW]**
Ammonia	191.24	0.74	3 852.904
	6 771.004	4.07	601.68
DME	195.26	0.83	4 273.118
	5 141.114	4.25	825.99
Propylen	212.12	0.89	4 293.103
	4 395.615	4.45	1 011.224
R152a	181.08	0.83	4 273.118
	5 113.595	4.53	886.69
R32	226.44	0.92	4 042.168
	4 465.878	4.25	951.18

Considering that the 5 working fluids we focused the study on, present a T_{max} close or higher than the critical temperature, it was found to be of interest to include in the analysis 2 more working fluids with lower critical temperatures, in order to find out if their associated SIC evolves in the same way. The chosen fluids are benzene and pentane, and

the analysis here presented includes the scenario of a variable heat source inlet temperature for a fixed $\dot{m}_{hot}$ of 10 kg/s and a $T_{cold,in}$ of 15 ºC.

It is important to highlight that special attention must be put to the high melting temperature that these two working fluids present at the ambient pressure when investigating their use in Rankine cycles, as the sink inlet temperature constitutes a limitation, not only because stablishing a condensing temperature limitation may worsen the efficiency of the cycle, but also because the working fluid may freeze if a too low sink heat temperature is reached (as it may happen during the coldest seasons). Benzene, for example, does not allow to work with a cooling water inlet temperature of 5 ºC.

Table 14 summarizes the obtained results for benzene and pentane. As it happened with the 5 previously analyzed and optimized working fluids, the SIC tends to decrease as the heat source inlet temperature increases. In this case, the SIC experiences a much more pronounced drop than the one it shows for the rest of working fluids, as the SIC that is obtained for low heat source temperatures is considerably high. This makes working fluids with high critical temperatures not to be attractive for low-temperature heat source applications. However, for high maximum cycle temperatures, the SIC reaches better values than the ones obtained for R32, R152a and propylene. The reason is that, at the highest hot source inlet temperature (250 ºC), benzene has not reached the maximum pressure limitation yet, while R32, R152a and propylene have, meaning that the former still has a high margin of potential of improvement.

If we plot in a graph the obtained SIC results for the 7 simulated working fluids as a function of the T_{max}/T_{crit} relationship (see Figure 20), we would see that, as the maximum temperature of the cycle increases, the plant SIC diminishes. It should be noted that the SIC variation is much more pronounced when T_{max}/T_{crit} increases from low values, while in those cases in which T_{max}/T_{crit} is high, increasing this relationship has a much lower impact on the obtained results.

Table 14. Benzene and pentane SIC optimization results

Working fluid	$T_{h,in}$ [ºC]	SIC [$/kW]	η_{II} [%]	Evaporator area [m²]	Condenser area [m²]	Power output [kW]
Benzene	120	10106.74	19.64	426.96	484.92	128.15
	150	7392.75	24.24	1102.08	380.40	249.88
	175	3631.23	27.65	395.12	316.02	387.70
	200	3184.43	27.87	494.02	367.73	514.01
	250	2304.34	30.75	615.61	398.36	868.50
Pentane	120	9212.28	22.07	848.67	204.61	143.99
	150	3516.15	28.53	190.94	166.53	294.09
	175	3109.42	31.67	25.57	307.65	444.01
	200	2366.23	33.06	218.75	250.27	609.71
	250	1883.71	29.87	179.70	247.81	843.49

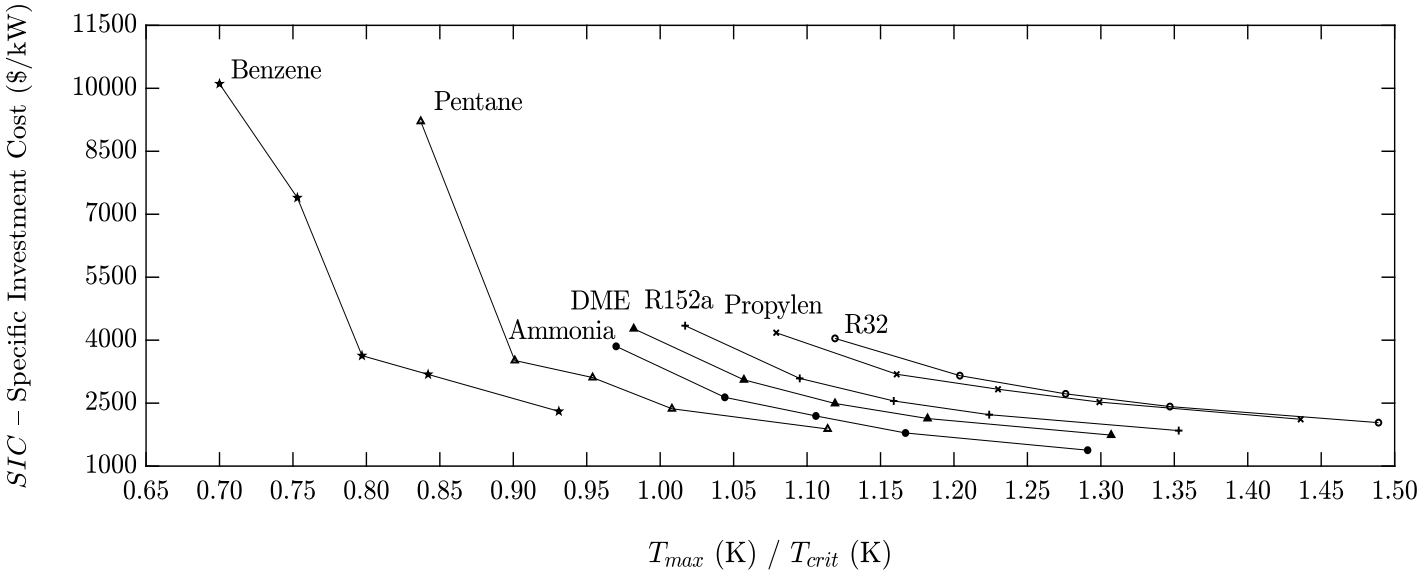

Figure 20. SIC results vs T_{max}/T_{crit} ($T_{sink,in}$ = 15 ºC, $\dot{m}_{hot}$ = 10 kg/s)

SIC values tend to stabilize once the maximum temperature of the cycle is equal or close to the critical temperature of the working fluid, because the maximum pressure limitation of the cycle does not allow for transcritical behaviors. For higher temperature relationships, increasing the cycle maximum temperature does only allow to achieve a higher power output by means of increasing the degree of super-heating, keeping the evaporation pressure constant and at its maximum value. For all the studied cases, this

higher power output can counteract the larger heat exchanger surfaces that are required for the higher heat duties, and the SIC keeps on diminishing even at high T_{max}/T_{crit}, although results show smaller deviations as T_{max} increases. For this reason, it is expected that, for temperatures higher than 250 ºC, there will be a point at which the SIC will not improve, what is more, the higher power output may not be able to balance the larger heat transfer surfaces and the SIC would increase. For benzene, maximum temperatures of 250 ºC are still below the fluid critical temperature, meaning that the SIC will keep on improving when increasing the heat source inlet temperature above this value as the evaporation pressure will keep on increasing. Once the maximum temperature reaches a value so that $T_{max}/T_{crit} \approx 1$, the SIC will still have certain potential of improvement by increasing the degree of super-heating. Therefore, benzene can be a suitable working fluid for high-temperature heat source applications.

Finally, it should be highlighted that the fact of stablishing the SIC as the objective function brings to SIC results with a clear and well-defined trend. However, in relation to the cycle performance, second-law efficiency results do not follow a specific pattern when minimizing the Specific Investment Cost of the plant.

10.4 Second-law efficiency optimization

It was before stated that the heat exchangers design, evaporation and condensing pressures, heat source inlet temperature, as well as other cycle parameters, have a great impact on both the plant cost and on its thermodynamic behaviour. For this reason, once the SIC optimization was carried out, we found it interesting to execute the same analysis by setting the second-law efficiency as the objective function (which is equivalent to maximizing the power output). Appendix F includes in Tables H, I, J, K and L the obtained results for all the scenarios for each one of the simulated working fluids when the second-law efficiency is set as the objective function. Just like it happened when collecting all SIC results, all the thermodynamic optimization results are going to be represented in a series of figures with the objective of being able to study the results tendency and come to conclusions in an easier way.

Figure 21 shows the second-law efficiency evolution with the heat source and heat sink inlet temperatures. The represented values have been taken for a 10 kg/s hot source case study because, once again, for any of the three different simulated mass flows, the results tendency is similar.

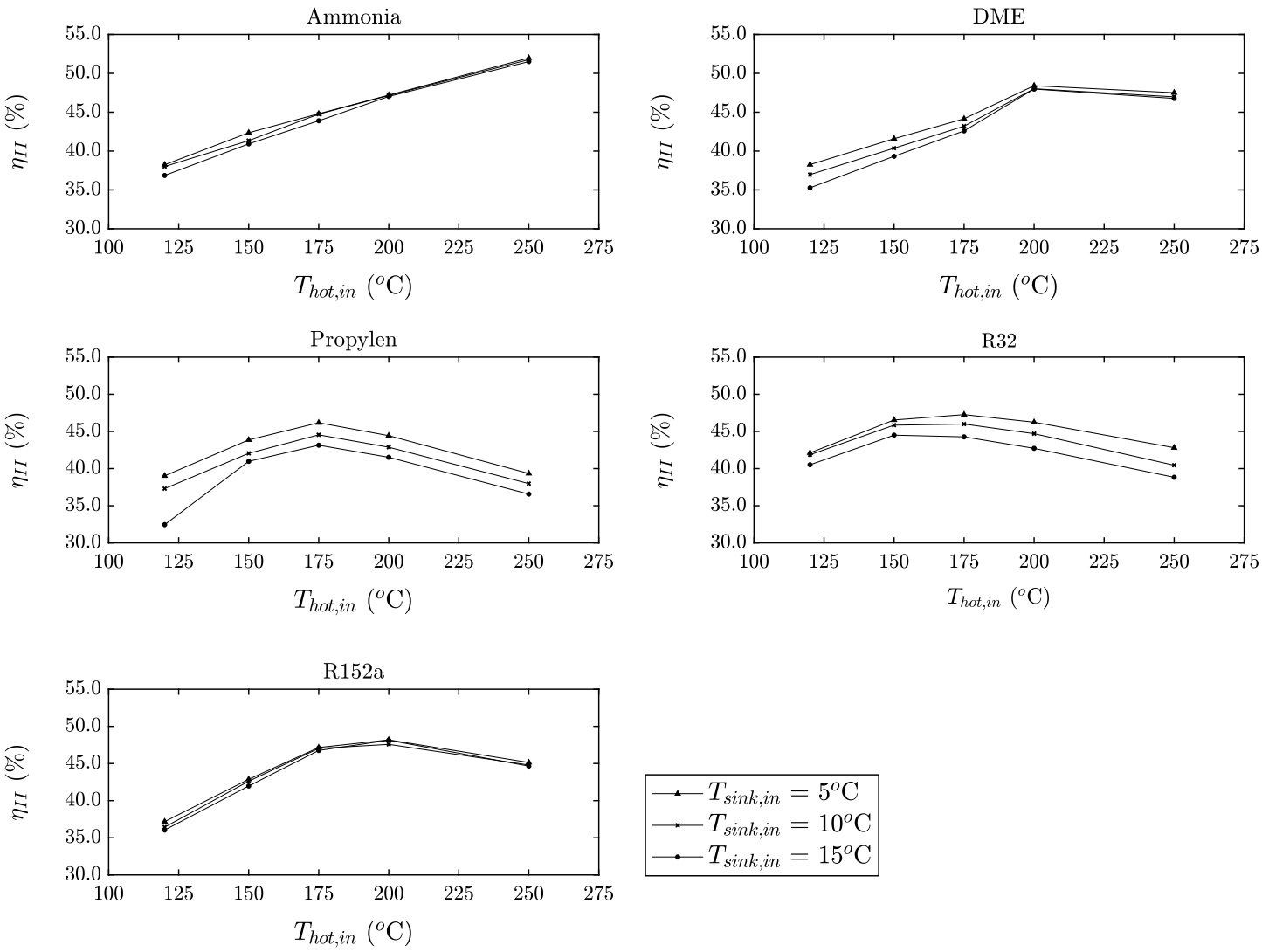

Figure 21. Second-law efficiency variation with $T_{hot,in}$ and $T_{sink,in}$ for different working fluids ($\dot{m}_{hot}$ = 10 kg/s)

As it can be observed in the figure, the second-law efficiency tendency when it is optimized is to increase until a specific heat source inlet temperature is reached and, for higher maximum temperatures, it starts dropping. The only exception is ammonia, for the one the cycle performance keeps on improving even when the maximum cycle

temperature reaches its highest value (250 ºC). The temperature for the one all working fluids find their best performance results corresponds to the point at which the evaporation pressure reaches its maximum allowed value. This is a sign to predict that cycles using working fluids with low critical pressures could find better efficiencies if their evaporation pressure could reach values closer to the critical one, although we cannot predict the way they would behave when operated under transcritical conditions, since the heat transfer processes would considerably differ from the sub-critical ones.

As the evaporation pressure reaches higher values when increasing the hot source inlet temperature, better temperature profile matches in the PrHE can be achieved, and, consequently, the exergy destruction in this component is reduced. However, when the maximum allowed pressure is reached, the evaporation pressure cannot increase any further, and the heat cannot be as well leveraged as before. Therefore, irreversibilities in the PrHE start increasing, and the system second-law efficiency drops.

Regarding the heat sink inlet temperature, for all studied working fluids, the second-law efficiency drops as it increases, as Figure 21 reflects. When optimizing the plant performance, the condenser pinch point tends to reach the lowest allowed value in all cases (5 ºC), in an effort to minimize the exergy destruction. If the cooling water inlet temperature increases, the condensing working fluid temperature is forced to increase as well, as the pinch point constraint must be met. Higher condensing temperatures do also imply higher condensing pressures, causing a cycle pressure ratio reduction. Hence, the expansion process through the turbine is more and more limited as the heat sink temperature increases, involving lower power outputs that finally lead to worse cycle performances.

The best Rankine cycle performance can be achieved for ammonia, at a $T_{hot,in}$ equal to 250 ºC, a heat source mass flow of 10 kg/s and a $T_{cold,in}$ equal to 5 ºC. The mentioned configuration presents a second-law efficiency of 51.97%, with a power output of 1605.41 kW. For R32 and propylene cases, the maximum second-law efficiencies are achieved when the maximum cycle temperature reaches 175 ºC, while, for DME and R152, the best performances arise for a hot water inlet temperature of 200 ºC. The reason is that R32 and propylene have a similar critical temperature which is lower than the one

DME and R152a present, meaning that the first two working fluids reach their maximum evaporation pressures at lower maximum cycle temperatures. For the two first mentioned working fluids (R32 and propylene), the maximum second-law efficiencies that can be achieved are 47.24% and 46.17%, with 754.48 kW and 736.93 kW power outputs respectively, while, for DME and R152a, the best cycle performances give second-law efficiencies of 48.41% and 48.18%, with 988.60 kW and 983.70 kW power outputs respectively. The power outputs that are obtained for the best cycle performances do not correspond to the maximum net powers that can be extracted from the cycle, as increasing the degree of super-heating and the working fluid mass flow when increasing the heat source inlet temperature can lead to higher power outputs, although it does not guarantee a better use of the increased heat input.

With relation to the heat source mass flow, its impact on the shape of the plotted curves is not remarkable, as the second-law efficiency tends to follow the same trend: it increases in a continuous way with the maximum cycle temperature for ammonia, while, for the rest of working fluids, it reaches a maximum at a specific heat source inlet temperature, and it starts dropping when overpassing this temperature. The only difference we may hammer home is that increasing the heat source mass flow tends to stabilize a bit the second-law efficiency curves, meaning that the performance behavior deviations that are found when moving from 150 ºC to 175 ºC or 200 ºC are not as remarkable for a mass flow of 50 kg/s as they are for 10 kg/s. Despite of this, the second-law efficiency drop when reaching a hot source inlet temperature of 250 ºC is more than evident in all cases (with ammonia exception). Also, the increased heat input that higher hot water mass flows provide leads to higher power outputs.

Even though the power output tendency is clear when varying the heat source mass flow, the second-law efficiency does not change in a clear way when moving from 10 kg/s to 25 kg/s or 50 kg/s. For example, for a $T_{hot,in}$ of 150 ºC and a $T_{cold,in}$ of 10 ºC, propylene's second-law efficiency increases by 2.90% when moving from 10 kg/s to 25 kg/s and by 3.45% when moving up to a mass flow of 50 kg/s. However, for the same working fluid and a scenario of $T_{hot,in}$ equal to 200 ºC, and $T_{cold,in}$ equal to 15 ºC, the second-law efficiency drops by 0.30% when moving from 10 kg/s to 25 kg/s and by 0.44% when increasing the hot water mass flow up to 50 kg/s. This reflects that heat source mass flow

variations do not have a clear direct impact on the cycle performance, as it causes important changes in factors such as the heat exchangers pressure drops or the heat transfer coefficients, whose combination may lead to variable and not-constant-tendency outputs.

As it was done for the SIC optimization, it might be of interest to add two working fluids with high critical temperatures to the analysis, in order to determine if they follow the same trends as the ones that have already been found. Once again, benzene and pentane have been chosen for a case study of $T_{cold,in}$ = 15 ºC, $\dot{m}_{hot}$ = 10 kg/s and a varying heat source inlet temperature. This time, the second-law efficiency has been set as the objective function.

Table 15 summarizes the obtained results, in which it can clearly be seen that, as it happened with amonia, the cycle second-law efficiency continuously increases with the maximum cycle temperature. The reason is that, as these working fluids have a high critical temperature, the maximum allowed pressure is not reached in none of the scenarios, meaning that the evaporation pressure can keep on increasing without reaching the stablished limitation. This means that the higher power output that can be achieved when the heat input rises leads to a better exploitation of the heat source for all the studied hot water inlet temperatures.

Table 15. Benzene and pentane second law efficiency optimization results

Working fluid	$T_{h,in}$ [ºC]	SIC [$/kW]	η_{II} [%]	Evaporator area [m^2]	Condenser area [m^2]	Power output [kW]
Benzene	120	53395.04	34.27	7031.40	1313.04	223.59
	150	33225.77	35.14	5017.09	5613.91	362.23
	175	15602.05	36.83	4458.18	2306.22	516.41
	200	7436.45	37.06	2355.86	2125.88	683.47
	250	5305.93	37.73	1473.92	3472.89	1065.73
Pentane	120	34627.63	35.70	5492.64	608.46	232.93
	150	28988.20	39.37	7007.61	961.96	405.82
	175	6613.45	41.77	471.13	2718.41	585.65
	200	5737.71	43.51	536.78	3239.94	794.06
	250	5452.45	43.64	1572.58	4354.01	1232.52

In this scenario in which the performance of the Rankine cycle has been optimized, plotting all the working fluids results in the same graph as a function of T_{max}/T_{crit} does not allow to come to clear conclusions as it could be done when optimizing the SIC, as no clear tendency is visible. What it can be assured after having analyzed working fluids with very different critical temperatures, is that those cycles that operate with high-critical-temperature working fluids have a strict performance limitation when used together with low-temperature heat sources.

10.5 Techno-economic and thermodynamic optimization comparison

Once all the results were obtained and analyzed for the SIC and the thermodynamic optimizations in a separate way, we observed that the results differed a lot from one optimization case to another. This means that some parameters of the cycle are experiencing considerable variations that have a direct impact on the cost, power output and efficiency of the cycle when setting different objective functions. With the objective of determining which are these factors and how much they affect the outputs and results, a comparative analysis between the techno-economic and the thermodynamic optimization results is presented in this section.

The first thing that stands out when analysing the main results is that the performance of the cycle is worse when the SIC is minimum than when the efficiency is optimized, while the cycle cost is higher when the second-law efficiency reaches its maximum value than when the SIC is set as the objective function. Although this may seem logical, it gives insight about the fact that focusing the design of the cycle on reducing the SIC leads to power plants with a poor performance, while, in case we are looking for the best thermodynamic behaviour of the plant, we will be doing it in detriment of a higher cost. To summarize: the most efficient Rankine cycle power plants have a much higher Specific Investment Cost than those ones with a medium-low efficiency, and the less costly Rankine cycle power plants have a worse performance than the more expensive ones.

For example, R32 can experience a performance improvement of 6.53% if, instead of minimizing the Specific Investment Cost of the plant, we focus on optimizing its functioning, and this is done with an associated extra SIC of 1188.07 $/kW (for a case study of $T_{cold,in}$ = 10 ºC, $\dot{m}_{hot}$ = 10 kg/s and $T_{hot,in}$ = 120 ºC). If we extrapolate this result, we could say that improving the cycle second-law efficiency by 1% would require an extra SIC of 181.83 $/Kw for the given case study. This difference is lower in case of using ammonia, which shows an extra SIC of 364.25 $/kW for an efficiency improvement of 8.02% (meaning an extra SIC of 45.41 $/kW per each 1% improvement for the same case study). On the other side, we can find R152a, which requires an extra SIC of 412.70 $/kW to increase the performance of the Rankine cycle by 1%. It needs to be recalled that these results vary with the heat source and heat sink inlet conditions; for example, ammonia may require an extra SIC of 127.67 $/kW per each 1% efficiency improvement when increasing the heat source inlet temperature up to 200 ºC. In spite of this, R152a always shows the highest SIC rise when looking for better cycle performances, being the associated extra cost of special importance for high heat source mass flows (it may reach extra SIC values up to 646.26 $/kW for performance improvements of 1% when the hot source mass flow is 50 kg/s), while ammonia always presents the lowest extra SIC when improving a 1% the efficiency of the Rankine cycle.

These performance and cost differences are a consequence of the different HTCs, pressure drops, degrees of super-heating, mass flows, evaporation and condensing pressures, etcetera, that result from the optimization. All these parameters will be further analyzed one by one in order to determine the values they reach depending on the objective function that is set for carrying out the cycle optimization.

Due to the great amount of results that were obtained after having run all simulations for the 7 different studied working fluids, the following analysis will only be focused on three working fluids with different characteristics. These working fluids are ammonia (inorganic working fluid), benzene (organic working fluid with a high critical temperature) and R152a (organic working fluid with a low critical temperature). In order to be able to generalize the results, the rest of working fluids results will also be checked

to guarantee that they follow the defined tendency as well, although plots will not be shown unless it is of special interest.

First of all, the T-s diagrams of the three analyzed working fluids will be shown in Figure 22, Figure 23 and Figure 24. These diagrams were obtained for a $T_{sink,in}$ of 15 ºC, a $\dot{m}_{hot}$ of 10 kg/s, and a varying $T_{hot,in}$. SIC and second law efficiency T-s diagrams have been placed together in order to make their comparison easier.

- Benzene T-s diagrams:

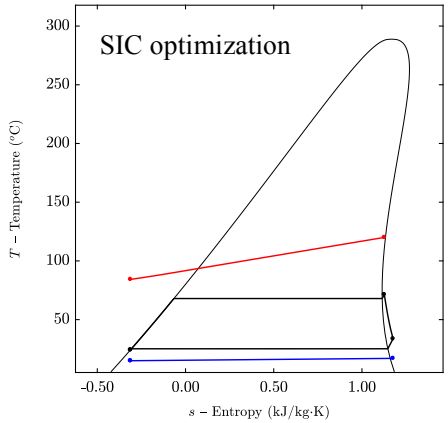

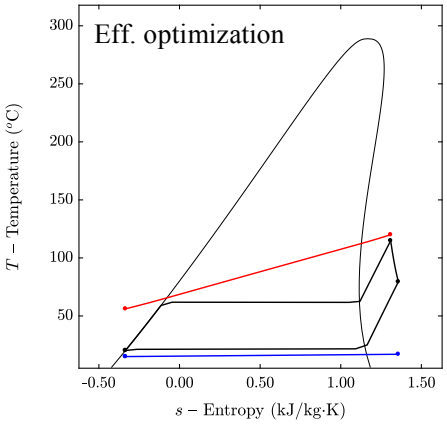

$T_{hot,in}$ = 120 ºC

SIC opt	Eff. opt
P_{evap} = 0.687 bar	P_{evap} = 0.488 bar
P_{cond} = 0.128 bar	P_{cond} = 0.084 bar
ΔT_{sup} = 3.39 ºC	ΔT_{sup} = 55.06 ºC

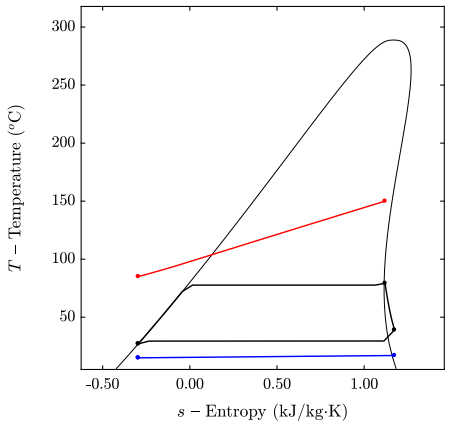

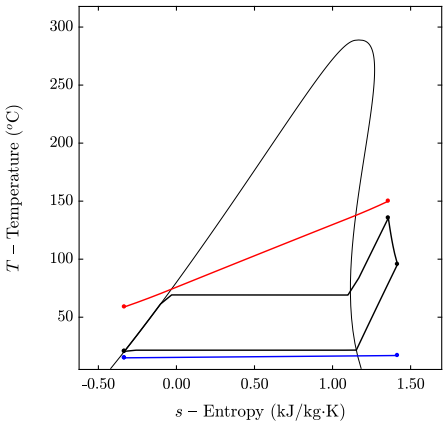

$T_{hot,in}$ = 150 ºC

SIC opt	Eff. opt
P_{evap} = 0.940 bar	P_{evap} = 0.712 bar
P_{cond} = 0.155 bar	P_{cond} = 0.108 bar
ΔT_{sup} = 1.53 ºC	ΔT_{sup} = 66.43 ºC

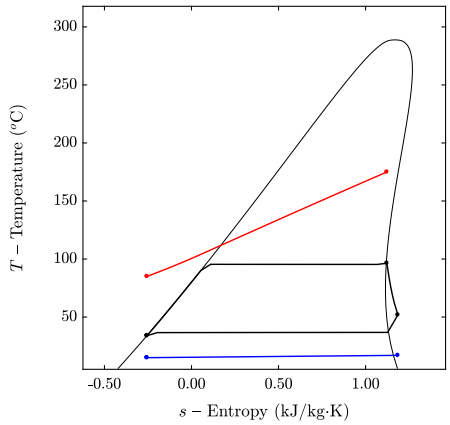

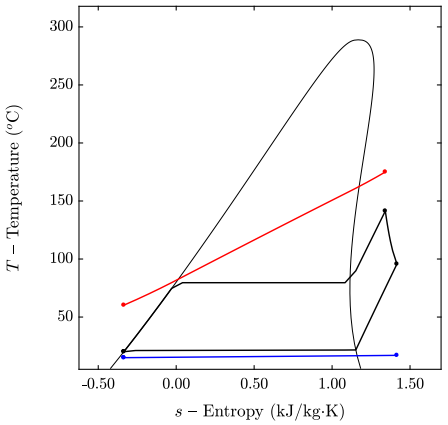

$T_{hot,in}$ = 175 ºC

SIC opt	Eff. opt
P_{evap} = 1.591 bar	P_{evap} = 0.999 bar
P_{cond} = 0.212 bar	P_{cond} = 0.109 bar
ΔT_{sup} = 1.04 ºC	ΔT_{sup} = 61.78 ºC

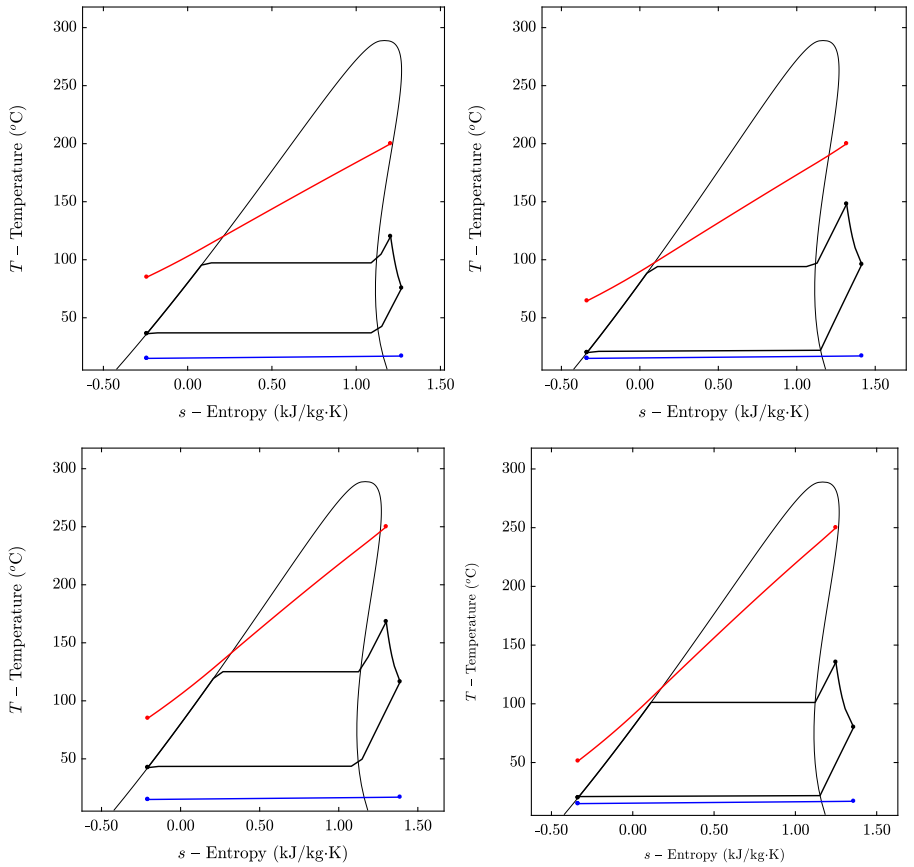

$T_{hot,in}$ = 200 ºC

SIC opt	Eff. opt
P_{evap} = 1.674 bar	P_{evap} = 1.531 bar
P_{cond} = 0.215 bar	P_{cond} = 0.105 bar
ΔT_{sup} = 22.81 ºC	ΔT_{sup} = 53.93 ºC

$T_{hot,in}$ = 250 ºC

SIC opt	Eff. opt
P_{evap} = 3.389 bar	P_{evap} = 1.865 bar
P_{cond} = 0.283 bar	P_{cond} = 0.110 bar
ΔT_{sup} = 43.24 ºC	ΔT_{sup} = 34.31 ºC

Figure 22. Benzene T-s diagrams for the SIC and thermodynamic optimizations for different hot source inlet temperatures ($T_{sink,in}$ = 15 ºC, $\dot{m}_{hot}$ = 10 kg/s)

- Ammonia T-s diagrams:

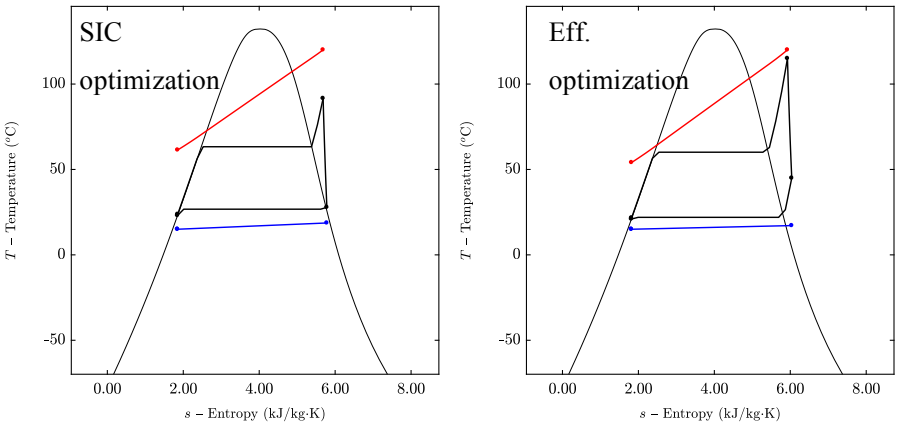

$T_{hot,in}$ = 120 ºC

SIC opt	Eff. opt
P_{evap} = 28.33 bar	P_{evap} = 26.22 bar
P_{cond} = 10.58 bar	P_{cond} = 9.13 bar
ΔT_{sup} = 28.31 ºC	ΔT_{sup} = 54.90 ºC

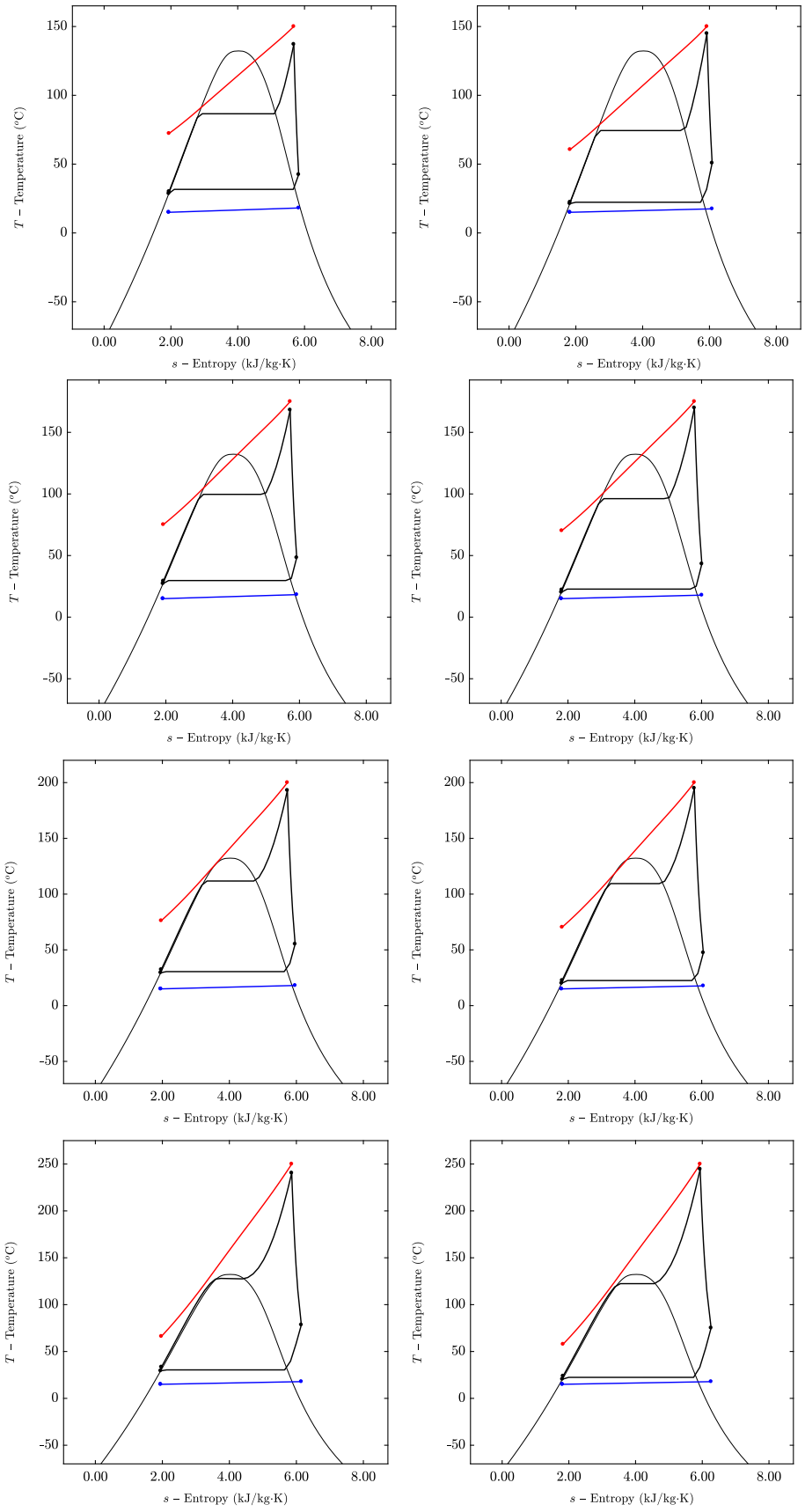

$T_{hot,in}$ = 150 ºC

SIC opt	Eff. opt
P_{evap} = 47.71 bar	P_{evap} = 36.62 bar
P_{cond} = 12.26 bar	P_{cond} = 9.23 bar
ΔT_{sup} = 50.48 ºC	ΔT_{sup} = 70.53 ºC

$T_{hot,in}$ = 175 ºC

SIC opt	Eff. opt
P_{evap} = 62.163 bar	P_{evap} = 57.97 bar
P_{cond} = 11.57 bar	P_{cond} = 9.36 bar
ΔT_{sup} = 60.85 ºC	ΔT_{sup} = 73.74 ºC

$T_{hot,in}$ = 200 ºC

SIC opt	Eff. opt
P_{evap} = 78.36 bar	P_{evap} = 74.94 bar
P_{cond} = 11.84 bar	P_{cond} = 9.28 bar
ΔT_{sup} = 81.31 ºC	ΔT_{sup} = 85.6 ºC

$T_{hot,in}$ = 250 ºC

SIC opt	Eff. opt
P_{evap} = 107.37 bar	P_{evap} = 95.17 bar
P_{cond} = 11.80 bar	P_{cond} = 9.26 bar
ΔT_{sup} = 112.99 ºC	ΔT_{sup} = 122.20 ºC

Figure 23. Ammonia T-s diagrams for the SIC and thermodynamic optimizations for different hot source inlet temperatures ($T_{sink,in}$ = 15 ºC, $\dot{m}_{hot}$ = 10 kg/s)

- R152a T-s diagrams:

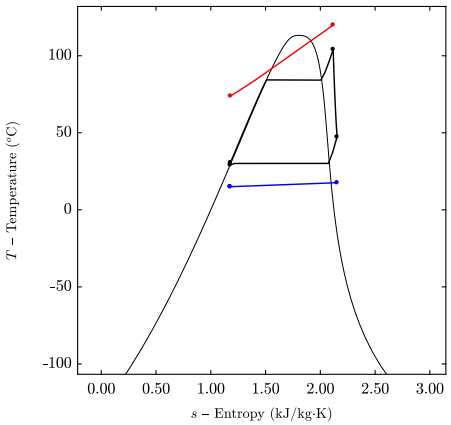

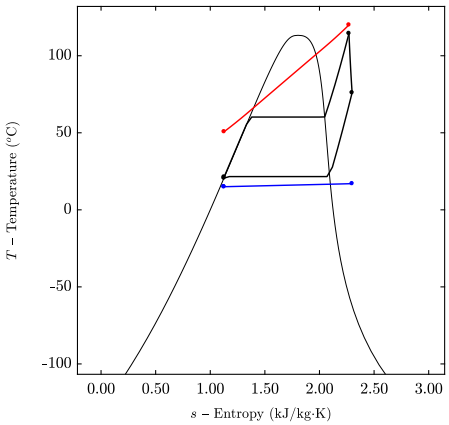

$T_{hot,in}$ = 120 ºC

SIC opt	Eff. opt
P_{evap} = 25.68 bar	P_{evap} = 15.08 bar
P_{cond} = 6.92 bar	P_{cond} = 5.38 bar
ΔT_{sup} = 19.93 ºC	ΔT_{sup} = 54.28 ºC

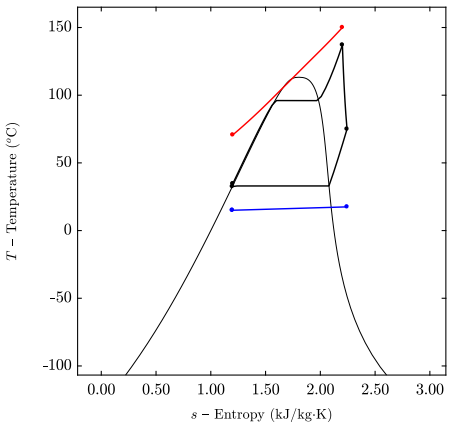

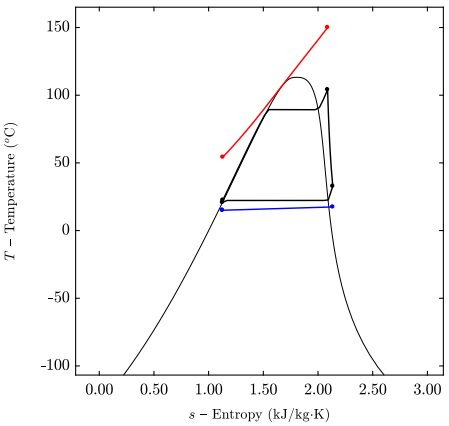

$T_{hot,in}$ = 150 ºC

SIC opt	Eff. opt
P_{evap} = 32.49 bar	P_{evap} = 28.45 bar
P_{cond} = 7.50 bar	P_{cond} = 5.49 bar
ΔT_{sup} = 41.17 ºC	ΔT_{sup} = 14.80 ºC

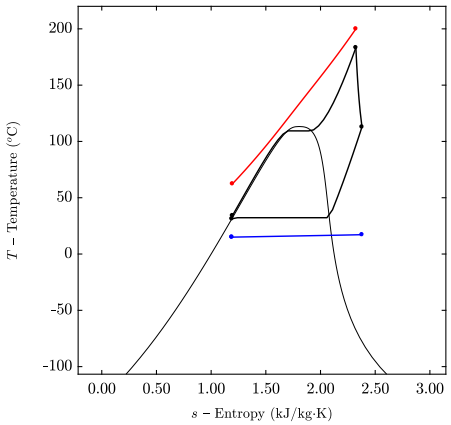

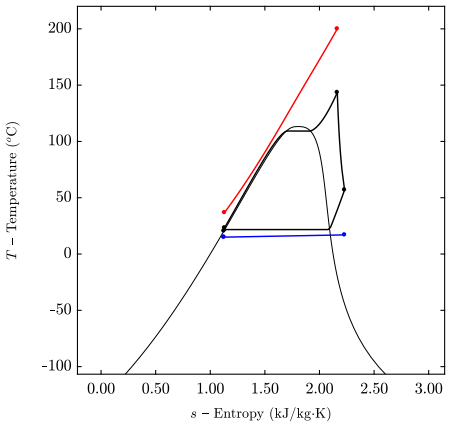

$T_{hot,in}$ = 175 ºC

SIC opt	Eff. opt
P_{evap} = 42.01 bar	P_{evap} = 38.03 bar
P_{cond} = 7.32 bar	P_{cond} = 5.44 bar
ΔT_{sup} = 51.46 ºC	ΔT_{sup} = 13.67 ºC

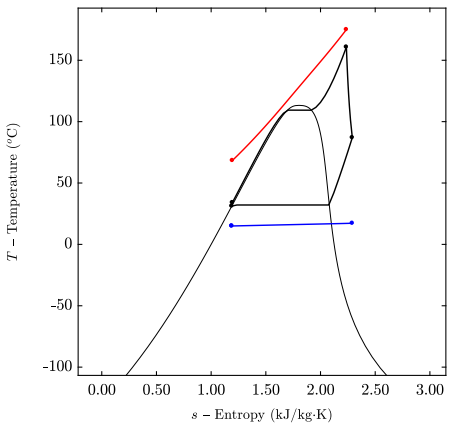

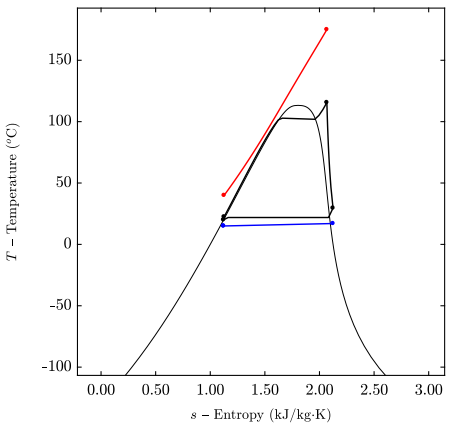

$T_{hot,in}$ = 200 ºC

SIC opt	Eff. opt
P_{evap} = 42.01 bar	P_{evap} = 42.01 bar
P_{cond} = 7.35 bar	P_{cond} = 5.40 bar
ΔT_{sup} = 74.06 ºC	ΔT_{sup} = 34.30 ºC

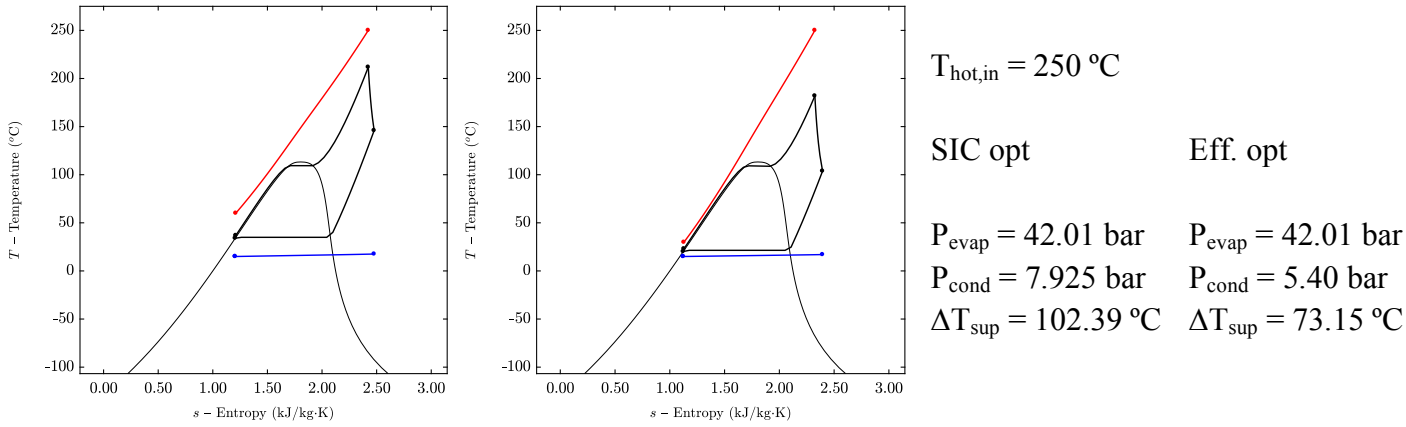

Figure 24. R152a T-s diagrams for the SIC and thermodynamic optimizations for different hot source inlet temperatures ($T_{sink,in}$ = 15 ºC, $\dot{m}_{hot}$ = 10 kg/s)

10.5.1 Evaporation pressure

By taking a look at the T-s diagrams, it can be seen that the working fluid optimal evaporation pressure tends to increase as the heat source inlet temperature increases, in both optimization cases and for all working fluids. Also, the evaporation pressure is always higher when optimizing the Specific Investment Cost than it is when maximizing the second-law efficiency, with the only exceptions of R152a when $T_{hot,in}$ = 200 ºC, and when $T_{hot,in}$ = 250 ºC (in these cases both cycle optimizations reach the highest allowed pressure).

While the SIC optimization is focused on finding a balance between the lowest possible cost and the highest possible power output, increasing the evaporation pressure results into something beneficial for this purpose because of two main reasons: the working fluid heat transfer coefficient and the pressure ratio increase. As the HTC is improved, the required PrHE heat transfer area decreases, meaning that the heat exchanger cost drops. The only limitation that higher evaporation pressures present when optimizing the SIC is the pinch point and LMTD reduction when the heat source and working fluid temperature profiles get closer, as it entails larger H.E surfaces. Therefore, the evaporation pressure when optimizing the SIC tends to increase until it reaches a point in which the improved

HTC and higher power output cannot counteract the effect of the larger surfaces which are a consequence of the smaller LMTDs.

The PrHE cost stops being important when optimizing the cycle second-law efficiency. This means that, in these optimization cases, the evaporation pressure tends to bring the heat source and working fluid temperature profiles as close as possible, with the objective of maximizing the exploitation of the available heat. Also, a better absorption of heat in the PrHE allows to increase the working fluid mass flow, which results into higher power outputs. These two considerations determine the performance of the Rankine cycle, and hence, its efficiency.

Something that can also be seen in the T-s diagrams is that the heat source temperature jump across the PrHE is much greater for the thermodynamic optimization cases. The reason is that this kind of optimization tends to maximize the use of the available heat, and, as more heat is absorbed by the working fluid, the temperature of the hot water out of the PrHE reaches lower values. This steeper heat source temperature profile, together with the minimum allowed pinch point in the evaporator when optimizing the performance of the cycle, allows to reduce the exergy destruction and to maximize the power output.

10.5.2 Condensing pressure

As it happens with the evaporation pressure, the working fluid condensing pressure is higher when optimizing the Specific Investment Cost than it is when optimizing the second-law efficiency of the cycle. However, in this case, the mentioned pressure does not show a clear tendency when the heat source inlet temperature varies, although for the thermodynamic optimization case it seems to be much more stable than for the SIC optimization.

It has to be recalled that minimizing the condenser area is essential to avoid high Rankine cycle costs when optimizing the SIC. In this case, increasing the condensing pressure involves better working fluid HTCs (because of the higher densities and temperatures it entails), allowing for a condenser area reduction. However, the fact of increasing the

condensing pressure does also limit the expansion process through the turbine in a way that the cycle power output drops. Furthermore, low condensing pressures can bring the working fluid and cooling water temperature profiles too close, causing a LMTD reduction that leads to large condenser surfaces. Therefore, the SIC optimization condensing pressure tends to find a value high enough so that the HTCs and the LMTD increase without causing a too important power output drop that may result into higher cycle SICs. This has a direct consequence on the cycle second-law efficiency that justifies the worse performance of the less costly cycles: as the exergy destruction in the condenser is higher when the LMTD increases, the performance of the Rankine cycle worsens.

For the thermodynamic optimization, the condensing pressure tends to reach low values to guarantee that the condenser pinch point reaches its minimum allowed value, that the LMTD is low enough to assure an efficient heat rejection process and that the power output is high. This leads to much more efficient processes, but also to much more costly components.

10.5.3 Logarithmic Mean Temperature Difference and pinch point

The Logarithmic Mean Temperature Difference in the cycle heat exchangers plays an important role when determining both the required heat exchangers surfaces and the heat exchange process efficiency. As the LMTD value increases, the surface that is needed to make the heat transfer process possible is reduced, leading to lower costs, although it does also have a negative impact on the cycle performance, as the exergy destruction increases.

Figure 25 shows the LMTD evolution through the condenser and PrHE for the SIC and thermodynamic optimizations. It can be observed that, in the PrHE, the LMTD tends to diminish in the pre-heating section, as the heat source fluid is cooled down while the working fluid is heated up in a counter-current heat exchange. Once the working fluid starts evaporating, the LMTD increases as the working fluid evaporation temperature remains constant while the hot water experiences a temperature reduction. When the working fluid reaches the saturated vapour state (point at which the LMTD finds its maximum value), the working fluid super-heating brings both temperature profiles closer again. In all cases, the minimum LMTD that is reached is lower for the thermodynamic

optimization than it is for the SIC optimization, as lower temperature differences imply minimizing the exergy destruction. These minimum LMTD values correspond to the primary heat exchanger point where the pinch point temperature is reached, which is found at the outlet of the pre-heating section in all cases. For the thermodynamic optimization, this pinch point temperature is always 5 ºC (the minimum allowed value), while it always reaches higher values for the SIC optimization.

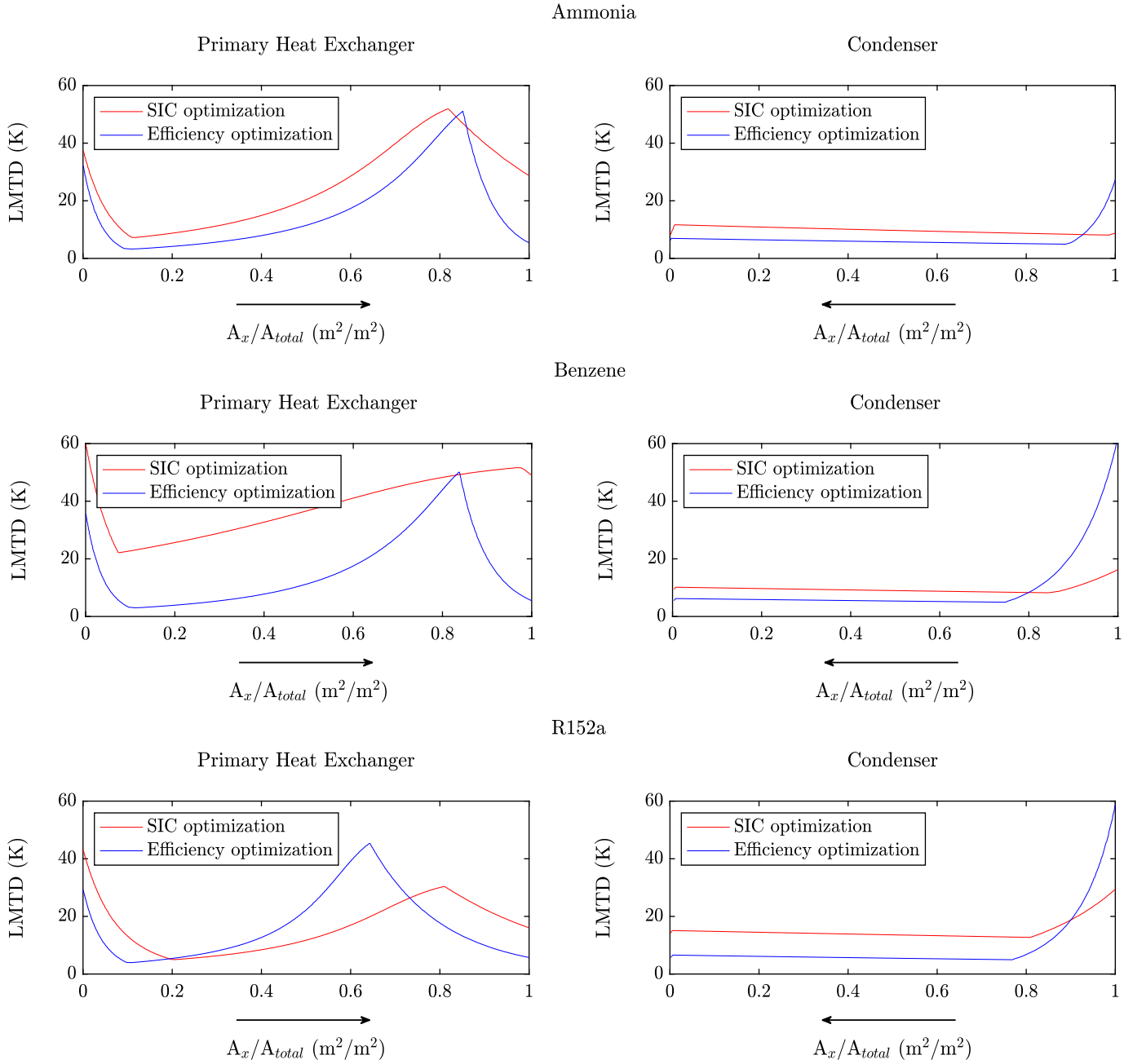

Figure 25. SIC and thermodynamic optimizations LMTD evolution through the PrHE and condenser ($T_{hot,in}$ = 120 ºC, $T_{sink,in}$ = 15 ºC, $\dot{m}_{hot}$ = 10 kg/s)

By taking a look at the LMTD at the inlet of the PrHE, it can be seen that it is greater for the SIC optimization than for the thermodynamic optimization. This is due to the higher temperature that the hot source fluid presents when leaving the H.E (we will see this in detail in Section 10.5.4).

At the evaporation section outlet, LMTDs for both optimizations reach similar values for ammonia and benzene, while, for R152a, a much higher LMTD can be observed for the efficiency optimization case. The optimal evaporation pressures for benzene and ammonia are not too different when optimizing the SIC and the cycle performance, but, for R152a, the thermodynamic optimization evaporation pressure presents a value that is more than 10.5 bar lower than the one obtained for the techno-economic optimization. This much lower evaporation pressure leads to a considerably greater difference between the H.E temperature profiles.

Something that stands out when taking a look at Figure 25 is the high LMTD that benzene presents in the PrHE when optimizing the system SIC. As this working fluid has a high critical temperature, it is forced to work at low pressures when the heat source inlet temperature is low. This entails low densities and evaporation temperatures that lead to very low HTCs, and hence, enormous heat transfer areas. To compensate this effect and minimize the SIC as much as possible, the LMTD tends to increase a lot.

The less steep shapes that LMTD curves present in the condenser if we compare them to the PrHE LMTD curves are a consequence of the smaller variations that the cooling water temperature experiences when it absorbs the rejected heat, provoking that the differences between the temperature profiles of the fluids that exchange the heat in the condenser keep an almost constant value during the constant-temperature condensing process.

Finally, we have already mentioned that, for all thermodynamic optimization cases, the pinch point in both the condenser and the PrHE reaches the minimum allowed value (5 ºC). However, for the SIC optimization, only ammonia's pinch point finds values close to the minimum ones (between 5 ºC and 8 ºC in the PrHE and 8 ºC and 13 ºC in the condenser). For the rest of working fluids, the pinch point temperatures reach higher values (for example, propylene may overpass a value of 18 ºC in the PrHE and 12 ºC in

the condenser). These differences all working fluids present when compared to ammonia are due to the better thermal properties that ammonia has, since, as its HTC is much higher than it is for the rest of working fluids, the heat transfer surfaces that it requires are lower. This entails that it can work at higher evaporation pressures and lower condensing pressures, as the optimization does not force the LMTD increase in a great extent, making it possible to diminish the pinch point in both heat exchangers.

Regarding the pinch point temperature evolution with the heat source inlet temperature when optimizing the system SIC, it tends to increase as the hot water inlet temperature rises, in both the PrHE and the condenser. The reason is that, as more heat is available and absorbed by the working fluid in the PrHE when the heat source temperature increases, the LMTD tends to be higher in order to compensate the larger surfaces that are required for greater heat duties. This also leads to higher degrees of super-heating, which entail larger pre-cooling surfaces in the condenser. With the aim of counteracting these extra pre-cooling areas and the larger condenser surfaces that are required to reject higher amounts of heat, the SIC optimization tends to increase the temperature differences in the condenser as well. Both LMTD growths imply higher pinch points values.

10.5.4 Heat source outlet temperature

The amount of heat that is absorbed by the working fluid determines the heat source temperature at the outlet of the primary heat exchanger. When optimizing the cycle second-law efficiency, making the most of the available heat is key to guarantee the best performance of the plant while, when executing the techno-economic optimization, the heat that is absorbed in the PrHE depends on the effect it has on the system Specific Investment Cost, as increased heat duties require larger H.E surfaces, which may or may not be counteracted by higher net power outputs.

For all working fluids, it was found that the hot source outlet temperature is always lower when optimizing the performance of the cycle than it is when optimizing its SIC, as it implies a better use of the heat and entails smaller temperature differences that minimize the exergy destruction. When comparing both kinds of optimization, benzene shows the most remarkable differences between the resulting optimal hot source outlet

temperatures. As this working fluid is forced to work at low operating pressures because of its high critical temperature, it presents poor HTCs, meaning that the heat transfer surfaces that are required per kW of exchanged heat are considerably high. For this reason, the techno-economic optimization solution tends to find the highest possible hot source outlet temperature, in an effort to minimize the heat duty and maximize the LMTD to compensate the big size of the components. However, when optimizing the performance of the plant, the cost of the H.E is not important anymore, and the focus of the optimization is to reduce the hot source outlet temperature to guarantee the best heat transfer process efficiency, something that might lead to unfeasible H.E sizes. Therefore, when benzene is the cycle working fluid, the heat source temperature at the outlet of the PrHE reaches the highest allowed value (i.e. 85 ºC) in all techno-economic optimization cases, while, for the thermodynamic optimization, the optimum hot water outlet temperature is always lower than 55 ºC.

10.5.5 Working fluid and cooling water mass flows

Mass flows in Rankine cycles determine some of the most important factors whose impact on the performance and cost of the system is decisive, such as the heat transfer coefficients, pressure drops and net power output. For this reason, each scenario entails a different set of optimum mass flows.

Figure 26 shows the working fluid and cooling water mass flows evolution with the hot source inlet temperature. As it can be seen, for both the techno-economic and the thermodynamic optimization, all mass flows increase with the increasing hot water inlet temperature.

When the objective of the optimization is to maximize the cycle second-law efficiency, the working fluid tends to absorb a high amount of heat from the hot source to make the most of the available heat. This heat input can be used in 2 different ways: increasing the degree of super-heating or increasing the amount of evaporated working fluid. The percentage of heat that is used with one aim or another depends on the balance that the power output finds with the recovered exergy, although it always results into increased working fluid mass flows.

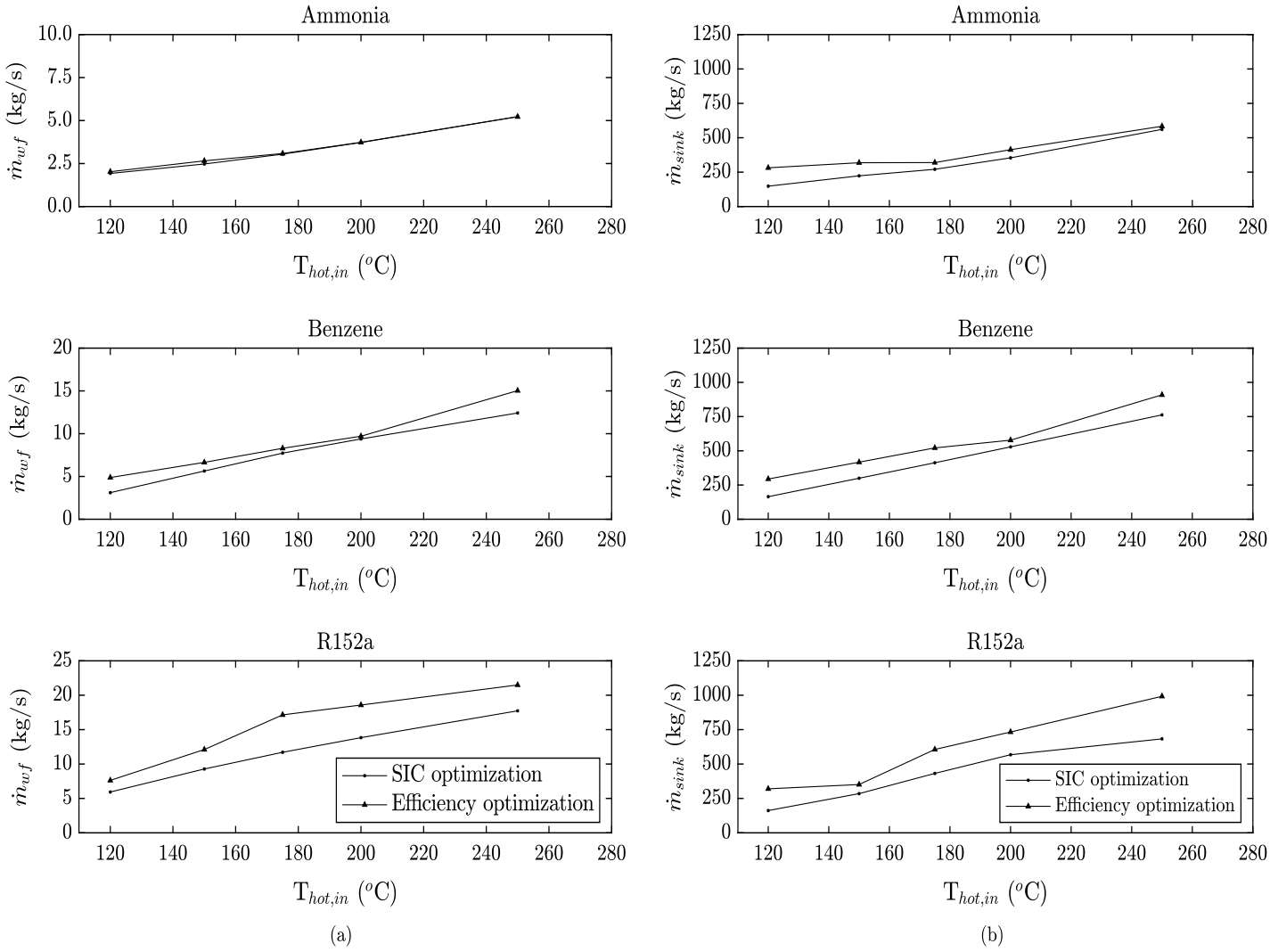

Figure 26. Working fluid (a) and heat sink (b) fluid mass flows evolution with the heat source inlet temperature ($\dot{m}_{hot}$ = 10 kg/s)

For the techno-economic optimization, increasing the amount of available heat has 3 direct consequences on the system: larger heat transfer areas are required to allow for greater heat duties, improved HTCs can be achieved because of the increased working fluid mass flows (involving smaller H.E surfaces) and higher power outputs can be obtained because of the higher degrees of super-heating and/or the higher working fluid mass flows. The working fluid mass flow is then determined by the balance between these 3 mentioned effects, making it hard to determine its evolution a-priori.

Something that can also be observed in Figure 26 is that the efficiency optimization working fluid mass flows are always higher than the ones that result from the SIC

optimization, even though the evaporation pressure that is reached during the techno-economic optimization is higher than the one obtained for the thermodynamic optimization. The reason is the better use of heat that the thermodynamic optimization allows for, making it possible to evaporate greater amounts of working fluid in spite of the fact that lower evaporation pressures imply that more heat is needed to evaporate 1 kg of working fluid (as the latent heat of vaporization decreases with the saturation pressure).

We have aforementioned that mass flows variations are closely related to changes in the system heat duties (presented in Figure 27). By relating Figure 26 and Figure 27, it can be observed that the higher mass flows that are obtained for the second-law optimization cases are consistent with the higher amounts of absorbed and rejected heat that this optimization case presents. Therefore, although determining how the system mass flows are going to change with the heat source inlet temperature is not simple a-priori, because of all the varying parameters they depend on, it is possible to predict whether they are going to increase or decrease by taking a look at the cycle heat flows evolution.

The heat that is rejected in the condenser evolves in the same way as the heat that is absorbed in the PrHE. This means that, as more heat enters the cycle, more heat has to be rejected to the sink. As a consequence, the cooling water mass flow experiences a rise when the heat source inlet temperature increases, as the cooling requirements are stricter.

The degree of increment that the cold water mass flow experiences when increasing the maximum cycle temperature is closely related to the thermal properties and the HTC of the working fluid. This means that working fluids with poor heat transfer coefficients require greater cooling loads for rejecting the same amount of heat than working fluids with much better heat transfer properties (such as ammonia). This is of special importance when designing the Rankine cycle power plant for locations with water scarcity issues, as, in some cases, such as when R152a is used as the cycle working fluid, the cooling load requirements may be very strict when optimizing the performance of the plant for high-temperature heat source applications. Under these conditions, it is important to study the heat transfer properties of the working fluid candidates, as they might determine the amount of cooling water that is required for the heat rejection process.

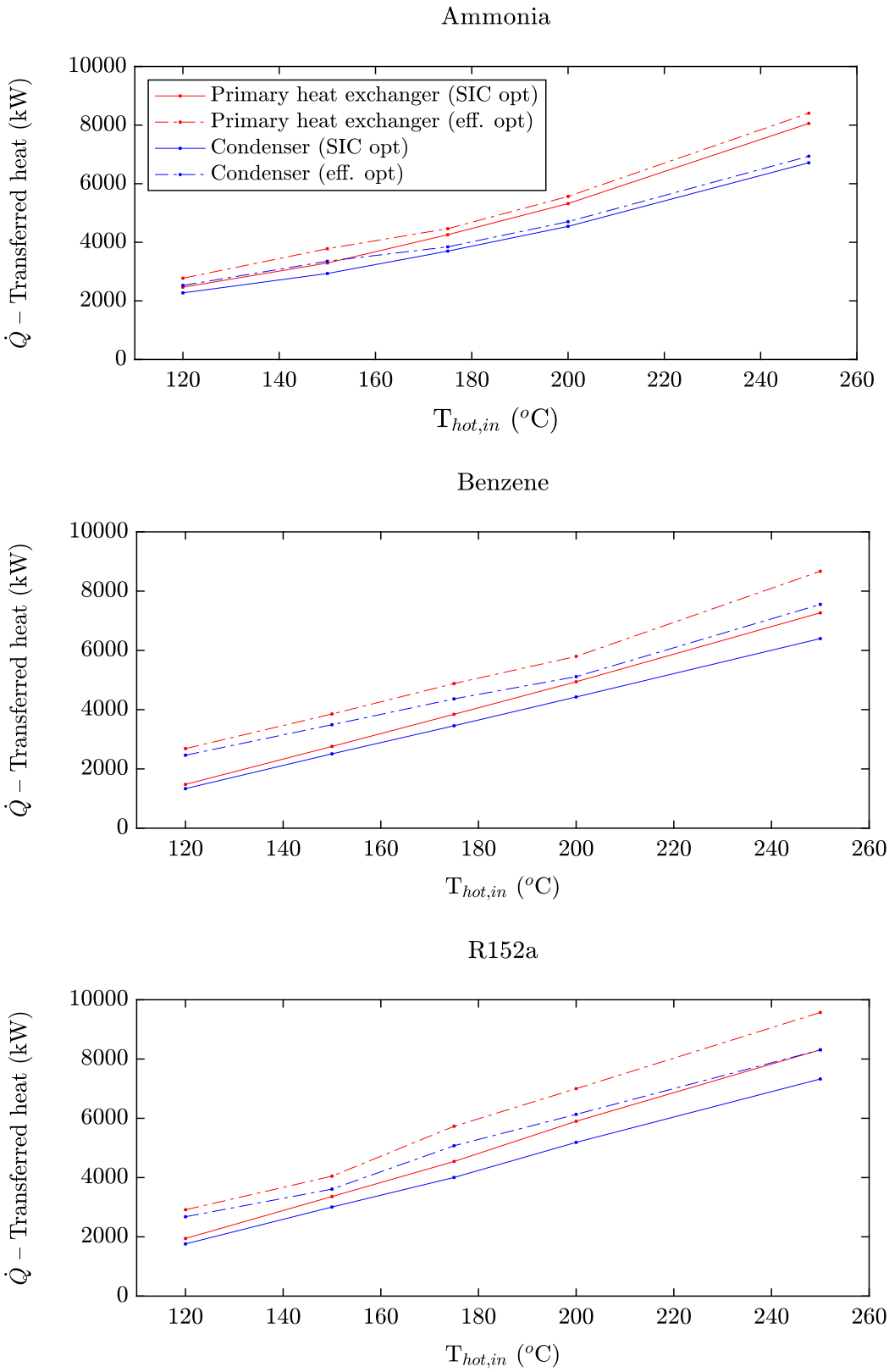

Figure 27. Heat absorbed and rejected by the working fluid in the Rankine cycle for different heat source inlet temperatures ($T_{sink,in}$ = 15 ºC, $\dot{m}_{hot}$ = 10 kg/s)

10.5.6 Degree of super-heating

The degree of super-heating that results from the thermodynamic and techno-economic optimization does not evolve in the same way when moving from one scenario to another.

In case of optimizing the Specific Investment Cost of the plant, the working fluid degree of super-heating has a constant increasing tendency with the heat source inlet temperature, which is determined by the equilibrium point at which the higher power output can counteract the larger H.E surfaces that are required to increase the vapour temperature at the outlet of the PrHE (see Figure 28). The only exception is found for benzene, for the one the techno-economic optimization leads to an almost saturated cycle when operating at low maximum cycle temperatures (120 ºC, 150 ºC and 175 ºC). This is a consequence of the low operating pressures and pressure ratios this fluid is forced to work with because of its high critical temperature, which cause an important worsening of its HTC and related net power output. The considerably larger heat transfer surfaces that are required to reach certain degree of super-heating cannot be compensated by the increased power output it entails, making the super-heating an unfeasible solution to optimize the system Specific Investment Cost. This does also explain why, for all the simulated scenarios, benzene can only find a maximum degree of super-heating lower than 60 ºC, while R152a and ammonia can overpass values of 100 ºC. This is especially interesting if we take into consideration that ammonia's vapour specific heat is much higher than the one benzene presents in the same state, meaning that the amount of heat that is required to increase the temperature of each unit mass of vapour working fluid by 1 ºC is much higher for the former. For example, for the scenario in which the heat source inlet temperature reaches 150 ºC, ammonia has a c_p of 5.591 kJ/kgK in the saturated vapour phase, while benzene's c_p is 1.868 kJ/kgK. Despite of this, ammonia reaches a 50.49 ºC degree of super-heating, and benzene, 1.53 ºC.

Regarding the thermodynamic optimization, the degree of super-heating tendency is not clear, and it is completely different for each working fluid. This means that determining the degree of super-heating when optimizing the performance of the plant is not possible a-priori, and there is no other way to find it than executing the optimization through MATLAB.

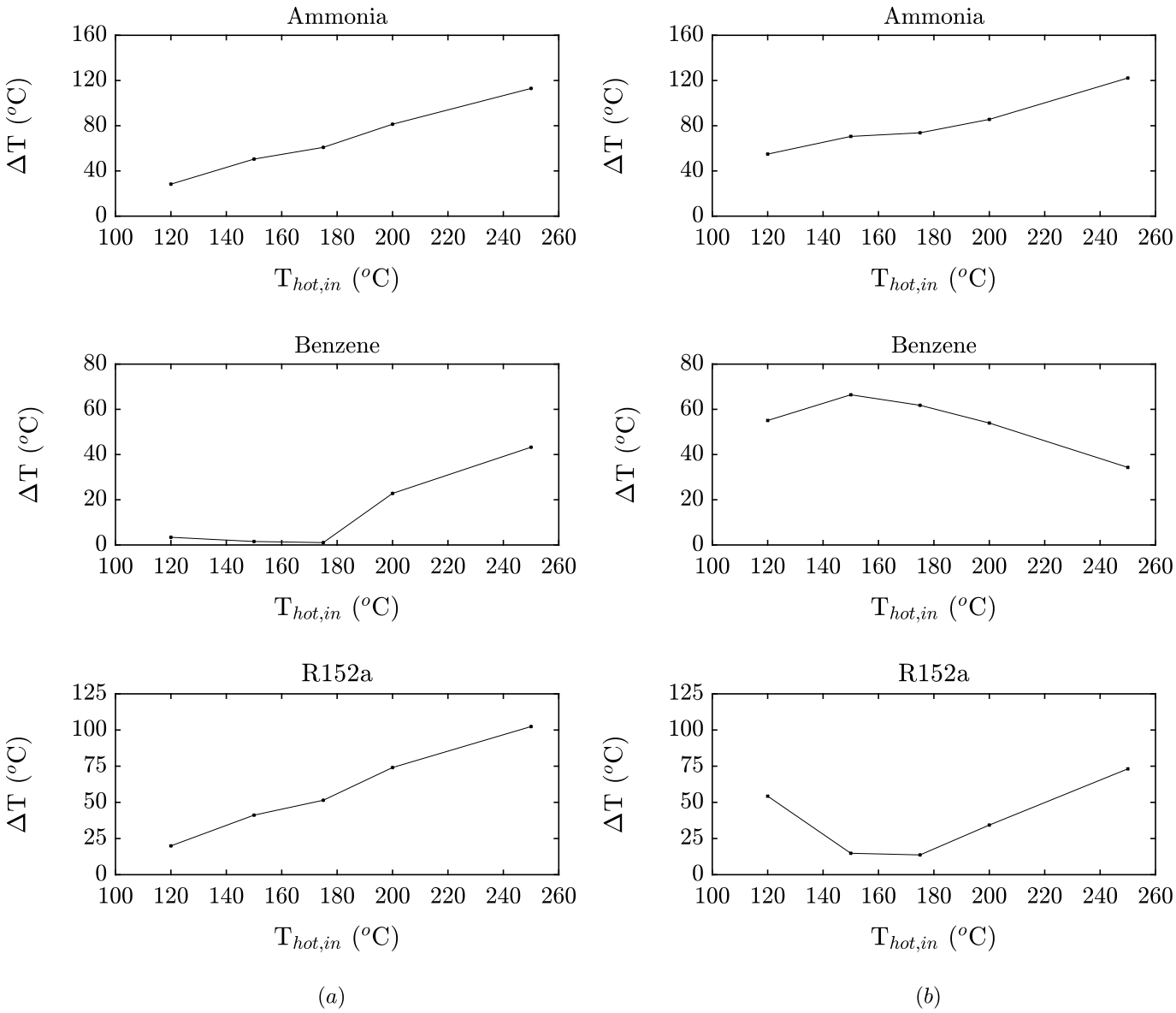

Figure 28. Degree of super-heating variation with the hot source inlet temperature for the SIC optimization (a) and the thermodynamic optimization (b)

10.5.7 Heat transfer coefficients

Heat transfer coefficients are of special importance when carrying out the techno-economic and the thermodynamic optimization, as they determine the H.E heat transfer surfaces, which have a direct impact not only on the cost of the plant, but also on the pressure drops that all fluids experience in the heat exchangers (and that determine the system performance because of being a source of irreversibility).

The main difficulty that the HTCs study gives rise to is that they are dependent on many different factors, making their value hard to predict. When analysing the different H.E configurations in Section 10.2, it could be checked that heat transfer coefficients experience large variations when the heat exchanger design is modified. Fluids properties do also have a major impact on the heat transfer coefficients values, as well as parameters such as the evaporation and condensing pressures or the degree of super-heating.

With the aim of determining the evolution behaviour of the HTCs, a deep analysis will be presented in this section. First, HTCs evolution for three different heat source inlet temperatures (120 ºC, 175 ºC and 250 ºC) and 2 different heat source mass flows (10 kg/s and 50 kg/s) are going to be studied for ammonia (for both objective functions solutions). Then, the same analysis will be applied to benzene and R152a, this time for two different heat source inlet temperatures and a heat source mass flow of 10 kg/s. In order to obtain more accurate plots and a better resolution of the results, the simulations were run again for a higher number of nodes in each heat exchanger (moving from 50 to 1000 nodes).

- Ammonia

  - SIC optimization

Figure 29 shows how the heat transfer coefficients evolve in the PrHE when ammonia is used as the cycle working fluid and the SIC is set as the objective function. As it can be observed, the fact of increasing the heat source mass flow entails changes of the HTCs values, although the tendency and shape of the curves are almost the same for all the different analysed heat source inlet temperatures. The impact that the hot water mass flow has on the working fluid HTC is almost negligible, while it is important when determining the one of the hot-side fluid. As the heat source mass flow is directly related to its heat transfer coefficient through the Reynolds number in a relation in the order of $Re^{0.55}$ (Mc Adams correlation), any increased mass flow leads to higher HTCs.

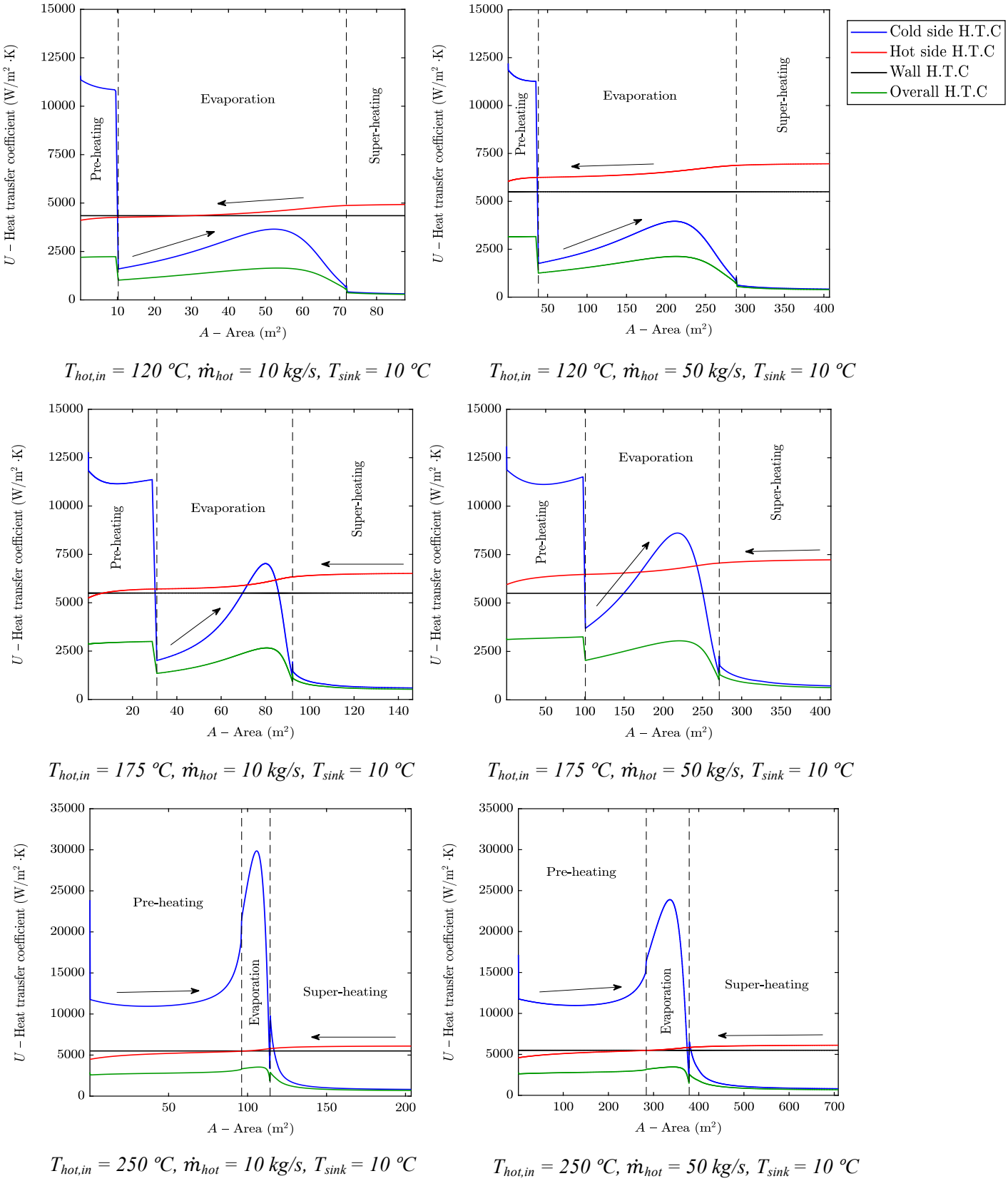

Figure 29. Heat transfer coefficients evolution through the PrHE for different heat source conditions when ammonia is used as the cycle working fluid (SIC optimization)

Regarding the fluid that limits the heat transfer process in the PrHE, Figure 29 shows that it depends on the maximum temperature of the cycle. When this temperature is relatively low, the working fluid constitutes the highest thermal resistance in almost all sections of the heat exchanger, meaning that special attention should be paid to the working fluid thermal properties when resorting to low-temperature heat source applications. As the $T_{hot,in}$ increases, the working fluid heat transfer coefficient evolution curve shows an important change of shape. The reason is that temperature is directly related to the transport properties of the fluid. As the temperature increases, the fluid thermal conductivity increases as well, while the fluid viscosity decreases. This leads to higher Reynolds and Nusselts numbers and, as a consequence, higher HTCs. This also causes an improvement of the hot side HTC, but not in a not too remarkable way.

Liquid-phase HTCs are much higher than vapour-phase HTCs (because of the higher density and higher thermal conductivity that all working fluids present in the liquid state). For this reason, ammonia HTC in the pre-heating section is so high that it does not limit the heat transfer process in none of the studied cases. This also implies that the area that is required to pre-heat the working fluid is so small that it represents a very low percentage of the overall PrHE surface.

Regarding the evaporation section, it can be seen that once ammonia reaches the saturated-liquid state, its heat transfer coefficient suddenly drops, as it enters the nucleate boiling phase (see Appendix A, “Boiling Regimes”). As ammonia evaporates, its heat transfer coefficient starts increasing and, at some points, it may overpass the hot-side HTC. This means that the fluid that limits the heat transfer process in the PrHE is not well-defined during the evaporation for medium-temperature heat source applications. There is a point at which the heat flux reaches its critical value, and the HTC of ammonia finds a peak. Once this point is crossed, ammonia’s heat transfer coefficient starts diminishing until it has completely evaporated. Figure 29 shows that the evaporation HTC peak is considerably higher when the heat source inlet temperature reaches 250 ºC. The reason is that higher hot source inlet temperatures entail higher heat fluxes, leading to considerably improved HTCs during the nucleate boiling process that result into evaporation areas that represent a minimum percentage of the overall PrHE surface.

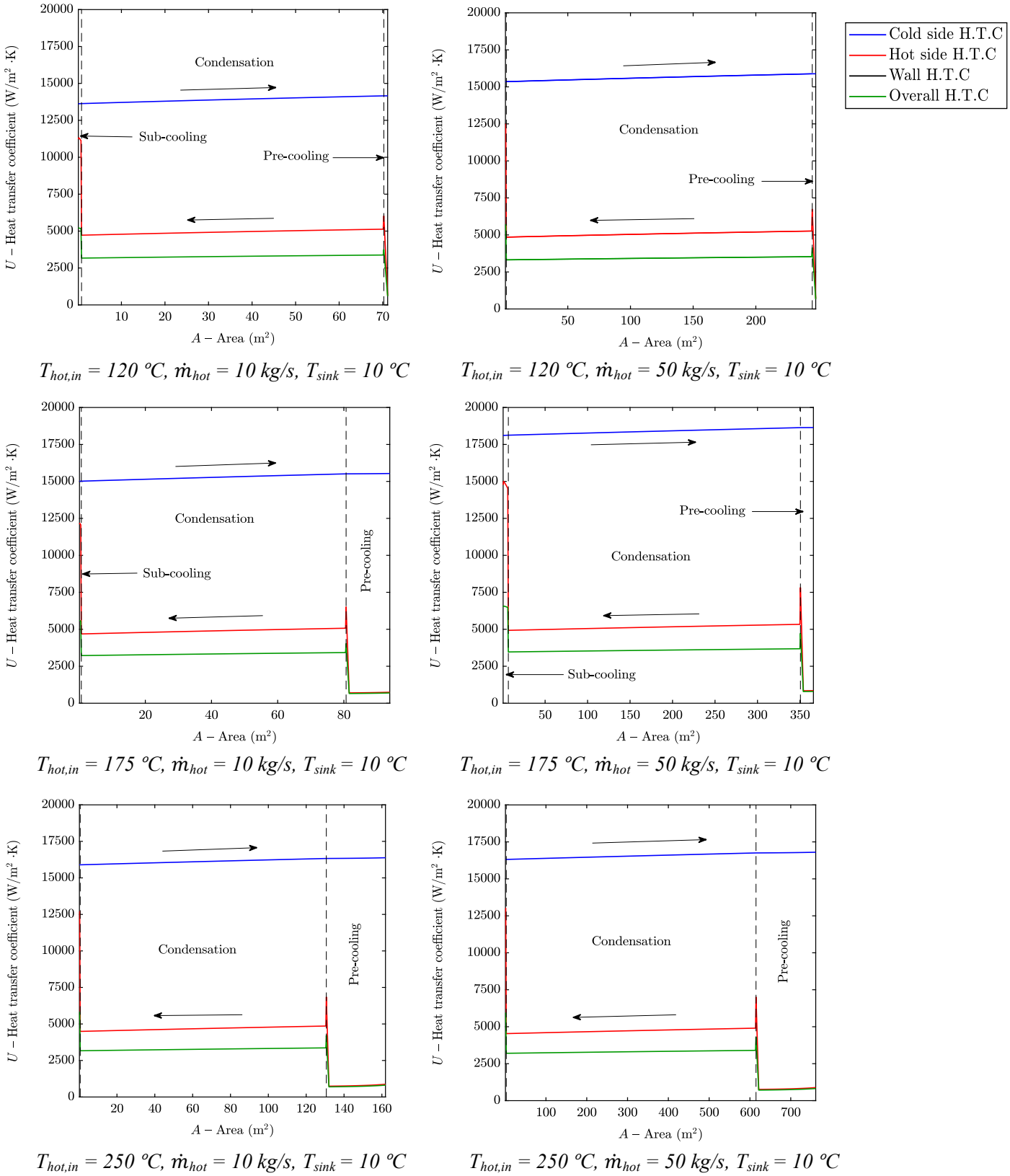

Figure 30. Heat transfer coefficients evolution through the condenser for different heat source conditions when ammonia is used as the cycle working fluid (SIC optimization)

Finally, with respect to the super-heating section, increasing the hot source inlet temperature implies reaching higher degrees of super-heating (as we have already seen in Section 10.5.6), which, together with the poor heat transfer coefficient that the working fluid presents in the vapour phase, results into the need of larger super-heating section surfaces.

When analysing the condenser HTCs when the Specific Investment Cost of the plant is optimized (see Figure 30), results show that their evolution tendency is much more stable than it was when analysing the ones obtained in the primary heat exchanger. This time, the conductivity heat transfer coefficient of the plates has not been plotted, as its value is so high that it does not limit the heat transfer process in none of the studied cases, and its impact on the overall HTC is negligible (although it is considered in the computations).

The low value that ammonia's HTC presents in the condenser pre-cooling section is again a consequence of the poor vapour thermal transfer properties. Once ammonia starts condensing, its heat transfer coefficient increases and keeps an almost constant value during the whole heat exchange process. Sub-cooling is presented in all cases, although the H.E area that it requires is small when compared to the overall condenser surface. The reason are the much better thermal transfer properties that the working fluid presents in the liquid phase. The light inclination that the cold-side heat transfer coefficient curves present is a consequence of the slight temperature jump the cooling water experiences when absorbing the heat from the working fluid.

The condenser size increases with the heat source inlet temperature because of the higher amount of heat that the working fluid must reject to the ambient. We have previously pointed out that the degree of super-heating rises as the hot source inlet temperature increases and, since this is also accompanied by higher turbine outlet temperatures, the need of pre-cooling to bring the super-heated vapour to the saturated conditions increases.

Regarding the effect of the heat source mass flow variations on the condenser heat transfer coefficients, it is almost negligible. Increasing the heat source mass flow implies higher heat inputs and hence, more heat must be rejected in the condenser. This leads to the need of greater cooling loads, which results into higher cold-side HTCs. However, as the heat

sink does never limit the heat transfer process in the condenser and its contribution to the overall HTC is almost negligible, condenser size variations when the heat source mass flow changes are just a consequence of the different amounts of heat that must be rejected in the heat exchanger.

- Thermodynamic optimization

Figure 31 and Figure 32 show how all heat transfer coefficients evolve through the PrHE and condenser respectively when the system second-law efficiency optimization is carried out.

By taking a look at the shapes of the curves plotted in Figure 31, it can be observed that they are similar to the ones that resulted from the techno-economic optimization (Figure 29). Once again, ammonia limits the heat transfer process in the evaporation and super-heating sections when a low-temperature heat source is used. As the heat source inlet temperature increases, the heat transfer limitation that the working fluid constitutes in the evaporation section losses weight until a temperature of 250 ºC is reached and the working fluid becomes the dominant thermal resistance only in the super-heating section.

Even though ammonia's HTC increases once the evaporation process starts, the peak it reaches when maximizing the second-law efficiency is much lower than it was when carrying out the techno-economic optimization. The main reason is that optimizing the performance of the plant leads to larger heat exchanger surfaces, which present lower associated heat fluxes. As the maximum evaporation heat transfer coefficient is reached at the maximum heat flux, any heat flux drop leads to a HTC worsening.

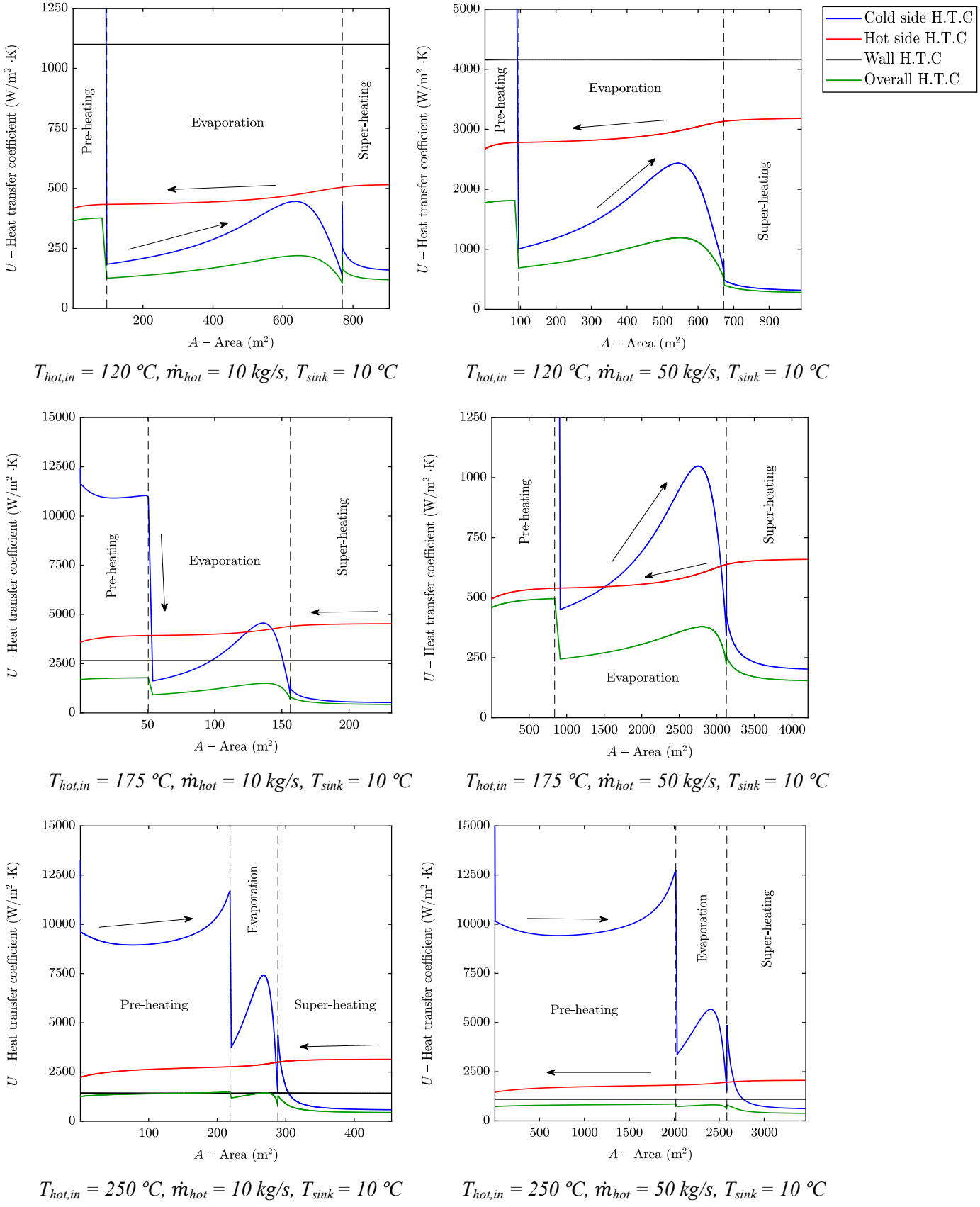

Figure 31. Heat transfer coefficients evolution through the PrHE for different heat source conditions when ammonia is used as the cycle working fluid (thermodynamic optimization)

With respect to the condenser heat transfer coefficients evolution when optimizing the performance of the cycle (see Figure 32), the deviations it presents with respect to the results obtained for the SIC optimization are not as remarkable as they were when analyzing the PrHE. The reason is that ammonia's HTC does not experience great variations when moving from one scenario to another. Therefore, the larger condenser heat transfer areas that the most efficient Rankine cycles require, against the most economical attractive ones, are a consequence of the optimum H.E designs that allow for minimizing the exergy destruction when higher amounts of heat must be rejected.

When comparing both optimization cases, it can be stated that the overall HTCs resulting from the thermodynamic optimization are lower than the ones obtained when executing the techno-economic optimization. The SIC optimization tends to look for the smallest possible heat transfer areas to reduce the cost of the heat exchangers to minima, hence, its tendency is to maximize the heat transfer coefficients. However, the thermodynamic optimization tends to look for large heat exchanger areas that entail lower pressure drops and, as a consequence, better cycle performances. For this reason, the thermodynamic optimization HTCs reach low values.

Once the hot source inlet temperature and mass flow variations impact on ammonia heat transfer coefficients were studied and analyzed, we observed that the fact of increasing the heat source mass flow has the same effect on all simulated working fluids, and that the medium hot source inlet temperature (175 ºC) is not required to define the tendency of the results when increasing the hot source inlet temperature from 120 ºC to 250 ºC. For this reason, for R152a and benzene analysis, only two hot source inlet temperatures (120 ºC and 250 ºC) and one heat source mass flow (10 kg/s) are going to be studied.

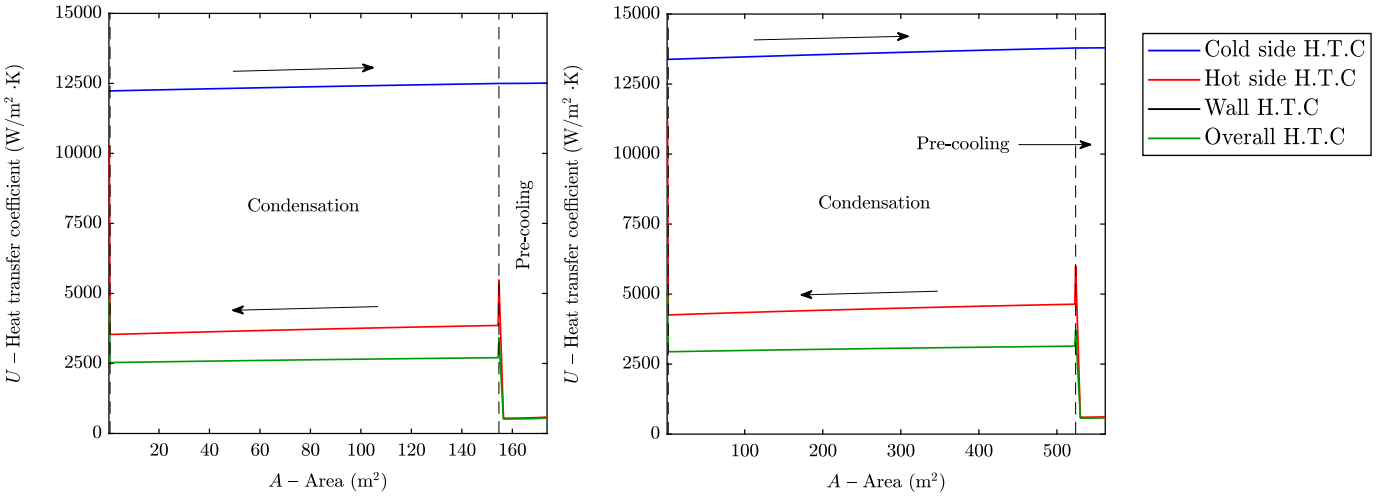

$T_{hot,in}$ = 120 ºC, $\dot{m}_{hot}$ = 10 kg/s, T_{sink} = 10 ºC

$T_{hot,in}$ = 120 ºC, $\dot{m}_{hot}$ = 50 kg/s, T_{sink} = 10 ºC

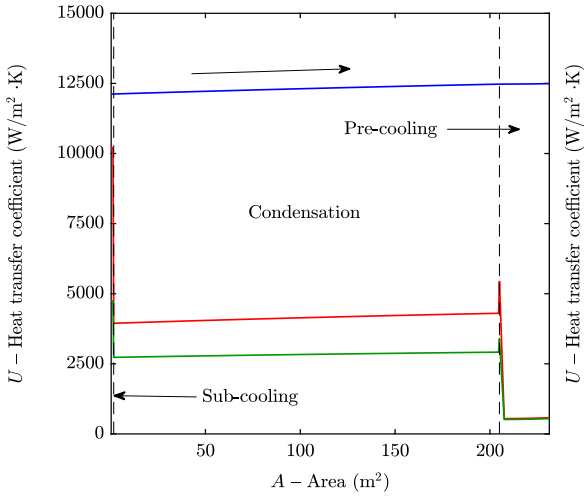

$T_{hot,in}$ = 175 ºC, $\dot{m}_{hot}$ = 10 kg/s, T_{sink} = 10 ºC

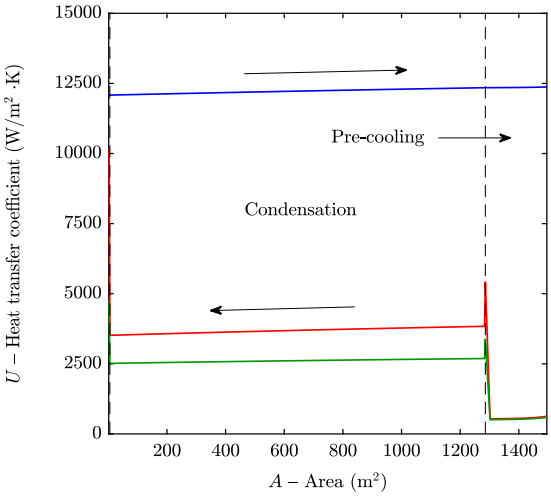

$T_{hot,in}$ = 175 ºC, $\dot{m}_{hot}$ = 50 kg/s, T_{sink} = 10 ºC

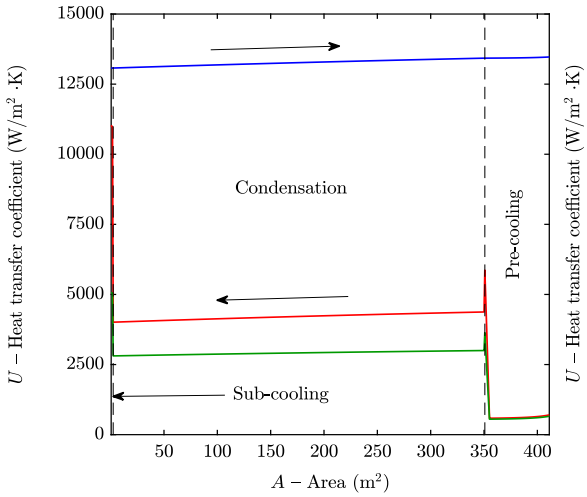

$T_{hot,in}$ = 250 ºC, $\dot{m}_{hot}$ = 10 kg/s, T_{sink} = 10 ºC

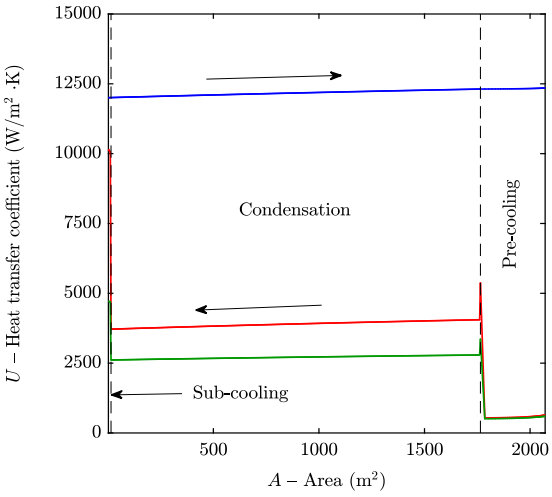

$T_{hot,in}$ = 250 ºC, $\dot{m}_{hot}$ = 50 kg/s, T_{sink} = 10 ºC

Figure 32. Heat transfer coefficients evolution through the condenser for different heat source conditions when ammonia is used as the cycle working fluid (thermodynamic optimization)

- Benzene

- SIC optimization

Figure 33 shows the HTCs evolution in both cycle heat exchangers when the system SIC is optimized and benzene is used as the working fluid.

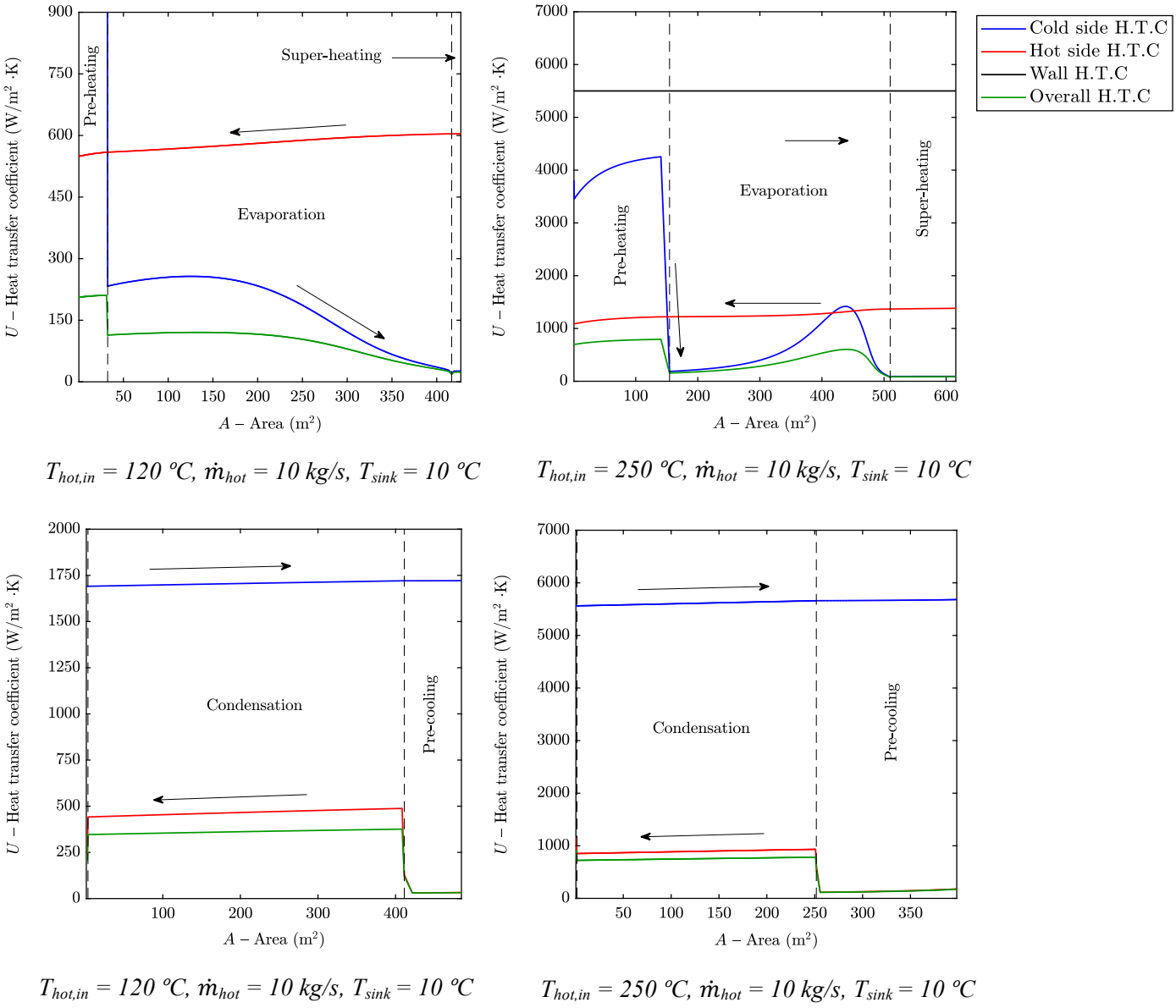

Figure 33. Heat transfer coefficients evolution through the primary heat exchanger and the condenser for different heat source conditions when benzene is used as the cycle working fluid (SIC optimization)

As the figure shows, increasing the hot source inlet temperature has the effect of improving the working fluid heat transfer coefficient, just like it happened with ammonia. However, for benzene, this growth is not as high as it was for ammonia and, even at high maximum cycle temperatures, benzene limits the heat transfer process in the evaporation section. This is a consequence of the low operating pressures benzene is forced to work at. Increasing the heat source inlet temperature allows for higher operating pressures, which considerably improve benzene's HTC.

- Thermodynamic optimization

When optimizing the cycle performance, benzene's HTCs evolution in the PrHE (see Figure 34) follows the same trend as the one it followed when optimizing the SIC, in the sense that it presents a very high heat transfer coefficient in the pre-heating section that considerably drops when evaporation starts. Once again, benzene limits the evaporation and super-heating heat exchange processes.

Even at the highest studied heat source inlet temperature (250 ºC), the peak that benzene's HTC reaches can only overpass the hot-side heat transfer coefficient in a very small region of the evaporation section, highlighting how low H.E heat fluxes are when operating with low T_{max}/T_{crit} fluids. Something that stands out when moving from the techno-economic optimization to the thermodynamic one, is the drop that the hot-side heat transfer coefficient experiences, which is especially relevant in the pre-heating section, as it constitutes the limiting thermal resistance and causes a considerable rise of the required pre-heating surface.

Benzene's heat transfer coefficient in the condenser does also follow the same trend in both optimization cases, with the only difference that it experiences a light drop when optimizing the performance of the Rankine cycle, because of the lower condensing pressures at which the cycle operates.

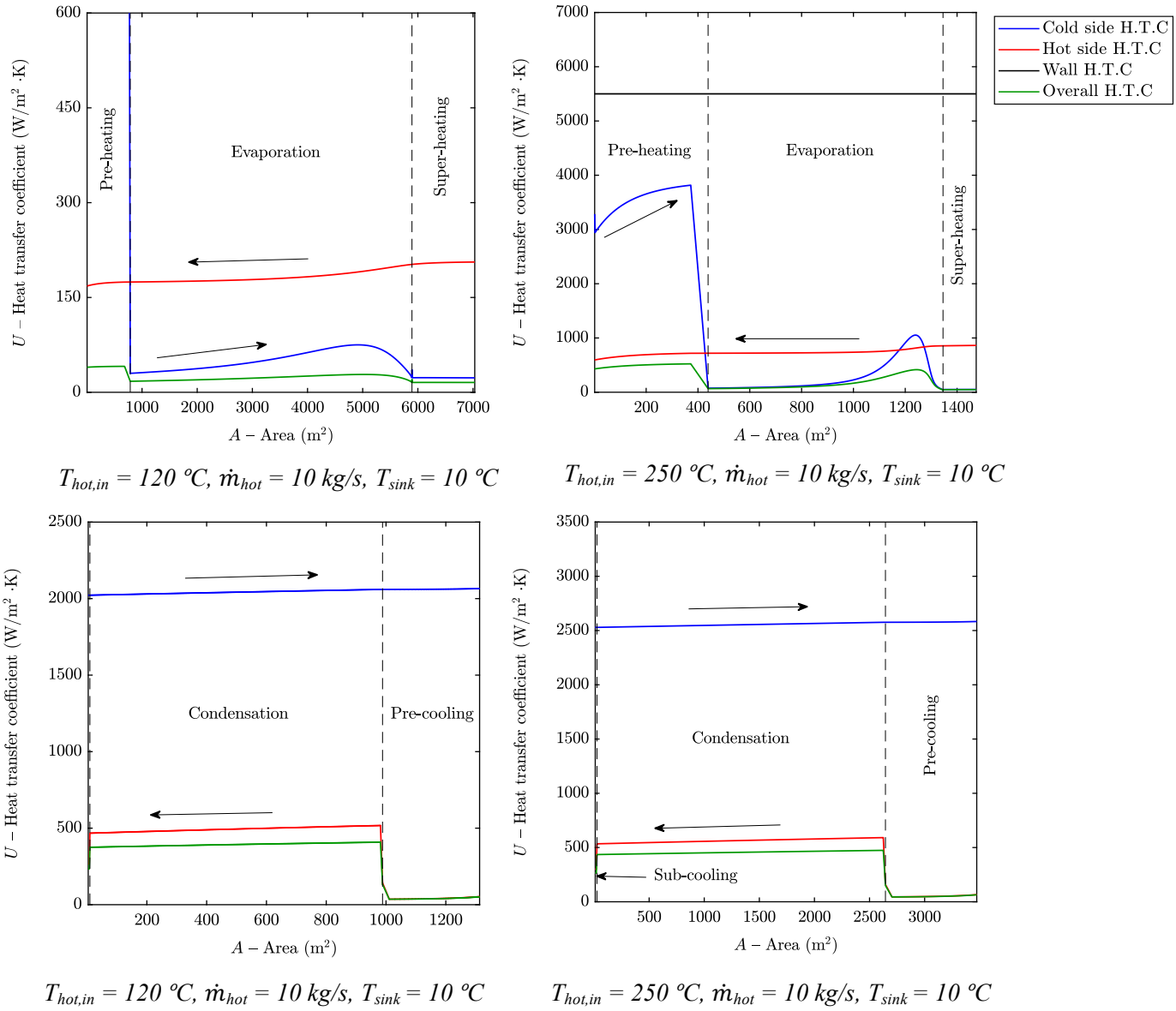

Figure 34. Heat transfer coefficients evolution through the primary heat exchanger and condenser for different heat source conditions when benzene is used as the cycle working fluid (thermodynamic optimization)

- <u>R152a</u>

- SIC optimization

The resulting heat transfer coefficients evolution obtained when optimizing the Specific Investment Cost of the R152a Rankine cycle (see Figure 35) is similar to the one that was

achieved for ammonia (Figure 31). The main reason is that R152a operates at evaporation pressures close to the critical one, leading to high heat transfer coefficients values that approach ammonia's HTCs much more than benzene's.

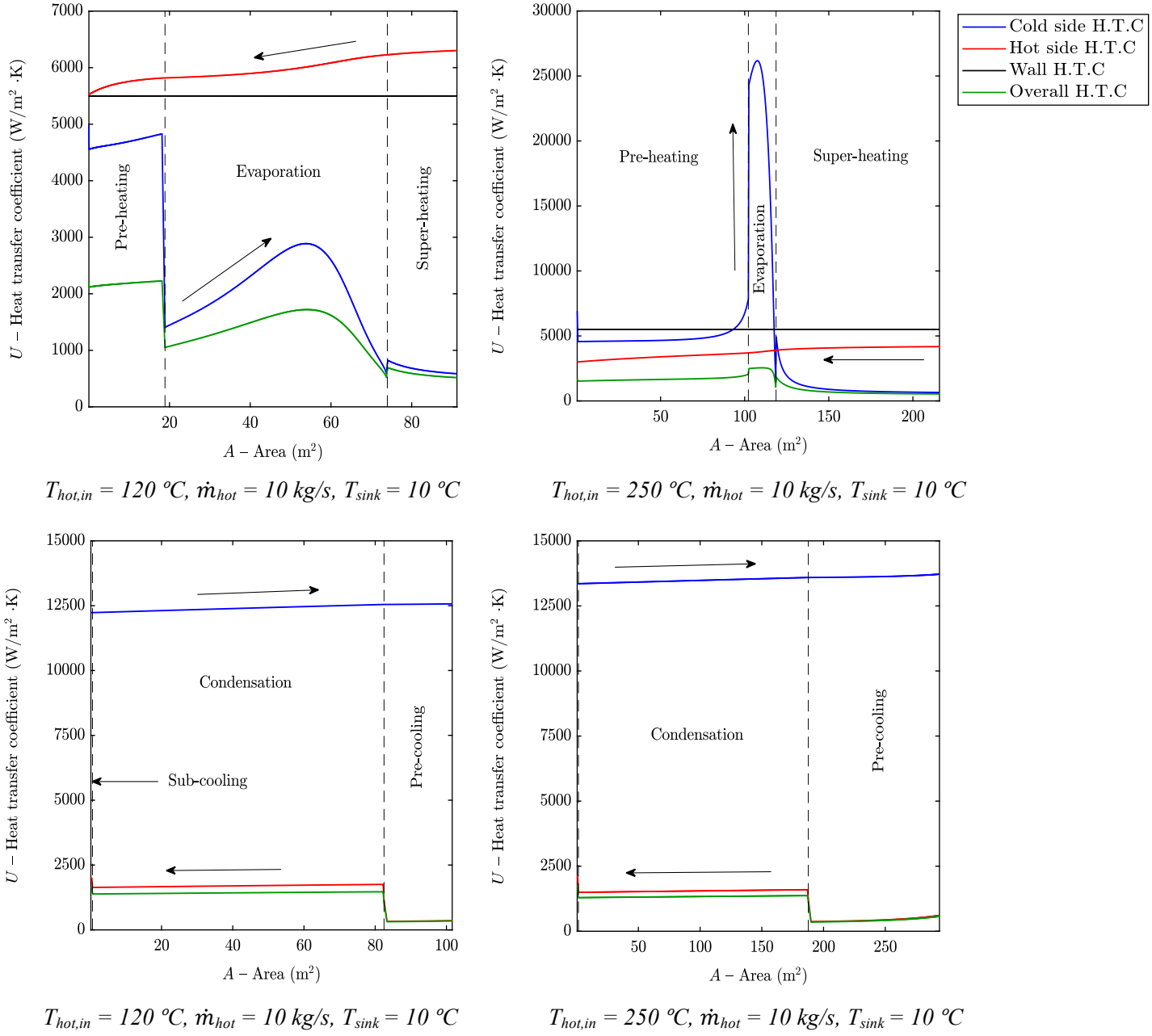

$T_{hot,in}$ = 120 ºC, $\dot{m}_{hot}$ = 10 kg/s, T_{sink} = 10 ºC

$T_{hot,in}$ = 250 ºC, $\dot{m}_{hot}$ = 10 kg/s, T_{sink} = 10 ºC

$T_{hot,in}$ = 120 ºC, $\dot{m}_{hot}$ = 10 kg/s, T_{sink} = 10 ºC

$T_{hot,in}$ = 250 ºC, $\dot{m}_{hot}$ = 10 kg/s, T_{sink} = 10 ºC

Figure 35. Heat transfer coefficients evolution through the primary heat exchanger and condenser for different heat source conditions when R152a is used as the cycle working fluid (SIC optimization)

In the PrHE, R152a constitutes the limiting thermal resistance in all sections until a sufficiently high hot source inlet temperature that allows to operate at high evaporation pressures is reached. This increased evaporation pressure entails much higher heat transfer coefficients, to the point of making R152a the heat transfer limiting fluid only in the super-heating section. Once again, the nucleate boiling regime allows to achieve a high HTC peak that makes the evaporation area represent an almost negligible percentage of the overall PrHE area.

The condenser heat transfer coefficients evolution, and hence its analysis, is exactly the same as the one we have previously described for ammonia. The increased pre-cooling section area that can be observed when increasing the heat source inlet temperature is a consequence of the higher degree of super-heating.

- Thermodynamic optimization

In relation to the thermodynamic optimization of R152a cycles, Figure 36 shows that, once again, the working fluid heat transfer coefficient has the same tendency as the one ammonia showed.

The main difference that can be observed when comparing R152a's and ammonia's results is that the nucleate boiling peak that the R152a heat transfer coefficient reaches at the highest maximum cycle temperature (250 ºC) is higher than the value it takes in the pre-heating section, while ammonia's HTC showed the contrary. Since ammonia requires smaller PrHE areas than R152a, the maximum heat flux that is reached during its evaporation process is higher, entailing higher HTCs peaks.

The different optimum condensing pressures that result from the thermodynamic and Specific Investment Cost optimizations are the cause of the deviations that the overall heat transfer coefficient experiences when setting different objective functions. The lower condensing pressures that optimizing the cycle performance entails, together with the smaller LMTDs and the greater heat duties that must be rejected, cause that this optimization case results into larger condenser sizes than the ones obtained when optimizing the SIC.

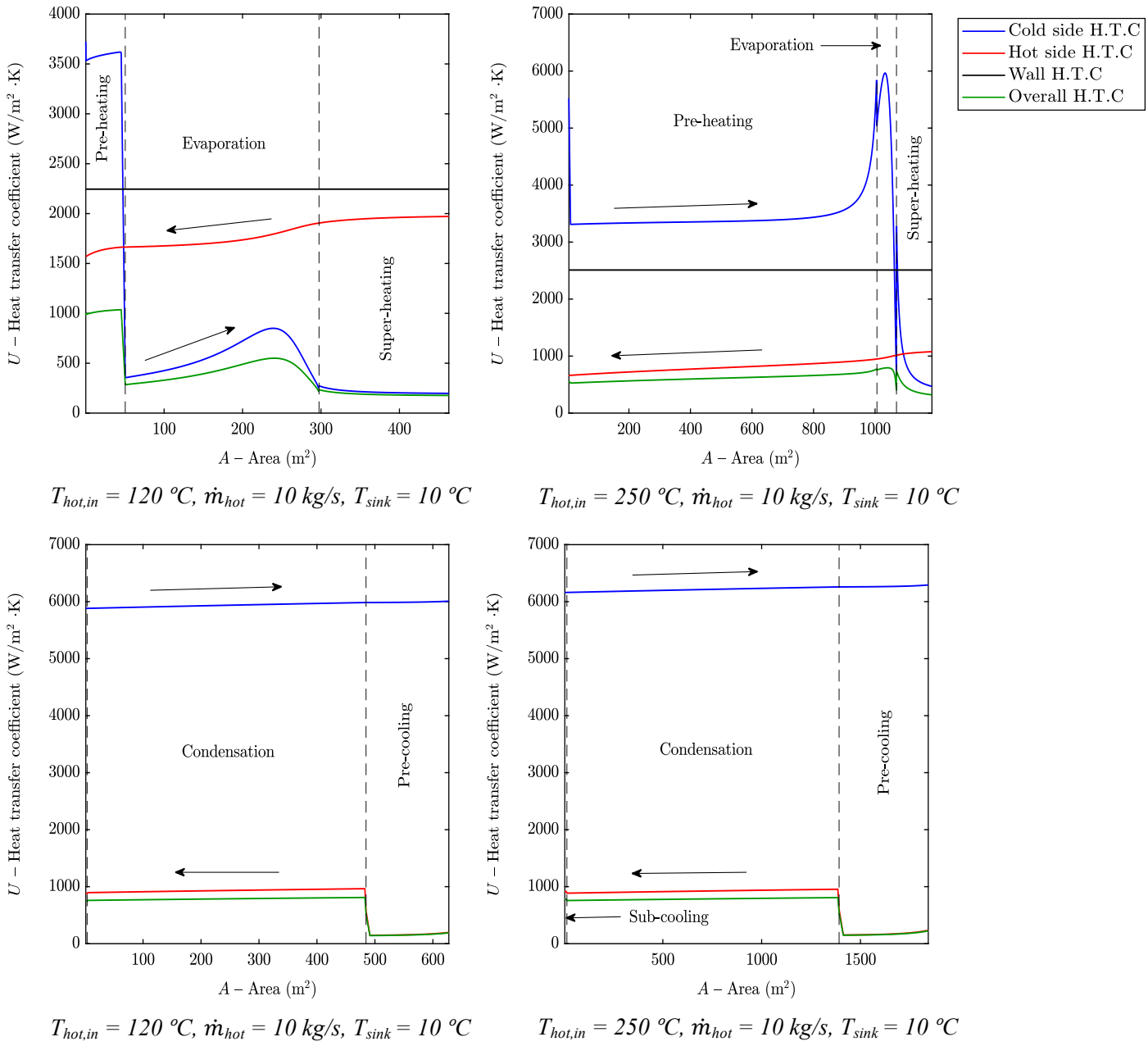

Figure 36. Heat transfer coefficients evolution through the primary heat exchanger and condenser for different heat source conditions when R152a is used as the cycle working fluid (thermodynamic optimization)

After having analyzed all working fluids heat transfer coefficients evolution through the cycle heat exchangers, it was found that ammonia cycles require the smallest pre-cooling

surfaces in the condenser. This is one of the main reasons why this working fluid does always reach the best Specific Investment Cost results. The explanation to this is closely related to the fact that ammonia is a wet working fluid, and the degree of super-heating it presents when leaving the turbine is lower than it is for the rest of organic working fluids (which are dry or isentropic), being much closer to the vapour saturated line.

10.5.8 Pressure drop

High fluid velocities in the heat exchangers can improve the HTCs to a great extent, although they also imply greater fluid pressure drops, which are a source of irreversibilities that deteriorates the plant performance. For this reason, the H.E allowed pressure drop is of main importance when determining the heat exchangers design, which considerably changes depending on the objective function choice.

The pressure drop results that were obtained after having carried out the techno-economic and thermodynamic optimization present important differences. While the SIC optimization tends to minimize the heat exchanger areas in an effort to optimize the system cost, the thermodynamic optimization tends to maximize the cycle second-law efficiency by minimizing the exergy destruction without taking into consideration the cost of the plant, resulting into large heat exchangers surfaces. As fluid velocities in the heat exchangers increase with the size of these components, friction effects, and hence pressure drops, reach higher values in the largest heat exchangers. For this reason, the techno-economic optimization does always result into much higher pressure drops than the performance optimization.

As an example, a case study of ammonia, a 10 kg/s heat source with an inlet temperature of 200 ºC, and a heat sink with an inlet temperature of 15 ºC, presents a hot-side pressure drop of 0.1% and a working fluid pressure drop of 8.79% in the PrHE after optimizing the SIC, while, for the same case study, optimizing the second-law efficiency leads to a shell-side pressure drop of 0.1% and a working fluid pressure drop of 2.86%. Regarding the PrHE required surface, it reaches a value of 146.20 m^2 in the first optimization case, and 311.83 m^2 in the second one, while the second-law efficiency increases from 42.31% to 43.90%, meaning that a large area increase is required for a little efficiency gain. This

is a clear example of how the heat exchanger design may determine the cycle cost (related to the heat exchangers area) and the cycle performance (related to the heat exchangers pressure drops).

When the heat source inlet temperature increases, the size of the system heat exchangers tends to increase as well, due to the need of enlarging the heat transfer areas for the greater heat duties. This has the effect of reducing the fluids pressure drops in the heat exchangers. However, as it was previously shown in Section 10.5.5, fluids mass flows do also increase with the heat source inlet temperature. Higher mass flows imply greater fluid velocities and hence, increased pressure drops. Therefore, the pressure drop evolution with the heat source inlet temperature does not follow a clear well-defined tendency, since its value depends on the balance between both described phenomena.

We need to highlight that the cooling water pressure drop in the condenser does not present a too relevant importance when it comes to optimize the Rankine cycle second-law efficiency or its Specific Investment Cost for two reasons:

1. Any change in the cooling-fluid transport properties that can arise because of the pressure drop it experiences has no influence on the condenser size, as the cold-side HTC is so high that it has an almost negligible effect on the overall heat transfer coefficient.

2. Great cooling-fluid pressure drops may imply stricter pumping requirements, but, as we have previously demonstrated, the power consumption that the pumps require is almost negligible in comparison with the turbine power output, so the pressure drop that the cooling fluid pump has to face does not lead to much reduced power outputs.

On the other side, any pressure drop that the working fluid may suffer in the Rankine cycle does have a great impact on both the performance and cost of the system. This is of importance when designing the primary heat exchanger, as the wide range of values that the inlet diameter can take may lead to low or high working fluid pressure drops depending on the defined objective function. Therefore, special attention should be paid

to the pressure drop the working fluid experiences in the primary heat exchanger, as it is key to determine the optimum design of the heat exchanger.

11 Conclusions

From the discussed results, the following conclusions have been extracted:

11.1 Different H.E configurations conclusions

1. Working fluids with a dimensionless temperature (T_{max}/T_{crit}) in a range between 0.97 and 1.02 give the best results when optimizing the Specific Investment Cost for all the different H.E configurations that can be implemented in the Rankine cycle with the plate and shell-and-tube heat exchangers. From the studied working fluids, the best results were obtained for ammonia, R152a, DME, propylene and R32 (none of them surpassing 4000 $/kW). These results show an agreement with S. Lemmens studies, who stated in [69] that investment costs of most ORC projects are in the 2000 – 4000 €/kW range.

2. When optimizing the Specific Investment Cost of Rankine cycles, wet working fluids normally yield better results than dry and isentropic working fluids with similar T_{max}/T_{crit} ratios. These working fluids require smaller pre-cooling surfaces, and their associated condenser cost is considerably lower. The most remarkable case is ammonia, which reaches the lowest SIC for all the studied H.E configurations.

3. A maximum evaporation pressure limitation had to be set to avoid transcritical cycles. All working fluids with a T_{max}/T_{crit} higher than 1.02 tend to work at the maximum allowed pressure, meaning that their potential of improvement is restricted. It is expected that better SIC results can be reached for these working fluids when operated under transcritical conditions, although limitations in our model did not allow to check it.

4. Fluids with a T_{max}/T_{crit} lower than 0.97 present high SICs that tend to increase as the temperature ratio is lower. These working fluids are forced to work at low operating pressures that imply low densities and temperatures that worsen their

HTC, leading to bigger and more expensive heat exchangers. S. Quoilin et al. [68] did also work with an operating temperature limitation to avoid transcritical cycles, reaching the same conclusions: high critical temperature working fluids involve working at low densities that cause an oversizing of the cycle components.

5. The H.E configuration that entails the lowest SIC is the one that resorts to the plate heat exchanger as both PrHE and condenser. This configuration allows to increase the power output by super-heating the vapour at the outlet of the H.E, without leading to a need of much larger heat transfer areas. This shows an agreement with the results obtained by H. Hajabdollahi et al. in [71], who carried out a comparative study for cost optimization of plate heat exchangers and shell-and-tube heat exchangers, concluding that the formers allow for a 13% reduction in the total cost compared to the shell-and-tube heat exchangers.

6. PS configuration[24] shows the second best SICs results, which do not present high deviations when compared to PP results. SP and SS configurations present the worst SIC results, and their use is not justified for low-temperature heat sources. These two last mentioned configurations entail an over-sizing of the cycle components and much lower power outputs.

7. When exploiting a low-temperature heat source, the working fluid limits the heat transfer process in the pre-heating and super-heating sections of the plate PrHE, while it is always the limiting fluid when the PrHE is of the shell-and-tube type. In the condenser, it does not matter the kind of H.E we implement: the working fluid always constitutes the highest thermal resistance. Therefore, special

[24] For the heat exchangers configurations abbreviations, the first letter refers to the type of primary heat exchanger, while the second one refers to the type of condenser. “P” is used for “plate heat exchanger” and “S”, for “shell-and-tube heat exchanger”.

attention should be paid to the working fluid thermal properties when designing the cycle heat exchangers to avoid limiting the heat exchange processes[25].

8. When using a shell-and-tube condenser, the contribution of this component to the overall cost has a meaningful importance, representing a great percentage of the power cycle SIC (higher than 50%). Both configurations that use plate condensers, show a much more balanced distribution of the overall cost between the PrHE, condenser and expander, although the condenser does always represent the greatest share of the overall cost, around 40%. This last assertion shows an agreement with the results obtained by Y. Nusiaputra et al. in [72], who stated that the main feature contributing to the cost of the system is the cooling-system, reaching shares that amount to 35% - 38% of the investment cost. Therefore, resorting to shell-and-tube condensers is hardly recommended if the cost of the system wants to be minimized.

11.2 SIC and thermodynamic optimizations conclusions

1. Increasing the heat source inlet temperature or its mass flow, and reducing the heat sink inlet temperature, lead to better SIC results for all the studied working fluids. The effect is greater for working fluids with high T_{max}/T_{crit}.

2. Large-capacity Rankine cycles have a higher cost than low-capacity Rankine cycles, although their related SIC is much lower because of the greater power outputs. This conclusion was also reached by S. Lemmens [69], who declared that larger geothermal projects have lower SICs, and J. Wang et al. [66], who concluded that increasing the exergy efficiency of Organic Rankine Cycles usually raises the overall capital cost of the system.

[25] No article covering which fluid limits the heat exchange process in different types of heat exchangers could be found in open literature.

3. Increasing the heat source inlet temperature implies higher evaporation pressures and better cycle performances until the working fluid reaches its maximum optimum allowed evaporation pressure. Once this point is reached, further temperature increases cause efficiency drops (for sub-critical cycles). These conclusions are the same for varying heat source mass flows. This is in consistency with conclusions reached by S. Quoilin et al. [68], M. Imram et al. [55], and D. Walraven et al. [73], who affirmed that, when optimizing the thermodynamic performance of an ORC, every fluid has a heat-source inlet temperature that maximizes the plant exergy efficiency.

4. Results in this work show that higher heat source inlet temperatures have almost no impact on the condensing pressure. This last assertion was also formulated by Y. Li et al. in [59], whose results showed that increasing heat source inlet temperatures lead to increased evaporation pressures but provoke little changes of the condensing temperatures.

5. Reduced condensing temperatures lead to better cycle performances. This is closely linked to the ambient temperature. D. Walraven et al. [74] came to the same conclusions after having executed the techno-economic optimization of a low-temperature geothermal heat source ORC for a varying dry-bulb temperature.

6. Improving the efficiency of Rankine cycles has an associated extra cost that yields to higher SICs. This conclusion was also reached by M. Imran et al. in [55]. Results reached in this work show that ammonia presents the lowest extra SIC when improving the performance of the cycle by 1%, while R152a is associated with the highest one. The extra SIC that is required when improving the cycle performance is even higher for large-capacity plants. This should be taken into consideration when designing power plants that are expected to operate at varying loads and require a high flexibility.

7. The hot source temperature out of the PrHE is much lower when optimizing the performance of the Rankine cycle than when its SIC is minimized, as the available heat is better used in a more efficient heat transfer process. This implies that the

less costly Rankine cycle power plants are more likely to be used with co-generation purposes than the most efficient ones, as the hot source fluid may leave the PrHE at temperatures up to 85 ºC (benzene case).

8. Lower pinch-point temperatures imply higher Specific Investment Costs and better system efficiencies. The same results tendency was obtained by J. Wang et al. in [66].

9. Improved SICs do always entail higher degrees of super-heating, with the exception of low critical temperature working fluids, for the ones the poor HTCs imply much larger heat transfer areas that cannot be compensated by slightly higher power outputs. This tendency is concordant with the one that N. Kazemi et al. [24] found when analyzing the effect of the degree of super-heating on the SIC of the system.

10. HTCs reach their highest value when the working fluid is in the liquid phase. This normally implies that the super-heating and the pre-cooling sections represent higher percentages of the overall H.E surfaces than the pre-heating and sub-cooling sections.

11. The fluid that limits the heat transfer process in each section of the PrHE depends on the T_{max}/T_{crit} relationship, while it is always the working fluid that limits the heat transfer process in all the condenser sections. As the impact of the cost of this component on the overall SIC is major, attention should be put to the working fluid transfer properties when designing the cycle, especially when high degrees of super-heating are required.

12. SIC optimizations yield high pressure drops that deteriorate the performance of the power plant. On the other side, the thermodynamic optimization may result into enormous H.E areas and costs, being consistent with what D. Walraven et al. asserted in [73], *"the efficiency of an ORC increases with increasing heat-exchanger surface"*. Also, M. Imran et al. [55] executed the system optimization in order to reach minimum values for both the H.E pressure drops and system

cost, finding that both objective functions are conflicting and no set of values can satisfy both conditions at the same time. These phenomena should be considered when designing the heat exchangers in order to avoid too poor systems' performances or/and considerably expensive unfeasible over-sized components.

11.3 Evaluation of objectives

This section has the purpose of evaluating the accomplishment of the objectives stated in Section 1.3.

1. A deep literature review was carried out, and all information and data regarding the design of Rankine cycles components, heat transfer correlations, cost correlations, etcetera, were presented in Chapters 3, 4, 5, 6 and 7.

2. A MATLAB code was developed to execute the steady-state cycle optimization of the Specific Investment Cost and the second-law efficiency. The code is able to compute all the thermodynamic states of the cycle and the required correlations to find the optimum solution. Furthermore, it was refined to decrease the computational time and proper documentation and descriptions of each one of the computed functions have also been included.

3. The model validation could not be carried out, and it constitutes the main limitation of this work. The lack of information in open literature did not allow for simulating any of the case studies that other authors analyzed, as our model requires assumptions and many different inputs that authors do not specify in their publications. Furthermore, considering the great amount of different correlations that can be used to simulate the same process but that give dissimilar results, no model like the one we presented in this work could be found, making the validation not possible to be executed. More reasons regarding this challenge were given in Section 10.1. In spite of this, conclusions in Section 11.1 and 11.2 include the agreement between the tendencies of the results obtained in this work and the

ones found in the literature. Even though the compared results are not numerically the same, their tendency is, showing the model reliability.

4. A specific case study (presented in Chapter 9) was selected for executing the Specific Investment Cost cycle optimization for different heat exchangers configurations and working fluids. The results and discussion of this case study were presented in Chapter 10.2.

5. From the results obtained in the previously mentioned case study, the most suitable heat exchanger configuration was selected for a specific set of working fluids, and the thermodynamic and techno-economic optimizations were carried out for different heat source and heat sink scenarios. Both optimization results were first analyzed in a separate way in Sections 10.3 and 10.4, and their comparison was given in Section 10.5.

6. Not only the best set of working fluids was included in this work, but also some others for which the thermodynamic and techno-economic optimization results were not so good. An analysis was carried out during the discussion process in Chapter 10, allowing for generalizing the results and coming to the conclusions presented in Section 11.1.

11.4 Further work

The development of this Master Thesis work has revealed how wide the field of Rankine cycles is and the numerous possibilities that its study offers. From the obtained conclusions, we found that this Thesis can be used to guide future work. Our suggestions for further work are:

1. It was set out that increasing the heat source inlet temperature implies much stricter cooling loads requirements. This may come with problems when the cycle is designed for water scarcity locations. For this reason, we suggest the study of Air-Cooled Condensers in order to determine how the cost of the power plant may

be affected by the fans consumption and the much larger H.E areas that the poor air HTCs would imply.

2. The work that was here presented included the techno-economic and thermodynamic optimization of Rankine cycles in a separate way, as one of the objectives of the Thesis was to determine how the different cycle parameters could affect the cost and performance of the power plant. It would be of interest to study how these cycle parameters behave when executing the thermodynamic and SIC optimizations in combination by means of the multi-objective optimization. A good approach would be to study different scenarios giving different weights to each one of the objective functions.

3. Studying the use of different kind of heat sources that entail much higher maximum cycle temperatures, such as waste heat recovery, could be interesting. This way, a more proper assessment for the use of high critical temperature working fluids could be given.

4. Studying other cost objective functions that include installation, instrumentation, land, licenses and research costs (among others) can lead to more realistic results that can be used to assess in a better and much more detailed way the construction of Rankine cycle power plants.

5. The heat transfer correlations that we decided to implement in our code were selected after having carried out a deep literature research. These were chosen taking into consideration the advice to use the most common and suitable ones. However, many different correlations that can be computed to drive the heat transfer process were found during the research, and not all authors agree on which ones give the most realistic approaches. As it could be seen in some of the plotted figures (such as Figure 36), the fact of having to resort to different source correlations for studying the HTC evolution of same working fluid, resulted in strange curves tendencies at the points where the different correlations coincided.

Implementing different heat transfer correlations than the ones we have used for the development of this Master Thesis may help to avoid discontinuities in the phase change locations. This could be helpful for moving forward in a field that seems to present a lack of consensus.

Bibliography

[1] E. Macchi, M. Astolfi, L. Bronicki, L. Bell, E. Lemmon, C. Invernizzi, D. Bonalumi, F. Casella, E. Martelli, L. Pierobon, G. Persico, M. Pini and P. Valdimarsson..., Organic Rankine Cycle (ORC) Power Systems. Technologies and Applications, E. Macchi and M. Astolfi, Eds., Elsevier, 2017.

[2] I. Encabo., R. Agromayor. and L. Nord, "Thermodynamic Optimization of an Organic Rankine Cycle for Power Generation from a Low Temperature Geothermal Heat Source," in *Proceedings of the 58th SIMS*, Reykjavik, 2017.

[3] M. Astolfi, M. Romano, P. Bombarda and E. Macchi, "Binary ORC (Organic Rankine Cycles) power plants for the exploitation of medium-low temperature geothermal sources - Part B: Techno-economic optimization," *Energy,* no. 66, pp. 435 - 446, 10 January 2014.

[4] T. Tartière and M. Astolfi, "IV International Seminar on ORC Power Systems, ORC 2017. A World Overview of the Organic Rankine Cycle Market," *Energy Procedia,* vol. 129, pp. 2-9, 13-15 September 2017.

[5] Knowledge Center for Organic Rankine Cycle, "History of ORC," [Online]. Available: http://www.kcorc.org/en/science-technology/history/. [Accessed October 2017].

[6] P. Colonna, E. Casati, C. Trapp, T. Mathijssen, J. Larjola, T. Turunen-Saaresti and A. Uusitalo, "Organic Rankine Cycle Power Systems: From the Concept to Current Technology Applications, and an Outlook to the Future," *Journal of Engineering for Gas Turbines and Power,* vol. 137, October 2015.

[7] J. Freeman, K. Hellgardt and C. Markides, "An assessment of solar-powered organic Rankine cycle systems for combined heating and power in UK domestic applications," *Applied Energy,* vol. 138, pp. 605-620, November 2014.

[8] M. Talukdar, "ADT Alarm Systems," 14 December 2016. [Online]. Available: http://www.adtalarmsystems.com/heat-exchanger-uses-in-various-industries/. [Accessed 20th October 2017].

[9] Turboden, "ORC plants for Industrial Heat Recovery," 2011. [Online]. Available: http://www.turboden.eu/en/public/downloads/11- COM.P-18-rev.4_HR_ENG.pdf.

[10] ORMAT, "Financial annual reports, 2012-2015," [Online]. Available: http://investor.ormat.com/GenPage.aspx?IID=4087066&GKP=302737.

[11] S. Goel, O. Herzog, A. Datta, D. R. Sonde, K. Deshpande, J. Fink and T. Schumacher, "Market potential study for organic Rankine cycle technology in India," *Indo-German Energy Forum,* June 2014.

[12] B. Tchanche, M. Pétrissans and G. Papadakis, "Heat resources and organic Rankine cycle machines," *Renewable and Sustainable Energy Reviews,* vol. 39, pp. 1185-1199, 2014.

[13] H. Chen, D. Goswami and E. Stefanakos, "A review of thermodynamic cycles and working fluids for the conversion of low-grade heat," *Renewable and Sustainable Energy Reviews,* vol. 14, p. 3059–3067, 2010.

[14] B. Junjiang and L. Zhao, "A review of working fluid and expander selections for organic Rankine cycle," *Renewable and Sustainable Energy Reviews,* vol. 24, p. 325–342, 2013.

[15] B. Saleh, G. Koglbauer, M. Wendland and J. Fischer, "Working fluids for low-temperature organic Rankine cycles," *Energy,* no. 32, pp. 1210-1221, 2007.

[16] M. Astolfi, E. Martelli and L. Pierobon, "Thermodynamic and technoeconomic optimization of Organic Rankine Cycle systems," in *Organic Rankine Cycle (ORC) Power Systems*, 1 ed., Milan; Lyngby, Elsevier Ltd., 2016, pp. 173 - 248.

[17] R. Agromayor and L. Nord, "Fluid selection and thermodynamic optimization of organic Rankine cycles for waste heat recovery applications," *Energy Procedia,* vol. 129, pp. 527-534, 2017.

[18] A. Schuster, S. Karellas and R. Aumann, "Efficiency optimization potential in supercritical Organic Rankine Cycles," *Energy,* no. 35, pp. 1033-1039, 2010.

[19] F. Haberle, M.-. Preibinger and D.-. Brüggermann, "Zeotropic mixtures as working fluids in Organic Rankine Cycles for low-enthalpy geothermal resources," *Renewable Energy,* vol. 37, no. 1, pp. 364-370, 2012.

[20] I. Pioro and S. Mokry, "19. Heat Transfer to Fluids at Supercritical Pressures," in *Heat Transfer - Theoretical Analysis, Experimental Investigations and Industrial Systems*, P. A. Belmiloydi, Ed., In-Tech, 2011, pp. 481-504.

[21] I.L.Pioro, H. Khartabil and R.B.Duffey, "Heat transfer to supercritical fluids flowing in channels - empirical correlations (survey)," *Nuclear Engineering and Design,* vol. 230, pp. 69-91, 27 October 2003.

[22] L. Tocci, T. Pal, I. Permazoglou and B. Franchetti, "Small Scale Organic Rankine Cycle (ORC): A Techno-Economic Review," *Energies,* no. 10, March 2017.

[23] R. Shah and D. Sekulic, in *Fundamentals of Heat Enchanger Design*, New York; Kentucky, John Wiley & Sons, 2003, pp. 1-74.

[24] N. Kazemi and F. Samadi, “Thermodynamic, economic and thermo-economic optimization of a new proposed organic Rankine cycle for energy production from geothermal resources,” *Energy Conversion and Management,* no. 121, pp. 391-401, 2016.

[25] F. T. Touceda, “2. Transferencia de calor en intercambiadores de placas. Estudio del proceso de ebullición forzada de la mezcla amoniaco/agua en intercambiadores de placas para equipos de refrigeración por absorción,” *Universitat Rovira i Virgili,* 2006.

[26] Sondex, “Plate Type Heat Exchangers: Operation & Maintenance Manual,” 26 April 2011. [Online]. Available: http://www.sondex-usa.com.

[27] M. Lazova, H. Huisseune, A. Kaya, S. Lecompte, G. Kosmadakis and M. d. Paepe, “Performance Evaluation of a Helicoidal Coil Heat Exchanger Working under Supercritical Conditions in a Solar Organic Rankine Cycle Installation,” *Energies,* no. 9, p. 432, 2016.

[28] G. Longo, “Refrigerant R134a condensation heat transfer and pressure drop inside a small brazed plate heat exchanger,” *Int. J. Refrig,* no. 31, pp. 780-789, 2008.

[29] S. Karellas, A. Schuster and A. Leontaritis, “Influence of supercritical ORC parameters on plate heat exchanger design,” *Appl. Therm. Eng,* no. 33, pp. 70-76, 2012.

[30] D. Walraven, B. Laenen and W. D'haeseleer, “Economic system optimization of air-cooled organic Rankine cycles powered by low-temperature geothermal heat sources,” *Energy,* vol. 80, pp. 104-113, 12 December 2014.

[31] W. Liu, C. W. D. Meinel and H. Spliethoff, “Techno-economic analysis of the sub-critical ORC with optimized heat transfer process,” in *3rd International Seminar on ORC Power Systems*, Brussels, Belgium, 2015.

[32] G. Li, “Organic Rankine cycle performance evaluation and thermoeconomic assessment with various applications part II: Economic assessment aspect,” *Renewable and Sustainable Energy Reviews,* no. 64, pp. 490-505, 7 July 2016.

[33] J. Zhou, Y.Li, Q. Gu and C. Shao, “Temperature Field Prediction of Rectangular Shell-and-Tube Heat Exchanger,” *J. Pressure Vessel Technology,* vol. 135, no. 6, 10 October 2013.

[34] Werner Sölken, “EWP. Explore the World of Piping,” 2008-2018. [Online]. Available: http://www.wermac.org. [Accessed January 25 2018].

[35] R. Brojan, “Thermopedia - Shell and Tube Heat Exchangers,” 11 February 2011. [Online]. Available: http://www.thermopedia.com. [Accessed January 2018].

[36] Tubular Exchanger Manufacturers Association (TEMA), Standards of the Tubular Exchanger Manufacturers Association, 7th ed., Tarrytown, 1988.

[37] S. Kakaç and H. Liu, Heat Exchangers Selection, Rating and Thermal Design, 2nd ed., Miami, Florida: CRC Press, 2002, p. 522.

[38] Armstrong, "Plate Heat Exchangers," *Armstrong. Efficient Heat Transfer in a Compact Design,* no. 113.12, 11 April 2016.

[39] S. Kakaç, Boilers, Evaporators and Condensers, 1st ed., Coral Gables, Florida: John Wiley & Sons, 1991.

[40] F. Angulo-Brown, "An ecological optimization criterion for finite-time heat engines," *Journal of Applied Physics,* vol. 69, p. 7465–7469, 1991.

[41] V. Holubec and A. Ryabov, "Efficiency at and near maximum power of low-dissipation heat engines," *Physical Review E,* vol. 92, no. 5, p. 052125, 18 November 2015.

[42] Y. Wang, "Unified Approach to Thermodynamic Optimization of Generic Objective Functions in the Linear Response Regime," *Entropy,* vol. 18, no. 5, p. 161, 26 April 2016.

[43] R. Agromayor and L. Nord, "Turbomachinery design for Rankine cycles in waste heat recovery applications," 2017.

[44] E.P.S Departamento de Ingeniería Térmica y de Fluidos, "Listado de correlaciones de transferencia de calor," Madrid, 2016 / 2017.

[45] A. Lakew and O. Bolland, "Working fluids fos low-temperature heat source," *Appl Therm Eng,* vol. 30, no. 10, pp. 1262-1268, 2010.

[46] C. Zhang, C. Liu, S. Wang, X. Xy and Q. Li, "Thermo-economic comparison of subcritical organic Rankine cycle based on different heat exchanger configurations," *Energy,* no. 123, pp. 728-741, 2017.

[47] S. Zhang, H. Wang and T. Guo, "Performance comparison and parametric optimization of subcritical organic Rankine cycle (ORC) and transcritical powe cycle system for low-temperature geothermal power generation," *Appl. Energy,* vol. 88, no. 8, pp. 2740-2754, 2011.

[48] M. Shah, "A general correlation for heat transfer during film condensation inside pipes," *International Journal of Heat and Mass Transfer,* vol. 22, no. 4, pp. 547-556, 1979.

[49] K. Okada, M. Ono, T. Tominura, T. Okuma, T. Konno and S. Ohtani, "Design and heat transfer characteristics of a new plate heat exchanger," *Heat Transfer Japanese Research,* vol. 1, pp. 90-95, 1972.

[50] H. Kumar, “The plate heat exchanger: construction and design,” in *1st UK National Conference on Heat Transfer*, Leeds, 1984.

[51] A. Wanniarachchi, U. Ratman, B. Tilton and K. Dutta-Roy, “Approximate correlations for Chevron-type plate heat exchangers. 30th National Conference,” *ASME - Publications - HTD,* vol. 12, no. 314, pp. 145-152, 1995.

[52] J. García-Cascales, F. Vera-García, J. Corberán-Salvador and J. Gonzálvez-Maciá, “Assessment of boiling and condensation heat transfer correlations in the modelling of plate heat exchangers,” *Int J Refrig,* vol. 30, no. 6, pp. 1029-1041, 2007.

[53] M. Toledo-Velázquez, P. Quinto-Díez, J. Alzelmetti-Zaragoza, S. Galvan, J. Abugaber-Francis and A. Reyes-León, “Delaware Method Improvement for the Shell and Tubes Heat Exchanger Design,” *Engineering,* vol. 6, pp. 193-201, 2014.

[54] C. Tribbe and H. Müller-Steinhagen, “Gas/Liquid Flow in Plate-and-Frame Heat Exchangers - Part I: Pressure Drop Measurements,” *Heat Transfer Engineering,* vol. 22, pp. 5-11, 2001.

[55] M. Imran, M. Usman, P. Byung-Sik and Y. Yang, “Comparative assessment of Organic Rankine Cycle integration for low temperature geothermal heat source applications,” *Energy,* no. 102, pp. 473-490, 14 March 2016.

[56] D. Green, Perry's Chemical Engineers' Handbook, 7th ed., Mc-Graw Hill, 1997.

[57] R. Turton, R. Bailie, W. Whiting and J. Shaeiwitz, Analysis, Synthesis and Design of Chemical Processes, 3rd ed., Pearson Education, Inc, 2009.

[58] H. Loth, J. Lysons and C. White, “Process Equipment Cost Estimation - Final Report,” United States of America.

[59] Y. Li, M. Du, C. Wu, S. Wu and C. Liu, “Economical evaluation and optimization of subcritical organic Rankine cycle based on temperature matching analysis,” *Energy,* no. 68, pp. 238-247, 2014.

[60] G. Qiu, H. Liu and S. Riffat, “Expanders for micro-CHP systems with organic Rankine cycle,” *App. Therm. Eng,* no. 31, pp. 3301-3307, 2011.

[61] Issue, Chemical Engineering Plant Cost Index. CEPCI June 2017, “SCRIBD,” 2017. [Online]. Available: https://es.scribd.com/document/352561651/CEPCI-June-2017-Issue. [Accessed 6 October 2017].

[62] E. Cayer, N. Galanis and H. Nesreddine, “Parametric study and optimization of a transcritical power cycle using a low temperature source,” *Appl. Energy,* no. 88, pp. 2740-2754, 2010.

[63] Z. Wang, N. Zhou, J. Guo and X. Wang, "Fluid selection and parametric optimization of organic Rankine cycle using low temperature waste heat," *Energy,* vol. 40, no. 1, pp. 107-115, 2012.

[64] A. Bejan, G. Tsatsaronis and M. Moran, Thermal Design and Optimization, John Wiley & Sons, 1996, pp. 333-401.

[65] M. Madhawa Hettiarachchi, M. Golubovic, W. Worek and Y. Ikegami, "Optimum design criteria for an Organic Rankine cycle using low-temperature geothermal heat sources," *Energy,* no. 32, pp. 1698-1706, 2007.

[66] J. Wang, Z. Yan, M. Wang, S. Ma and Y. Dai, "Thermodynamic analysis and optimization of waste heat recovery Organic Rankine Cycles," *Appl. Therm. Eng,* no. 31, pp. 2885-2893, 2011.

[67] Y. Feng, Y. Zhang, B. Li, J. Yang and Y. Shi, "Sensitivity analysis and thermoeconomic comparison of ORCs (organic Rankine cycles) for low temperature waste heat recovery," *Energy,* no. 82, pp. 664-677, February 2015.

[68] S. Quoilin, S. Declaye, B. Tchanche and V. Lemort, "Thermo-economic optimization of waste heat recovery Organic Rankine Cycles," *Appl. Therm. Eng,* no. 31, pp. 2885-2893, 2011.

[69] S. Lemmens, "Cost Engineering Techniques and Their Applicability for Cost Estimation of Organic Rankine Cycle Systems," *Energies,* vol. 9, no. 485, p. 18, 23 June 2016.

[70] F. Táboas, M. Vallès, M. Bourouis and A. Coronas, "Flow boiling heat transfer of ammonia/water mixture in a plate heat exchanger," *International Journal of Refrigeration,* vol. 33, pp. 695-705, 21 December 2009.

[71] H. Hajabdollahi, M. Naderi and S. Adimi, "A comparative study on the shell and tube and gasket-plate heat exchangers: The economic viewpoint," *Applied Thermal Engineering,* vol. 92, pp. 271-282, 2016.

[72] Y. Nusiaputra, H.-J. Wiemer and D. Kuhn, "Thermal-Economic Modularization of Small, Organic Rankine Cycle Power Plants for Mid-Enthalpy Geothermal Fields," *Energies,* vol. 7, no. 7, pp. 4221-4240, 2014.

[73] D. Walraven, B. Laenen and W. D'haeseleer, "Comparison of shell-and-tube with plate heat exchangers for the use in low-temperature organic Rankine cycles," *Energy Conversion and Management,* vol. 87, pp. 227-237, 2014.

[74] D. Walraven, B. Laenen and W. D'haeseleer, “Minimizing the levelized cost of electricity production from low-temperature geothermal heat sources with ORCs: Water or air cooled?,” *Applied Energy,* vol. 142, pp. 144-153, 13 January 2015.

[75] Y. Cengel, “Chapter 10: Boiling and condensation,” in *Heat Transfer. A Practical Approach*, 2 ed., McGraw-Hill Higher Education, 2003, pp. 515-561.

[76] E. Saunders, Heat Exchangers - Selection, Design and Construction, New York: Wiley & Sons, 1988.

[77] United Nations Development Programme, 2017. [Online]. Available: http://www.undp.org/content/undp/en/home/sustainable-development/environment-and-natural-capital/montreal-protocol.html. [Accessed 10 December 2017].

Glossary

Back work ratio

Relationship between the pump power consumption and the turbine power production.

Baffle

Panels used in heat exchangers and other industrial processes tanks with the aim of supporting the tubes and determining the flow direction.

Brayton Cycle

Thermodynamic cycle in which a compressible working fluid is compressed, heated up and expanded to convert thermal energy into mechanical work.

Chevron angle

Angle that the plates corrugations present with respect to the x-horizontal axis.

Condenser

Device that is used to condense vapour into liquid. For our cycle, it also allows for the pre-cooling and sub-cooling of the working fluid.

Darcy friction factor

Dimensionless number that describes the pressure losses due to friction in pipes and open-channel flows.

Degree of freedom

Independent variable parameter of the optimization process whose value determine the rest of parameters of the problem.

Fluid, cooling

Substance that absorbs the heat that the working fluid rejects in the condenser.

Fluid, dry

Substance with a T-s diagram positive slope vapour saturation curve.

Fluid, heating

Substance that provides the heat that the working fluid absorbs in the primary heat exchanger.

Fluid, isentropic

Substance with a T-s diagram infinite slope vapour saturation curve.

Fluid, wet

Substance with a T-s diagram negative slope vapour saturation curve.

Fluid, working

Substance that is continuously evaporated, expanded, condensed and pumped in the Rankine cycle.

Fouling

Accumulation of residues on the heat exchanger surfaces.

Heat flux

Flow of heat per unit of area; flow of energy per unit of area and unit of time.

Heat sink

Any system that is able to receive and absorb heat.

Heat source

Any system that is able to provide and reject heat.

Heat transfer coefficient

Quantitative number that characterizes the transition of thermal energy between two substances at different temperatures.

Hydraulic diameter

Term that allows to generalize round tubes calculations to non-circular tubes. It is defined as 4 times the ratio of the cross-sectional area of the flow and the wetted perimeter.

Limiting fluid

Substance that presents the highest thermal resistance during a heat transfer process.

Logarithm Mean Temperature Difference (LMTD)

Logarithmic mean value taken over all the local temperature differences existing between the fluids exchanging heat in a heat exchanger.

Number, Boiling

Dimensionless parameter defined as a ratio of mass flow rates per unit area, involving the heat flux and latent heat of vaporization.

Number, Nusselt

Dimensionless number defined as the ratio of convective to conductive heat transfer.

Number, Prandlt

Dimensionless number defined as the ratio of viscous diffusion rate and thermal diffusion rate.

Number, Reynolds

Dimensionless number defined as the ratio of inertial forces and viscous forces.

Objective function

Equation to be optimized by mathematical programming means.

Pinch point temperature

Minimum temperature difference between hot and cold fluids exchanging heat in a heat exchanger.

Pitch layout

Way in which the tubes are placed in a shell-and-tube heat exchanger.

Pressure ratio

Ratio between the working fluid highest and lowest operating pressures in a thermodynamic cycle.

Primary heat exchanger

Device that is used in Rankine cycles to evaporate liquid into vapour. For our cycle, it also allows for the pre-heating and super-heating.

Rankine Cycle

Thermodynamic closed cycle in which the working fluid is continuously evaporated, expanded, condensed and pumped back to the initial state in order to convert thermal energy into mechanical work.

Rankine Cycle, Organic

Rankine cycle in which the working fluid is an organic substance.

Rankine Cycle, saturated

Thermodynamic cycle in which the working fluid leaves the primary heat exchanger as saturated vapour.

Rankine Cycle, transcritical

Thermodynamic cycle in which the working fluid evaporation pressure is above its critical pressure.

Rankine Cycle, super-heated

Thermodynamic cycle in which the working fluid leaves the primary heat exchanger as super-heated vapour.

Specific heat

Amount of heat per unit of mass that is required to increase the temperature of a substance by one degree Celsius.

Steady-state conditions system

System whose variables do not change with time.

Sub-cooling

Action of reducing the temperature of saturated-liquid substances at a given condensing pressure.

Super-heating

Action of increasing the temperature of saturated-vapour substances at a given evaporation pressure.

Wetted perimeter

Perimeter of a cross sectional area that is in contact with the fluid that flows through it.

Appendices

Appendix A: Boiling regimes

Boiling is the heat transfer mechanism that the working fluid follows during the evaporation. This mechanism has a pattern of 4 different regimes that can be represented by means of the boiling curve (Figure A.1)[26].

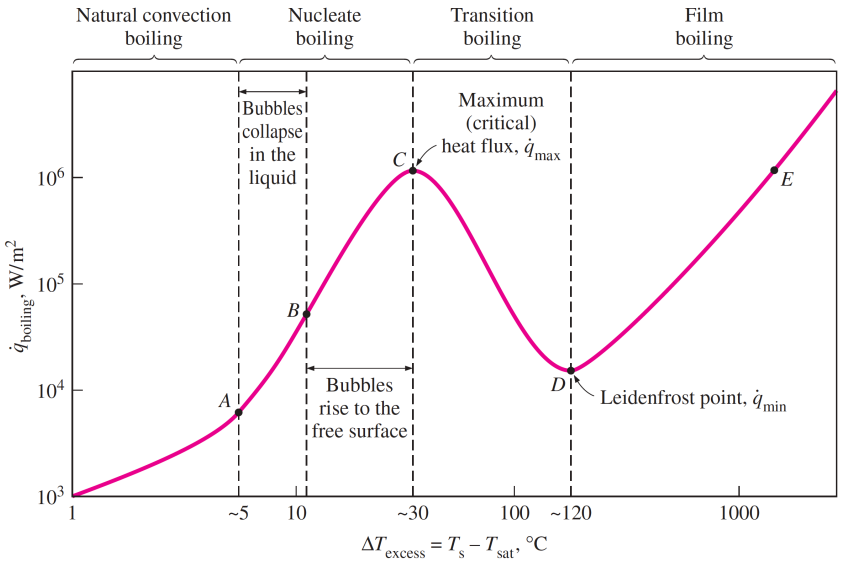

Figure A.1. Typical boiling curve for water at 1 atm [75]

The 4 regimes that can be observed in the figure and that rule the boiling heat transfer mechanism are:

Natural convection boiling

In this regime, the fluid has not reached the saturation temperature and it is sub-cooled liquid. The heat transfer process is then governed by natural convection.

[26] Even though the figure represents the boiling curve for water, the general shape is the same for all working fluids. Its specific shape is dependent on the H.E surface material and the fluid pressure, but it has no relation with the H.E geometry [82].

Nucleate boiling

The saturation temperature is reached and the fluid starts evaporating. Bubbles appear at various preferential sites on the heating surface and they are dissipated in the liquid until a sufficiently higher surface temperature is reached. At this point, much more bubbles start forming in a large number of nucleation sites, creating columns of vapour in the liquid. Liquid entrainment and evaporation cause large heat fluxes and heat transfer coefficients in this region [75]. The heat flux keeps on increasing until it reaches a maximum.

Transition boiling

Once the surface temperature that makes the heat flux reach its highest value is overpassed, the working fluid enters the transition boiling regime. The heating surface is completely covered in vapour, which acts as an insulation because of its low thermal conductivity and leads to decreasing heat fluxes. This regime is unstable, and avoided in practice. Both nucleate and film boiling occur at the same time [75].

Film boiling

In the transition boiling, as the heat flux is reduced, the film boiling gains weight against the nucleate boiling. When the heating surface reaches a specific temperature, the heat flux takes its minimum value, and the film boiling regime starts. The unstable film of vapour that was appearing during the transition boiling stabilizes and, even though it is still limiting the heat transfer process because of its low conductivity, it allows increased heat fluxes and HTCs as the heating surface temperature rises. In this regime, the heat transfer is governed by radiation of the vapour film [75].

Typical boiling processes do not follow the boiling curve point by point. What it really happens is that, once the maximum heat flux is reached at point C, there is a sudden H.E surface temperature jump that moves the process to point E, entering directly in the film

boiling regime. The heat flux at this point must be controlled in order to avoid danger of burnout that may melt the H.E manufacturing material.

Appendix B: Constants for the gasketed-plate heat exchanger correlations

Table A. Constants for single-phase heat transfer and pressure loss calculation in gasketed-plate heat exchangers [50, 76]

Chevron Angle	Heat Transfer			Pressure Loss		
	Reynolds number	C_h	n	Reynolds number	K_p	m
≤ 30º	≤ 10	0.718	0.349	< 10	50.000	1.000
	> 10	0.348	0.663	10 – 100	19.400	0.589
				> 100	2.990	0.183
45º	< 10	0.718	0.349	<15	47.000	1.000
	10 – 100	0.400	0.598	15 – 300	18.290	0.652
	> 100	0.300	0.663	> 300	1.441	0.206
50º	< 20	0.630	0.333	< 20	34.000	1.000
	20 – 300	0.291	0.591	20 – 300	11.250	0.631
	> 300	0.130	0.732	> 300	0.772	0.161
60º	< 20	0.562	0.326	< 40	24.000	1.000
	20 – 400	0.306	0.529	40 – 400	3.240	0.457
	> 400	0.108	0.703	> 400	0.760	0.215
65º	< 20	0.562	0.326	50	24.000	1.000
	20 – 500	0.331	0.503	50 – 500	2.800	0.451
	> 500	0.087	0.718	> 500	0.639	0.213

Appendix C: Constraints for the cycle

Inequality constraints:

$$c_1 = \frac{h_3 - h_{liq}(p_1)}{h_{max} - h_{min}} \qquad c_2 = -\frac{h_5 - h_{vap}(p_5)}{h_{max} - h_{min}}$$

$$c_3 = -\frac{h_6 - h_{vap}(p_6)}{h_{max} - h_{min}} \qquad c_4 = -\frac{\Delta T_{evap} - \Delta T'_{evap}}{\Delta T'_{evap}}$$

$$c_5 = -\frac{\Delta T_{cond} - \Delta T'_{cond}}{\Delta T'_{cond}} \qquad c_6 = -SIC$$

Equality constraints:

$$c_7 = \Delta p_{hot,PrHE} - \Delta p'_{hot,PrHE} \qquad c_8 = \Delta p_{wf,PrHE} - \Delta p'_{wf,PrHE}$$

$$c_9 = \Delta p_{wf,cond} - \Delta p'_{wf,cond} \qquad c_{10} = \Delta p_{cold,cond} - \Delta p'_{cold,cond}$$

Appendix D: Results for the SIC optimization of 18 different working fluids and 4 different H.E configurations

Table B. Results obtained for 18 different working fluids and 4 different H.E configurations

Working fluid (Class)	T_{max}/T_{crit} [K/K]	Conf.	SIC [$/kW]	η_{II} [%]	Evaporator area [m^2]	Condenser area [m^2]	Power output [kW]
Butane (Alkane)	0.925	PP	4389.070	28.970	111.236	188.873	208.590
		SP	4518.103	28.533	174.580	169.180	205.304
		PS	5942.999	19.334	50.984	214.149	139.218
		SS	7246.796	17.381	128.641	256.708	125.149
Isobutane (Alkane)	0.964	PP	4112.973	32.522	119.169	184.697	234.082
		SP	4485.261	28.694	169.049	161.279	206.475
		PS	6553.388	19.591	261.317	178.571	141.076
		SS	7309.207	18.772	121.433	309.073	135.147
Pentane (Alkane)	0.837	PP	5013.093	21.550	87.719	151.987	155.234
		SP	5968.710	26.360	302.807	312.640	189.657
		PS	7459.764	18.845	79.508	396.137	135.624
		SS	9737.930	13.872	200.731	335.385	99.804
Propane (Alkane)	1.063	PP	4030.016	31.221	84.668	141.335	224.906
		SP	4206.584	31.373	156.712	138.403	225.985
		PS	6033.677	23.121	70.532	255.765	166.409
		SS	6098.562	22.943	80.389	243.971	165.603
C2 Butene (Alkene)	0.902	PP	4365.780	28.716	106.550	185.247	206.780
		SP	4382.232	25.920	135.170	120.655	186.470
		PS	5739.456	20.362	48.241	218.399	146.633
		SS	7322.220	17.213	156.801	244.131	123.882
Propylen (Alkene)	1.079	PP	3904.920	35.490	71.324	186.078	255.711
		SP	3943.740	32.679	112.847	117.822	235.607
		PS	6090.213	24.211	61.447	275.675	174.275
		SS	7309.207	18.772	121.433	309.073	135.147
Propyne (Alkyne)	0.977	PP	3773.596	30.082	46.008	115.247	216.850
		SP	4126.030	30.022	160.703	128.288	216.195
		PS	5183.268	22.506	43.815	188.887	162.084
		SS	6275.795	19.866	96.393	224.375	143.202
Cyclopropane (Cycloalkane)	0.987	PP	3761.142	29.900	45.851	105.644	215.740
		SP	4020.770	30.502	144.548	116.847	219.629
		PS	5163.578	23.609	48.952	204.665	169.982
		SS	6144.522	19.518	92.643	194.116	140.803
DME (Ether)	0.982	PP	3689.640	30.800	44.928	108.054	221.896
		SP	3992.686	31.678	135.972	137.736	228.064
		PS	5868.731	20.321	28.401	222.121	146.333
		SS	5989.894	20.850	87.843	216.212	150.221

R22 (HCFC)	1.065	PP	3937.291	28.856	54.990	95.246	208.008
		SP	4021.290	31.274	105.785	122.031	225.651
		PS	5457.010	19.823	54.636	124.718	142.648
		SS	5951.403	21.728	66.736	211.905	157.028
R134a (HFC)	1.051	PP	4157.880	31.420	89.407	175.983	226.175
		SP	4272.120	32.660	152.159	182.287	235.128
		PS	6071.032	21.762	51.661	244.067	156.647
		SS	6178.545	21.713	78.551	246.869	156.707
R152a (HFC)	1.017	PP	3781.610	30.730	48.053	117.425	221.395
		SP	3959.792	29.598	106.480	104.002	213.199
		PS	5895.471	24.233	36.803	341.931	174.464
		SS	6131.205	20.812	92.794	226.177	150.030
R245ca (HFC)	0.878	PP	4707.780	27.900	103.398	236.384	201.049
		SP	5188.890	25.111	195.290	203.943	180.655
		PS	7393.122	16.703	49.532	307.925	120.276
		SS	9183.911	13.731	177.869	285.835	98.802
R245fa (HFC)	0.920	PP	4633.380	23.640	47.807	156.069	170.895
		SP	4974.950	27.410	191.135	221.897	197.233
		PS	6346.576	16.564	45.659	184.090	119.224
		SS	8093.052	16.105	147.741	297.148	115.917
R32 (HFC)	1.119	PP	3655.890	35.047	69.476	116.293	252.492
		SP	3804.026	35.326	122.803	127.695	254.878
		PS	5841.536	24.541	52.516	277.971	176.595
		SS	6291.601	26.786	256.159	318.179	192.770
R1234yf (HFO)	1.069	PP	4206.760	31.622	88.831	181.994	227.638
		SP	4417.650	30.052	120.570	175.390	216.368
		PS	6387.021	22.851	70.795	288.519	164.478
		SS	6427.165	24.191	113.859	315.843	174.719
R1234ze (HFO)	1.028	PP	3974.454	31.067	57.562	142.617	223.685
		SP	4164.570	29.570	92.599	136.795	213.049
		PS	5873.268	19.976	60.898	180.133	143.761
		SS	6485.804	19.017	68.760	218.691	137.310
Ammonia (Inorganic)	0.970	PP	3166.050	33.450	38.072	64.954	242.264
		SP	3480.119	29.989	120.994	47.234	216.026
		PS	4654.080	25.117	36.022	162.938	180.880
		SS	5334.639	21.700	175.817	111.833	156.147

Appendix E: SIC optimization result

Table C. Ammonia SIC optimization results

Hot source mass flow [kg/s]	$T_{c,in}$ [ºC]	$T_{h,in}$ [ºC]	SIC [$/kW]	η_{II} [%]	Evaporator area [m^2]	Condenser area [m^2]	Power output [kW]
10	5	120	3225.791	32.715	120.120	71.257	260.586
		150	2451.862	36.628	157.998	87.967	439.741
		175	2008.149	38.084	151.309	88.248	608.053
		200	1686.786	42.387	174.697	115.357	865.673
		250	1291.365	46.960	209.070	161.363	1450.682
	10	120	3480.119	29.989	120.994	47.234	216.026
		150	2484.474	36.786	116.357	78.817	410.031
		175	2074.741	39.622	153.993	99.684	593.518
		200	1734.622	42.193	140.049	109.812	815.132
		250	1321.767	46.993	194.174	153.379	1388.682
	15	120	3852.904	29.297	87.652	71.137	191.236
		150	2638.406	34.276	116.735	55.943	353.782
		175	2194.741	38.180	107.323	103.976	535.806
		200	1789.218	42.313	146.194	101.147	772.220
		250	1378.755	47.112	203.594	161.895	1330.954
25	5	120	2180.574	32.090	241.024	160.659	634.872
		150	1614.431	35.521	281.923	184.059	1066.265
		175	1314.534	37.856	284.835	209.703	1511.268
		200	1105.563	41.088	355.807	243.311	2097.194
		250	831.469	45.928	411.671	360.539	3546.985
	10	120	2267.892	30.975	231.001	120.481	558.274
		150	1673.136	34.927	250.392	159.837	973.247
		175	1369.179	37.875	290.214	207.837	1418.342
		200	1129.249	41.388	318.008	230.261	1998.954
		250	863.351	46.142	426.437	381.297	3408.898
	15	120	2440.103	30.027	196.943	119.290	491.247
		150	1780.066	32.537	230.983	200.038	906.723
		175	1437.591	36.953	233.574	210.804	1295.868
		200	1178.438	41.505	321.557	239.047	1893.496
		250	886.722	46.357	416.841	368.453	3273.922
50	5	120	1654.781	32.089	482.013	321.402	1269.722
		150	1193.120	34.163	465.857	340.538	2051.140
		175	956.415	37.295	488.973	410.006	2977.561
		200	793.077	39.281	534.797	417.823	4011.261
		250	601.683	43.840	692.224	589.477	6771.004
	10	120	1746.210	31.156	425.954	283.749	1122.862
		150	1240.830	34.149	449.505	305.723	1902.936
		175	1000.494	36.452	525.286	307.704	2731.318
		200	820.400	39.332	508.600	406.298	3798.727
		250	619.413	44.330	651.816	629.928	6549.910
	15	120	1856.870	30.194	407.100	247.770	987.950
		150	1304.600	34.180	436.888	300.861	1763.818
		175	1035.096	36.702	413.867	365.823	2576.298
		200	852.633	39.664	518.515	394.960	3618.931
		250	659.441	44.974	708.934	761.226	6352.231

Table D. DME SIC optimization results

Hot source mass flow [kg/s]	$T_{c,in}$ [ºC]	$T_{h,in}$ [ºC]	SIC [$/kW]	η_{II} [%]	Evaporator area [m^2]	Condenser area [m^2]	Power output [kW]
		120	3826.720	30.808	161.006	134.048	245.273
		150	2812.321	35.274	165.887	169.559	423.367
	5	175	2311.461	38.106	162.301	205.842	608.385
		200	1993.068	38.518	198.021	205.384	786.573
		250	1633.709	37.815	263.358	277.475	1168.007
		120	3992.686	31.678	135.972	137.736	228.064
		150	2939.627	34.64	167.035	151.012	385.879
10	10	175	2420.745	36.530	167.334	174.041	547.114
		200	2055.045	38.061	159.274	193.395	735.010
		250	1681.470	37.588	233.380	269.116	1110.637
		120	4273.118	29.906	139.071	110.019	195.258
		150	3055.277	35.125	163.696	144.591	362.223
	15	175	2491.815	36.757	149.609	161.123	515.686
		200	2133.207	37.976	163.532	183.103	692.731
		250	1738.254	36.412	219.451	254.096	1028.441
		120	2630.525	29.494	297.120	284.427	582.826
		150	1913.207	32.685	319.042	312.442	980.889
	5	175	1568.820	35.895	351.316	400.934	1432.758
		200	1346.117	37.235	366.846	486.471	1900.914
		250	1101.732	35.919	487.875	607.222	2773.558
		120	2780.650	27.570	261.927	227.428	496.084
		150	1991.203	32.029	254.274	306.574	891.911
25	10	175	1632.478	35.705	353.363	373.855	1336.819
		200	1385.281	37.547	371.463	453.460	1812.802
		250	1136.770	35.763	472.120	591.615	2641.711
		120	2976.590	27.399	289.708	208.288	447.175
		150	2135.511	31.710	319.617	281.680	817.617
	15	175	1712.156	35.398	341.658	368.470	1241.209
		200	1444.550	37.867	427.998	435.539	1726.822
		250	1165.390	35.392	377.818	602.282	2499.070
		120	1960.714	27.115	421.495	428.834	1071.783
		150	1477.136	30.506	564.755	571.986	1830.799
	5	175	1172.636	33.197	544.344	637.351	2650.043
		200	1011.665	36.342	655.548	865.626	3710.471
		250	825.991	33.290	807.378	951.111	5141.114
		120	2045.566	26.631	450.950	325.298	958.608
		150	1559.233	31.132	571.588	591.201	1734.014
50	10	175	1242.657	33.140	607.381	626.294	2481.538
		200	1034.614	35.427	625.056	724.221	3421.105
		250	843.584	32.742	636.519	990.024	4837.097
		120	2211.279	26.604	405.804	380.157	868.244
		150	1576.624	29.267	419.025	437.466	1509.565
	15	175	1266.562	32.727	477.672	577.778	2295.664
		200	1076.822	35.923	610.890	768.106	3276.421
		250	888.655	32.313	744.402	910.586	4563.212

Table E. Propylene SIC optimization results

Hot source mass flow [kg/s]	$T_{c,in}$ [ºC]	$T_{h,in}$ [ºC]	SIC [$/kW]	η_{II} [%]	Evaporator area [m^2]	Condenser area [m^2]	Power output [kW]
10	5	120	3700.099	33.574	134.166	131.180	267.552
		150	2868.796	36.894	157.548	172.402	442.925
		175	2458.790	37.532	197.814	214.380	599.187
		200	2200.361	35.978	222.241	238.836	734.612
		250	1893.753	32.258	252.948	314.809	996.313
	10	120	3943.740	32.679	112.847	117.822	235.607
		150	3059.215	36.759	184.161	172.063	409.611
		175	2673.037	36.201	219.057	217.999	542.174
		200	2385.804	34.309	229.607	243.097	662.646
		250	2014.857	30.138	254.514	285.109	890.547
	15	120	4176.361	32.454	115.904	106.184	212.115
		150	3187.898	35.775	148.677	162.819	369.034
		175	2830.961	35.419	214.212	214.664	496.756
		200	2525.088	33.158	219.013	237.857	604.777
		250	2115.155	29.006	195.311	289.582	819.436
25	5	120	2565.108	32.141	295.271	271.238	635.557
		150	1991.898	35.498	333.704	406.152	1065.384
		175	1723.460	33.842	413.078	415.570	1350.706
		200	1555.943	33.826	456.808	561.535	1726.636
		250	1311.141	29.780	505.701	649.614	2299.772
	10	120	2741.351	31.816	271.860	262.373	573.360
		150	2106.188	35.340	368.141	388.139	984.377
		175	1829.880	33.887	386.071	454.677	1268.753
		200	1648.223	32.848	431.198	560.228	1585.719
		250	1383.168	28.990	489.004	665.609	2141.361
	15	120	2925.477	30.959	253.515	235.779	506.098
		150	2241.622	34.995	367.051	383.670	902.430
		175	1942.498	33.278	372.056	454.333	1166.801
		200	1752.643	31.623	427.677	527.922	1441.951
		250	1456.824	27.245	422.397	614.626	1923.796
50	5	120	1934.346	31.595	487.258	490.725	1250.494
		150	1502.241	32.809	509.838	674.582	1969.367
		175	1298.910	33.609	692.823	808.219	2682.666
		200	1221.600	30.392	776.086	939.960	3102.731
		250	1011.224	28.463	862.514	1196.705	4395.615
	10	120	2076.478	30.263	440.266	450.692	1090.275
		150	1623.770	32.113	580.895	636.520	1788.961
		175	1388.834	31.654	602.822	741.216	2370.287
		200	1281.401	28.705	641.112	894.548	2771.555
		250	1064.648	26.454	805.360	1039.324	3908.260
	15	120	2269.235	28.643	402.275	426.507	936.556
		150	1727.832	31.987	573.431	643.714	1649.589
		175	1497.255	31.426	576.815	858.992	2203.620
		200	1335.972	27.981	587.860	832.244	2551.612
		250	1133.181	24.803	727.698	1008.240	3502.740

Table F. R152a SIC optimization results

Hot source mass flow [kg/s]	$T_{c,in}$ [ºC]	$T_{h,in}$ [ºC]	SIC [$/kW]	η_{II} [%]	Evaporator area [m^2]	Condenser area [m^2]	Power output [kW]
10	5	120	3875.326	38.245	295.051	218.936	302.222
		150	2843.804	34.295	160.060	157.738	411.708
		175	2352.095	38.236	193.336	203.642	610.570
		200	2095.369	39.477	227.149	274.177	806.209
		250	1713.817	36.505	238.055	322.766	1127.768
	10	120	3959.792	29.598	106.480	104.002	213.199
		150	2963.132	34.390	145.453	153.001	383.257
		175	2459.927	37.980	188.034	194.465	568.953
		200	2149.545	39.078	208.913	259.343	754.709
		250	1781.175	35.146	246.955	285.612	1038.828
	15	120	4345.105	27.698	91.199	101.621	181.077
		150	3089.174	34.084	156.283	134.977	351.619
		175	2551.866	37.972	168.480	197.166	532.713
		200	2224.672	38.515	217.040	233.433	702.549
		250	1845.427	34.609	215.779	293.891	977.495
25	5	120	2706.607	29.220	326.692	293.353	577.526
		150	1939.996	32.875	294.519	342.570	986.793
		175	1617.034	36.037	367.771	449.962	1438.533
		200	1399.005	36.264	415.253	501.027	1851.492
		250	1146.258	34.206	442.967	653.485	2641.718
	10	120	2807.602	27.102	213.471	243.451	487.993
		150	2021.914	33.153	289.806	328.407	923.688
		175	1671.151	35.377	347.131	396.920	1324.655
		200	1477.499	35.560	424.582	522.261	1734.931
		250	1203.127	34.067	405.215	710.273	2516.400
	15	120	2970.926	28.432	255.078	240.096	464.694
		150	2125.889	33.690	292.837	337.676	868.781
		175	1749.222	35.964	363.240	405.824	1261.144
		200	1576.600	35.082	446.076	529.678	1617.880
		250	1265.403	34.463	581.033	649.284	2434.689
50	5	120	2048.858	27.305	463.769	499.832	1079.521
		150	1456.803	31.540	485.206	598.251	1893.323
		175	1212.598	35.144	637.605	798.442	2805.617
		200	1065.552	35.543	782.438	937.878	3628.906
		250	886.687	33.112	867.858	1218.396	5113.595
	10	120	2168.301	27.102	426.942	487.015	975.987
		150	1542.634	31.692	503.698	602.693	1765.862
		175	1279.573	34.523	650.903	758.664	2585.527
		200	1106.628	35.161	723.722	920.675	3394.992
		250	915.692	30.934	777.201	1045.439	4569.959
	15	120	2443.753	26.674	333.721	626.368	871.072
		150	1641.591	30.278	507.911	532.353	1561.181
		175	1348.953	34.142	606.754	764.165	2394.559
		200	1156.402	34.896	688.537	914.731	3182.492
		250	977.040	29.689	617.417	1153.451	4192.863

Table G. R32 SIC optimization results

Hot source mass flow [kg/s]	$T_{c,in}$ [ºC]	$T_{h,in}$ [ºC]	SIC [$/kW]	η_{II} [%]	Evaporator area [m^2]	Condenser area [m^2]	Power output [kW]
10	5	120	3560.565	35.024	132.365	122.519	279.354
		150	2726.170	38.814	171.672	166.459	466.102
		175	2385.467	40.054	207.994	240.931	639.519
		200	2142.293	37.786	223.188	253.598	771.530
		250	1789.698	35.202	277.697	323.302	1087.338
	10	120	3804.026	35.326	122.803	127.695	254.878
		150	2900.643	38.712	159.969	180.097	431.418
		175	2545.590	38.158	185.956	231.391	571.443
		200	2271.004	36.001	240.250	233.744	695.207
		250	1915.440	33.393	229.170	348.552	986.975
	15	120	4042.168	34.586	118.825	108.993	226.438
		150	3154.870	37.854	189.879	179.908	390.559
		175	2721.102	37.342	219.874	223.146	523.530
		200	2417.729	34.341	207.125	240.936	626.409
		250	2035.162	32.632	299.851	337.522	921.895
25	5	120	2383.495	34.520	287.060	227.257	683.674
		150	1928.958	37.692	401.269	400.935	1131.461
		175	1641.552	37.817	408.452	527.572	1509.413
		200	1462.625	37.826	482.884	642.852	1930.880
		250	1226.156	33.551	523.824	734.537	2590.626
	10	120	2533.379	34.144	258.431	226.589	615.699
		150	2057.420	36.798	373.323	98.390	1025.888
		175	1794.308	36.665	420.383	552.950	1372.885
		200	1608.855	34.837	510.252	585.352	1681.775
		250	1319.508	31.357	528.333	706.476	2316.172
	15	120	2731.700	33.305	243.302	213.005	544.987
		150	2221.541	35.973	338.407	424.312	927.710
		175	1910.635	34.708	405.892	498.787	1216.984
		200	1713.544	32.287	441.930	524.927	1472.530
		250	1407.967	29.268	403.950	713.835	2066.784
50	5	120	1776.052	34.589	476.531	436.639	1370.300
		150	1406.357	37.541	640.319	703.759	2253.768
		175	1241.110	34.772	700.770	781.023	2775.556
		200	1136.037	33.334	720.201	1014.741	3403.132
		250	951.175	28.919	787.421	1101.703	4465.878
	10	120	1891.870	32.732	359.514	404.006	1180.922
		150	1562.942	35.304	636.695	715.334	1966.982
		175	1350.112	32.722	603.852	755.873	2450.234
		200	1202.150	31.858	708.917	949.576	3075.888
		250	1020.328	28.137	816.772	1192.014	4156.914
	15	120	2103.212	32.421	426.261	428.095	1060.795
		150	1724.217	33.637	647.295	715.622	1734.842
		175	1485.128	32.296	680.249	869.212	2264.683
		200	1340.899	31.209	804.103	1025.531	2846.069
		250	1124.204	27.965	925.019	1272.947	3949.169

Appendix F: Second law efficiency optimization results

Table H. Ammonia thermodynamic optimization results

Hot source mass flow [kg/s]	$T_{c,in}$ [ºC]	$T_{h,in}$ [ºC]	SIC [$/kW]	η_{II} [%]	Evaporator area [m^2]	Condenser area [m^2]	Power output [kW]
10	5	120	3891.131	38.235	303.495	218.871	302.357
		150	2837.909	42.357	350.717	246.763	508.307
		175	2491.253	44.801	478.444	330.372	715.13
		200	2033.442	47.199	409.353	382.21	963.828
		250	1524.267	51.974	419.149	515.576	1605.405
	10	120	3844.354	38.011	256.778	158.476	273.492
		150	2870.962	41.342	330.99	181.643	460.48
		175	2427.323	44.754	359.221	288.193	670.303
		200	2367.288	47.149	789.159	339.604	910.362
		250	1560.468	51.762	414.729	485.733	1529.77
	15	120	6145.414	36.860	903.863	173.748	240.494
		150	3296.718	40.922	465.351	198.250	421.864
		175	2365.737	43.897	231.644	231.298	615.600
		200	2058.655	47.024	311.829	307.625	857.741
		250	1582.067	51.512	454.451	411.178	1455.153
25	5	120	3028.861	38.260	865.493	548.956	755.778
		150	2020.186	42.011	711.146	627.774	1260.79
		175	1823.774	44.382	698.939	669.568	1771.164
		200	1303.125	47.044	623.46	814.065	2401.558
		250	1152.927	51.808	1470.149	1135.083	4000.542
	10	120	2874.573	36.96	742.614	316.013	664.919
		150	2024.862	40.602	723.646	405.565	1130.496
		175	1880.24	43.413	952.01	793.151	1625.29
		200	1309.723	46.673	513.157	730.229	2253.229
		250	1223.886	50.739	1521.588	1166.801	3748.241
	15	120	2765.937	35.404	389.647	295.036	577.697
		150	2237.894	40.307	767.875	471.781	1039.393
		175	2006.628	42.968	1062.662	707.769	1505.412
		200	1464.482	45.733	714.587	765.112	2085.418
		250	1177.037	50.529	1140.874	1152.034	3568.041
50	5	120	2437.947	37.939	1464.936	1036.676	1499.225
		150	1639.434	42.08	1355.399	1258.227	2525.15
		175	1317.449	44.836	1272.092	1648.898	3579.081
		200	1244.927	46.992	1976.163	1940.589	4798.508
		250	926.592	51.947	2282.877	2448.877	8022.669
	10	120	2281.132	37.003	1281.763	615.36	1331.525
		150	1903.414	41.002	1847.404	1048.798	2283.293
		175	1449.465	43.438	1601.348	1407.323	3254.044
		200	1018.978	46.37	1262.211	1215.452	4477.412
		250	907.126	51.579	1989.801	2275.227	7620.565
	15	120	2209.006	35.979	890.062	561.914	1174.307
		150	1674.531	40.493	1231.049	797.906	2087.928
		175	2678.051	42.972	4214.547	1495.475	3012.820
		200	1138.633	45.898	1309.480	1375.238	4187.057
		250	1170.692	51.123	3462.191	2071.318	7219.915

Table I. DME thermodynamic optimization results

Hot source mass flow [kg/s]	$T_{c,in}$ [ºC]	$T_{h,in}$ [ºC]	SIC [$/kW]	η_{II} [%]	Evaporator area [m^2]	Condenser area [m^2]	Power output [kW]
10	5	120	5893.805	38.256	655.354	577.437	302.292
		150	3574.93	41.588	264.891	631.838	499.091
		175	3077.168	44.155	308.558	828.638	704.838
		200	2634.333	48.408	437.133	965.319	988.598
		250	2262.835	47.505	573.601	1375.208	1467.451
	10	120	4776.516	36.969	269.556	352.03	266.054
		150	3480.965	40.371	196.452	478.785	449.731
		175	4393.144	43.204	1151953	944.679	646.879
		200	2735.803	48.017	523.771	858.937	927.2
		250	2345.735	46.976	606.738	1307.359	1388.178
	15	120	5585.377	35.272	374.026	347.238	230.129
		150	3658.228	39.325	285.966	391.449	405.438
		175	3254.556	42.597	292.402	683.029	597.443
		200	3092.62	47.975	451.422	1131.044	874.955
		250	2821.756	46.772	1075.963	1468.955	1321.02
25	5	120	4471.339	38.226	943.134	1648.134	755.162
		150	3728.91	42.297	1688.243	2058.029	1268.982
		175	2502.786	46.3	1225.029	2045.291	1848.346
		200	2502.231	48.786	1174.273	3557.53	2491.807
		250	1881.392	47.227	1645.826	3454.649	3646.7
	10	120	4910.784	36.454	1117.054	1401.114	655.704
		150	3074.277	40.256	1171.332	1257.023	1120.963
		175	3376.749	44.267	1906.994	2553.985	1657.12
		200	2305.492	48.6	1069.139	2822.216	2346.559
		250	2027.504	46.96	1970.268	2166.086	3469.054
	15	120	4954.948	35.940	1023.025	1192.784	586.317
		150	2750.623	39.352	712.384	979.946	1014.265
		175	2703.94	42.649	1112.322	1738.353	1495.305
		200	2370.642	48.147	1480.652	2226.811	2195.821
		250	2833.949	46.249	3672.542	3476.355	3265.558
50	5	120	3355.608	37.724	1952.381	1970.208	1490.208
		150	2342.961	41.647	1390-251	3054.550	2498.928
		175	2325.564	46.316	2592.512	4140.166	3697.908
		200	1831.171	48.398	2146.695	4823.882	4942.119
		250	3774.988	47.469	9138.223	9226.817	7330.984
	10	120	3131.094	37.044	1327.863	1787.707	1333.056
		150	2985.788	40.717	2195.564	3267.018	2267.387
		175	3333.064	45.125	3700.956	5514.995	3378.634
		200	1842.702	48.146	2210.751	4308.087	4649.06
		250	1605.828	47.073	2773.309	5845.162	6954.879
	15	120	3682.457	35.000	1568.597	1686.156	1141.899
		150	2133.993	38.922	912.803	1894.195	2006.817
		175	3247.426	44.035	3621.574	4460.988	3087.442
		200	2012.839	47.777	2479.709	4226.682	4358.089
		250	1953.225	46.464	4171.237	5524.521	6562.059

Table J. Propylene thermodynamic optimization results

Hot source mass flow [kg/s]	$T_{c,in}$ [ºC]	$T_{h,in}$ [ºC]	SIC [$/kW]	η_{II} [%]	Evaporator area [m^2]	Condenser area [m^2]	Power output [kW]
10	5	120	4591.191	39.024	321.290	380.562	308.367
		150	3660.146	43.863	445.076	565.744	526.376
		175	3755.191	46.169	891.568	921.077	736.931
		200	3730.208	44.432	1334.801	1084.089	907.162
		250	2352.675	39.341	561.158	983.645	1215.104
	10	120	4508.071	37.299	204.196	295.638	268.442
		150	3669.269	42.055	373.693	469.834	468.406
		175	5268.002	44.541	1913.842	791.046	666.899
		200	3852.292	42.876	1330.018	934.501	827.863
		250	2415.431	37.974	444.089	949.907	1121.997
	15	120	4942.214	36.026	204.589	288.139	235.084
		150	3924.069	40.974	310.255	499.008	422.676
		175	3462.407	43.146	382.534	700.093	605.102
		200	3933.203	41.521	1197.278	864.623	757.217
		250	2652.420	36.566	502.312	996.441	1032.793
25	5	120	3477.873	39.961	541.038	1160.397	784.139
		150	4467.570	46.089	2934.274	1866.803	1382.7
		175	2521.117	46.259	1481.533	1747.721	1846.152
		200	2321.001	45.060	1114.918	2686.488	2300.575
		250	2606.326	39.809	3009.696	3129.988	3073.796
	10	120	4742.967	39.05	1519.554	1013.434	702.412
		150	3517.132	44.954	1555.597	1663.969	1251.932
		175	3223.725	45.044	1973.914	2131.097	1686.103
		200	2223.596	43.231	1219.352	1895.981	2086.928
		250	2059.252	38.254	127.704	2856.391	2825.7
	15	120	4303.213	38.897	1028.341	824.095	634.627
		150	2905.306	43.584	606.054	1334.431	1123.83
		175	2838.469	43.593	1093.473	1911.265	1528.609
		200	3412.979	41.223	2648.485	2015.052	1879.466
		250	1953.495	36.283	1134.033	2187.382	2561.961
50	5	120	3275.742	39.583	1711.79	2205.028	1564.113
		150	3554.864	46.080	3896.18	3694.19	2765.448
		175	2312.343	45.805	2526.496	3916.115	3656.925
		200	1943.624	44.590	2265.207	4473.285	4553.032
		250	1661.002	39.296	2703.49	4883.995	6068.534
	10	120	3130.681	39.046	876.945	2299.602	1406.016
		150	2624.515	45.509	1993.534	3027.013	2534.355
		175	3571.574	44.829	4859.071	4160.286	3356.377
		200	5827.267	42.79	9596.685	4953.743	4131.002
		250	1938.73	38.198	3295.711	5082.253	5643.13
	15	120	3536.467	37.866	1638.308	1631.545	1235.65
		150	2457.156	43.484	1235.064	2618.608	2242.548
		175	3746.545	43.211	4840.936	3628.242	3029.427
		200	2039.018	41.085	1892.648	3805.89	3746.856
		250	1886.283	36.261	2684.174	4639.61	5120.695

Table K. R152a thermodynamic optimization results

Hot source mass flow [kg/s]	$T_{c,in}$ [ºC]	$T_{h,in}$ [ºC]	SIC [$/kW]	η_{II} [%]	Evaporator area [m^2]	Condenser area [m^2]	Power output [kW]
10	5	120	4314.171	37.179	147.712	379.685	293.962
		150	4051.998	42.872	214.098	964.240	514.511
		175	5185.045	47.149	1753.649	1364.268	752.549
		200	3749.021	48.179	917.801	1779.908	983.697
		250	2418.78	45.137	584.453	1478.542	1394.171
	10	120	6780.704	36.433	577.832	676.496	262.157
		150	3538.375	42.615	166.222	574.898	474.758
		175	5197.012	47.032	1680.606	1211.806	704.203
		200	3154.707	47.576	732.913	1102.096	918.836
		250	2944.23	44.795	1102.647	1658.536	1323.576
	15	120	6902.572	36.044	462.969	627.520	235.218
		150	3780.117	41.969	189.770	557.903	432.762
		175	5353.484	46.753	1608.025	1161.566	655.547
		200	3391.301	47.190	794.567	1114.103	860.864
		250	3260.205	44.649	1184.769	1842.988	1261.070
25	5	120	4138.949	37.936	862.609	1391.88	749.417
		150	3951.475	43.244	1591.665	2543.066	1297.427
		175	3310.039	47.594	1719.239	3323.696	1899.471
		200	2652.609	47.645	1946.759	3096.786	2456.733
		250	2411.461	45.338	2569.551	4129.08	3500.932
	10	120	6408.685	36.552	1912.84	1676.624	657.506
		150	3305.623	43.066	549.381	2245.876	1199.203
		175	2390.368	46.726	835.842	1909.588	1750.014
		200	3510.075	47.034	2520.133	4140.917	2294.648
		250	3206.474	44.883	3320.172	5434.706	3315.351
	15	120	5151.726	35.919	816.31	1490.26	585.936
		150	3336.107	42.635	588.965	1926.149	1098.947
		175	2988.130	46.282	1818.367	1747.611	1622.537
		200	4033.323	46.839	3194.269	3964.851	2159.845
		250	2190.043	44.154	2185.642	2949.436	3117.715
50	5	120	8602.269	37.446	2985.974	8601.147	1479.556
		150	3457.637	42.772	2490.315	4931.628	2567.239
		175	3072.330	47.631	3276.362	6332.736	3802.186
		200	3370.995	48.283	5045.706	8312.973	4978.794
		250	2029.831	45.285	3517.126	7873.254	6993.781
	10	120	5630.254	36.577	3215.482	3042.273	1315.937
		150	2318.056	41.051	1367.8	2583.033	2286.625
		175	3071.049	47.216	2876.94	6085.652	3535.133
		200	2869.812	48.083	4035.929	6658.529	4643.109
		250	3225.542	44.881	5867.798	10862.295	6630.483
	15	120	7107.509	35.908	3872.746	3088.977	1171.626
		150	3034.825	40.163	2275.081	2693.605	2070.841
		175	2033.179	45.659	1285.951	3503.618	3201.479
		200	3709.486	47.400	5570.910	6778.226	4332.482
		250	2427.025	43.850	4561.262	7226.265	6192.805

Table L. R32 thermodynamic optimization results

Hot source mass flow [kg/s]	$T_{c,in}$ [ºC]	$T_{h,in}$ [ºC]	SIC [$/kW]	η_{II} [%]	Evaporator area [m^2]	Condenser area [m^2]	Power output [kW]
10	5	120	4412.36	42.117	399.98	355.486	332.851
		150	3289.086	46.540	438.814	470.407	558.633
		175	3027.083	47.263	612.521	654.602	754.479
		200	2895.996	46.244	886.795	791.394	944.175
		250	2195.367	42.809	698.229	913.973	1322.271
	10	120	4992.099	41.86	522.936	322.405	301.177
		150	3585.402	45.845	442.845	498.612	510.617
		175	3363.896	45.993	684.919	682.815	688.76
		200	2991.414	44.697	789.538	764.082	863.1
		250	2236.661	40.452	594.594	811.044	1195.231
	15	120	4529.674	40.511	183.764	284.35	264.516
		150	3641.118	44.497	400.815	411.333	458.786
		175	3422.659	44.270	609.038	588.055	620.9
		200	2992.225	42.723	597.019	699.019	779.187
		250	2476.321	38.827	703.534	822.28	1096.677
25	5	120	3876.463	39.578	893.909	721.319	645.675
		150	2805.249	44.667	1024.455	1033.078	1151.359
		175	2635.088	44.814	1453.327	1403.54	1571.092
		200	2346.083	43.123	1542.953	1660.916	1966.138
		250	2965.363	38.912	3724.627	2364.007	2747.473
	10	120	3568.658	41.333	75.285	733.196	743.59
		150	2836.549	45.951	1198.648	1237.205	1279.448
		175	2638.931	46.004	1554.636	1675.711	1722.263
		200	2256.704	44.677	1636.608	1824.392	2179.964
		250	1909.376	40.95	1878.847	2187.907	3024.904
	15	120	3449.264	42.197	955.659	936.066	833.858
		150	2432.910	46.852	622.901	1439.652	1406.804
		175	2413.051	47.037	1627.803	1514.882	1877.091
		200	2691.872	46.518	2632.457	2181.343	2374.362
		250	1909.089	43.028	2147.439	2437.044	3322.417
50	5	120	3196.113	42.186	2181.513	1842.398	1667.483
		150	3179.114	46.797	3857.649	2924.534	2807.884
		175	2249.171	47.037	3261.744	3030.541	3754.206
		200	3382.192	46.504	6730.299	4295.759	4747.298
		250	2055.172	43.173	4926.593	5222.586	6647.487
	10	120	3463.163	41.198	2102.72	1835.956	1483.382
		150	2267.274	45.499	2129.788	1982.847	2533.868
		175	2468.385	45.971	3108.164	3385.566	3442.545
		200	2254.315	44.434	3621.672	3699.379	4290.73
		250	2501.099	40.538	6057.529	4438.462	5988.691
	15	120	3706.070	39.148	2545.38	898.603	1277.234
		150	2936.196	44.605	2525.403	2659.978	2299.588
		175	4125.727	45.068	6096.709	2907.153	3159.153
		200	3031.458	43.270	4835.999	4145.554	3945.756
		250	2114.311	39.188	4530.462	4064.119	5534.168